REVIEWS OF

MODERN PHYSICS

VOLUME 38, NUMBER 3 JULY 1966

A Survey of Fast-Neutron Reactions*

N. CINDRO

Institute "Ruder Bošković," Zagreb, Yugoslavia

A survey of recent experimental and theoretical results (January 1963–July 1965) on fast-neutron-induced reactions is presented. The first part gives an outline of present reaction mechanism theories that may be useful for an experimentalist. A semiclassical and a more exact description of both direct and equilibrium processes is given and a brief discussion of intermediate processes included. The second part gives the experimental results relevant to the understanding of the mechanism of the interaction of neutrons with nuclei: energy spectra, angular distributions, and total cross sections. Finally, a survey is presented of the results and possibilities of utilising fast neutrons for nuclear structure investigations.

CONTENTS

INTRODUCTION

Reactions induced by fast neutrons are probably one of the experimentally hardest fields in nuclear physics, but the information that can be obtained therein is worth the effort and time spent in building special experimental apparatus and performing experiments incomparably longer than the ones where charged-particle beams are used. Moreover, when, in the last decade intense 14-MeV neutron beams became readily available, fast-neutron physics became in many respects the "poor man's physics." It is thus not surprising that in spite of the hardships involved a large number of experimental (and theoretical) papers have been published in recent years.

This survey aims to give an insight in fast-neutron reaction investigations. Of course, we are not able to explore every detail of this work. Our interest is concentrated on the problems concerning the mechanism of the interaction of fast neutrons with nuclei, and, to a somewhat lesser degree, the inferences about the nuclear structure that one can obtain from these interactions. Thus the interesting problems concerning the n–p and n–n scatterings and some of the few-body topics are omitted. It is necessary also to speak of the progress in experimental techniques utilized in the research work with fast neutrons. Considerable progress has, in fact, been achieved in recent years in this field.

The task of reviewing such a vast field of research as fast-neutron reactions poses immediately the problem of systematizing the presentation. In this systematization one might define a partition either by the energy scale or by the reaction products. Another systematic way of presentation would be according to the measured physical quantities, such as total cross sections, energy spectra, and angular distributions. It is our feeling that none of these systematic approaches is completely useful for the space at our disposal. Thus we shall rather divide the information collected in the last few years (January 1963 to approximately July 1965) according to its purpose: reaction mechanism investigations, nuclear structure studies, optical model and related topics.

* Based on a series of lectures held at the Third Winter School of Nuclear Physics, Villars, Switzerland, January 1965.

This is not always possible because some of the studies interweave structure, mechanism, and other information.

Thus the master plan is as follows: In Sec. I we review studies of reaction mechanism and related parameters obtained by means of energy spectra and angular distributions, total cross sections, and excitation function measurements and isomeric ratio measurements and analysis. Section II contains scattering and optical model studies while, finally, in Sec. III we review data about nuclear structure that can be obtained from fast-neutron reactions.

I. STUDIES OF REACTION MECHANISMS AND RELATED PROBLEMS

The problem of establishing the mechanism of the interaction between nucleons with nuclei is as old as nuclear physics itself, and so far it has not been successfully solved. There exist two different approaches to this basic problem, one that can be called black box or model treatment, the other, more recent, that can be connected with the employment of the many-body methods in nuclear physics.

In the first formulation the dynamics of the nuclear many-body system was dismissed as impossible to handle and the real state of affairs was substituted by a mathematically solvable model. Evaporation, direct reaction theories, and the optical model fall into this category. These models yield expressions for the cross sections, the polarization, and angular distributions without really solving the complete dynamical problem.

The second approach consists essentially in extending to the problem of nuclear reactions the many-body methods used in the study of nuclear structure. It is based on the idea that the unbound continuous states of the collision problem can be treated analogously to the bound levels of nucleons in the atomic nucleus.

The obvious difficulty with this approach is the problem of joining the internal region in which all nucleons interact to the external region in which the system is split into two or more particles. Much effort is being spent on solving this and other problems and it is probably true that a complete theory of nuclear interactions will ultimately follow the lines of the many-body approach. It is also true, however, that so far only a limited class of nuclear phenomena have been quantitatively understood and explained on the basis of many-body calculations. The bulk of our knowledge about the mechanism of interaction still comes from the black box approaches. (*Note added in proof.* From the time this survey was completed, the situation has greatly evolved in favor of the many-body treatment of nuclear problems.) Thus we concentrate on reaction mechanism models and analyse the existing data in terms of direct and compound nucleus theories. In the following pages we outline briefly the main reaction mechanisms. A more detailed description is given in the analysis of experimental data. The reader is also referred to several existing reviews like the one of Ericson[1] for the compound nucleus and of Austern[19] and Glendenning[21] for direct processes.

A. Reaction Mechanism Theories

A commonly employed partition divides the nuclear reactions according to their time duration. Although mathematically we can treat only the extremes—the infinitely short and infinitely long (equilibrium) interactions—it has become customary to consider the reactions which take place within a time comparable to the transit time of energetic nucleons through atomic nuclei (10^{-22} sec) as direct reactions, involving the excitation of only a few of the numerous degrees of freedom available in the nucleus. The reactions lasting one or more orders of magnitude longer are treated as equilibrium processes leading to long lived compound states. The domain inbetween the two extreme cases are the intermediate reactions which made their appearance in nuclear physics only recently.

1. Compound Nucleus Theory: Basic Assumptions

We start by stating the basic ideas and formulating the main equations that govern the extreme case of a slow reaction, the compound nucleus process. When the incident particle interacts with the target nucleus in such a way that its energy and momentum are evenly distributed through the nucleus, a long lived equilibrium system, called the compound nucleus is created. A typical feature of the system in equilibrium is that it is entirely determined by the constants of motion of the system and its size and shape; it is entirely independent of the details of the formation of the system.[1] Thus the mathematical treatment of a compound nuclear system in many ways parallels the treatment of classical thermodynamic systems, such as a liquid drop or radiative emission from a blackbody.

The analogy of an equilibrium system in nuclear reactions and a classical thermodynamic system, as foreseen by Bohr, carries several important implications. As already mentioned, the behavior of a system in equilibrium, in particular its decay, is independent of its mode of creation. The Bohr assumption of a nuclear reaction as a decay of a system in thermodynamic equilibrium (the compound nucleus) leads straightforwardly to the formulation of the expression for the cross section of a nuclear reaction,

$$X(a, b)Y$$

in the form[2]

$$\sigma(a, b)=\sigma_c(a)P_c(b), \tag{1.1}$$

where $\sigma_c(a)$ is the cross section for the formation of the metastable compound system from the incident particle a and the target nucleus X, and $P_c(b)$ the probability that the compound system, once formed,

will decay by emission of particles b. The independence of the modes of creation and decay ("loss of memory" in the compound nucleus) is reflected by the factorization of the cross section.

The compound nucleus as an equilibrium system is created as a result of subsequent scattering of nuclear particles, and the time necessary to attain such equilibrium is of the order of nuclear relaxation times. Hence, considerations based on nuclear recurrence times are important when considering the applicability of the compound nucleus theory to nuclear processes. It is well known that the recurrence time for a wave packet with an energy spread much larger than the level spacing formed of the compound nucleus is of the order of

$$2\pi h/D$$

for nonoverlapping equidistant levels of spacing D. It is thus that the criteria for the applicability of the Bohr assumption are most commonly discussed in terms of the overlap of compound state levels, which can be easily reduced to incident particle energy and target nucleus mass, rather than in terms of a time duration scale.

For incident particles of low energy the levels of the compound nucleus are well separated, and their width Γ is much smaller than their spacing D. The lifetime of such levels

$$\tau=\hbar/\Gamma$$

is much larger than the recurrence time $(2\pi h/D)$ of the system and the Bohr conditions are widely met.[3] Our main interest lies however, in the region of several MeV of incident energy where with increasing excitation of the compound nucleus its lifetime grows shorter as more and more exit channels become available. As the levels become less defined and start overlapping it is not possible any longer to make a general statement about an equilibrium system based on recurrence times. The applicability of the compound nucleus mechanism can, however, be understood in a different way. The energy spread of the incident beam here plays an essential role. For a given energy of excitation several overlapping states will, in general, contribute to the process. These states will interfere: however, there is an averaging effect due to the finite energy spread of the incident beam while an additional averaging is caused by transitions to different final states.

At this point we make use of the statistical hypothesis of the randomness of phases.[4,5] The phases between the different transition amplitudes interfere, and, provided they are randomly distributed, the averaging over the fluctuations inside the energy spread of the incident beam leads to the cancellation of cross-term contributions to the reaction cross section. Thus the statistical hypothesis of random phases of compound nucleus states is equivalent to saying that the contribution of cross terms to the transition amplitude is negligible and most of the transitions come from diagonal terms. Accordingly, the problem can still be treated as a classical one.

The success of the compound nucleus model in explaining intermediate energy nuclear reactions constitutes only an *a posteriori* argument for the validity of the statistical hypothesis.

The mathematical treatment of the compound nucleus theory can be considerably simplified if certain semiclassical concepts and pictures are adopted. Formulas derived in this way are applicable only to reactions leading to continuously populated final states, but in this range their validity is not necessarily less general. The advantage of such a treatment is that it gives a more straightforward insight to the meaning of expressions and parameters that govern a statistical process. For this reason we start with a presentation of the semiclassical treatment of the statistical theory.

2. *Statistical Theory: A Semiclassical Treatment*

The treatment of a nuclear reaction as an equilibrium process implies the knowledge of the two factors, $\sigma_c(a)$ and $P_c(b)$, entering Eq. (1.1). The cross section for compound nucleus formation $\sigma_c(a)$ is most readily calculated from the optical model, as the reaction cross section σ_R (i.e., the total cross section σ_T diminished by the shape elastic cross section σ_{SE})

$$\sigma_R=\sigma_T-\sigma_{SE}.$$

In equating the compound nucleus formation cross section σ_c to the optical model reaction cross section σ_R one tacitly assumes that every nuclear interaction takes place through the formation of a compound nucleus. This is certainly an overestimate of σ_c. The extent of this overestimation is discussed later on; however, the analysis of inelastic scattering data confirms the plausibility of this assumption.[7] The calculation of σ_c is rather complicated and requires the use of fast computers. However, several sets of calculated optical model cross sections are available both for charged particles[8,9] and neutrons.[10] Codes are also available for calculating cross sections using different local and nonlocal optical potentials.

The determination of the second term in (1.1), governing the decay of the compound nucleus, is less straightforward, although considerable progress has been made towards a better understanding of the use of different parameters involved. Derivation of a suitable form of $P_c(b)$ is based on the principle of detailed balance.[1,6] We merely give the final result and add a few comments on its validity. It can be shown that the probability per unit time of the compound nucleus decaying into an open channel leading to the emission of a particle ν with energy in the interval $(\epsilon_\nu, \epsilon_\nu+d\epsilon_\nu)$ is given by

$$P_\nu(\epsilon_\nu)d\epsilon_\nu=g_\nu\cdot(8\pi\mu_\nu\epsilon_\nu/\hbar^2)\sigma_\nu^*(\epsilon_\nu)[\rho_\nu(E_\nu)/\rho_c(E_c)], \tag{1.2}$$

where g_ν, μ_ν, and ϵ_ν are the spin weight $(2s_\nu+1)$, the reduced mass, and the energy of the emitted particle ν, respectively, and $\sigma_\nu^*(\epsilon_\nu)$ the cross section for the compound nucleus formation by the inverse process (absorption of particle ν with energy ϵ_ν by the residual nucleus). The level density factors $\rho_\nu(E_\nu)$ and $\rho_c(E_c)$ represent the level densities of the residual and compound nuclei at the corresponding excitations.

Equation (1.2) represents the basic equation governing the decay of the compound nucleus. It is based on the principle of detailed balance which in this case (overlapping levels) has a meaning only if applied to the average transition probability for the energy interval $\pm\Gamma$.

Using (1.1) and (1.2) we can readily deduce the cross section for a compound nuclear reaction. The total probability of decay of a compound nucleus is the sum of all particle probabilities over all kinds of particles and all ranges of energies:

$$P=\sum_\nu \int P_\nu(\epsilon_\nu)\, d\epsilon_\nu.$$

Thus the cross section for a specific emission is determined by the competition of different modes of decay, $P_\nu(\epsilon_\nu)/P$, which we can write explicitly by the aid of (1.1) and (1.2)

$$\sigma(a;\epsilon_\nu)\, d\epsilon_\nu=\sigma_c(a)\cdot\frac{g_\nu\mu_\nu\epsilon_\nu\sigma_c^*(\epsilon_\nu)\rho_\nu(\epsilon_\nu)\, d\epsilon_\nu}{\sum_\nu g_\nu\mu_\nu\int_0^{\epsilon_{\lim}}\epsilon_\nu\sigma_c^*(\epsilon_\nu)\rho_\nu(\epsilon_\nu)\, d\epsilon_\nu} \tag{1.3}$$

where the symbols have been explained before and the upper limit in the integral is obtained from energy conservation requirements. This is the well-known Weisskopf-Ewing formula for the emission into a particular exit channel in a nuclear reaction.[5]

Expression (1.3) shows that the decay of the compound nucleus, whose probability of formation is given by σ_c, is governed by the available phase space modified by a penetrability factor $\sigma_c^*(\epsilon_\nu)$. So far we have no way of measuring experimentally the cross section for the formation of the compound nucleus by the inverse reaction, which, as a rule will take place with the residual (now target) nucleus in an excited state. So we assume that this cross section is equal to the previously defined simple compound nucleus formation cross section (or, in essence, to σ_R), an assumption borne out by results. Having more or less established the meaning and value of the penetration factor σ_c^*, we discuss the level densities which are a crucial parameter in the determination of spectral shapes and total cross sections.

There are good grounds for the treatment of the nucleus as a system of fermions moving in an average potential. This model, called also the Fermi gas model, accounts for the rapid increase of level densities with excitation energy by the very additivity of energy of states in a system of fermions. In this model the problem of calculating the level densities is a combinatorial one, and can be treated in the usual thermodynamic way.

In the Fermi gas model the number of levels with a given energy E and angular momentum J is given by

$$\Omega(E,J)=[(2J+1)/\pi^{\frac{1}{2}}(2cT)^{\frac{3}{2}}]\times\exp[-(J+\tfrac{1}{2})/2cT]\rho(E), \tag{1.4}$$

where

$$\rho(E)=\text{const.}\ (E+t)^{-\frac{5}{4}}\exp[2(aE)^{\frac{1}{2}}]. \tag{1.4a}$$

We have introduced several new parameters in the formulas (1.4) and (1.4a). The level density parameter a is proportional to the single-particle spacing g_0 near the Fermi energy and related to the Fermi energy ξ_0 itself by

$$a=\tfrac{1}{6}(\pi^2 g_0)=\tfrac{1}{4}[\pi^2(A/\xi_0)]. \tag{1.5}$$

As the Fermi energy of a gas is independent of the number of particles (nucleons) in the gas

$$\xi_0=(3/\pi)^{\frac{2}{3}}\tfrac{9}{4}(\hbar^2/2Mr_0^2) \tag{1.5a}$$

(M and r_0 are the nucleon mass and radius respectively), the experimentally derived values of the level density parameter a should present a rough proportionality with the mass number A. For appropriate nucleon radii ($r_0=1.1-1.2$ F) the value of the Fermi energy $\xi_0=31$ MeV, which gives for a the value of $A/8$. This indeed, is the case.[11] Later on we introduce a more detailed theory that introduces shell effects in the level densities by means of j-dependent a values.

The parameter a is also related to the thermodynamic temperature t by a quadratic dependence

$$E=at^2-t \tag{1.6}$$

which, in essence, is the "equation of state" for a Fermi gas.

It can be shown that the value of $c\hbar^2$ in this model is equal to the rigid body moment of inertia, and the nuclear (to be distinguished from the thermodynamic) temperature T is given by

$$T^{-1}=[d\ln\rho(E)/dE]=(a/E)-\tfrac{5}{2}(2E+t)^{-1}. \tag{1.7}$$

The factor $2cT$ in the exponential of (1.4) is the well-known spin cutoff factor $2\sigma^2$.

The form of the level density energy dependence given in (1.4) is not the one usually employed under the name of Fermi gas model. One should notice, however, that as E becomes large, the preexponential factors

$$(E+t)^{-\frac{5}{4}}\quad\text{and}\quad t^{-\frac{5}{2}}$$

vary as

$$E^{-\frac{5}{4}}\quad\text{and}\quad E^{-\frac{3}{4}},$$

respectively, thus giving rise to the high-energy limit form of the level density

$$\rho(E) \propto E^{-2} \exp\left[2(aE)^{\frac{1}{2}}\right] \tag{1.8}$$

which is the commonly employed form. It is questionable, however, how and when this limit is reached in most of the neutron experiments analyzed.

The free fermion gas model is an essential basis of our treatment of nuclei, represented as a system of free, noninteracting nucleons. This picture is in many respects too crude, in the first place because the residual interaction effects are neglected. The importance of these effects is seen in the odd–even differences in nuclear level densities. In order to incorporate at least some of these residual interaction effects (pairing, shell structure etc.) one extends the Fermi gas model by artificially shifting the zero energy levels in odd–A and even–even nuclei by an amount varying up to 2 MeV. Phenomenologically this energy shift can be correlated to the energy necessary to break up a pair of nucleons. Thus the even–even nucleus behaves similarly to the odd–odd nucleus once a pair has been broken and the same number of particles results in each case, however, with an excitation energy decreased by the amount necessary to break up the pair (pairing energy). Thus, if the pairing energy is equal to 2δ, we can write

$$\rho_{\text{odd–odd}}(E) = \rho_{\text{odd–}A}(E-\delta) = \rho_{\text{even–even}}(E-2\delta) \tag{1.9}$$

the odd–A nuclei being somewhat intermediate. Values of δ (negative) obtained from mass formulas are listed in Cameron.[12]

The formulas (1.4)–(1.8) represent the mathematical outcome of the Fermi gas theory. Although other models of nuclear level densities are available, most of the analyses has been performed with this model.

Bohr, Mottelson, and Pines[13] have proposed a model based on the analogy between the spectra of excited nuclei and those of a superconducting metallic state. The essential feature of this model is that above a certain critical energy the nucleus behaves as a common Fermi gas, except that the energy of excitation is measured from a Fermi energy which lies above the even–even mass surface. This model gives, among other things, a different value of the spin cut-off parameter $2\sigma^2$, which is consistently above the free Fermi gas model value.

The salient feature of the nuclear level densities, their fast increase with excitation energy, can be taken into account by the simple expression (constant temperature model)

$$\rho(E) \propto \exp(E/T), \tag{1.10}$$

where T is a parameter often called the nuclear temperature. The expression (1.10) is actually the extreme application of the evaporation concept to atomic nuclei, and although plausible, it is not based on a proper nuclear model. Nevertheless many satisfactory results have been obtained using this expression.

3. *Statistical Theory: General Case*

The formalism developed in the preceding section could be applied to those transitions that lead only to a continuum of final states. There is no reason why compound nucleus reactions should not lead to well separated states with definite spins and parities. In this section we develop a formalism that provides for both cases, in the sense that the case of transitions to many final states can be obtained by appropriate summation of transition probabilities to individual states.[14,15] The account is mostly based on Ref. 16.

The theory is again based on the assumption that all states of the compound nucleus which can be excited on the basis of conservation of energy, angular momentum, and parity do participate in the reaction, but that the formation and decay of the compound nucleus take place in an incoherent way. Thus the cross section for a reaction induced by a particle of energy ϵ_0 and intrinsic spin i on a target with spin I leading to the emission of a particle with energy ϵ and spin i' and a residual nucleus of spin I' is given by[16]

$$\sigma(\alpha \mid \alpha') = \pi\lambda^2 \sum_{J,j,l\ j',l'} [(2J+1)/(2i+1)(2I+1)] \times (T^J{}_{\alpha' j' l'} T^J{}_{\alpha,j,l} / \sum_{\alpha'',j'',l''} T^J{}_{\alpha'',j'',l''}), \tag{1.11}$$

where l is the orbital angular momentum of the incoming particle, $j=I+i=J-l$ its channel spin, while l' and $j'=J-l'$ are the corresponding values for the emitted particle. The symbols α and α' mean a set of values characterizing the entrance and the exit channels, respectively, while T stands for penetrabilities.

The sums in (1.11) are submitted to the ordinary laws of angular momentum and parity conservation. The former law requires that only those terms that satisfy

$$|J-l| \leq j \leq J+l$$
$$|J-i| \leq j \leq J+i$$
$$|J-l'| \leq j' \leq J+l'$$
$$|J'-i'| \leq j' \leq J+i'$$

(J stands for the compound nucleus angular momentum) can be included in the first sum in (1.11). Conservation of parity requires that the sum runs over all final states consistent with

$$(-1)^{l''}\pi_q = (-1)^{l}\pi_{\text{initial}}$$
$$(-1)^{l''}\pi_p = (-1)^{l}\pi_{\text{initial}}.$$

Finally the energy conservation restricts the sum in the denominator to levels with energy $E<\epsilon_0$. Similarly, the second (double primed) sum goes over all possible ways through which the compound nucleus can decay when the decay characterized by α', j', l' can occur.

Equation (1.10) gives the total cross section for the emission of a particle to a specific final state, regardless of the direction of emission. The angular distribution of emitted particles is given by

$$\sigma\langle\alpha \mid \alpha'\Omega\rangle = \tfrac{1}{4}\lambda\!\!\!^{-2} \sum_{J,l,j,l',j'} \frac{(-1)^{j'-j}}{(2i+1)(2J+1)} \frac{T^J{}_{\alpha jl} T^J{}_{\alpha' j' l'}}{\sum_{\alpha'' j'' l''} T^J{}_{\alpha'' j'' l''}} \times i^{-2L} \sum_L Z(lJlJ; jL) Z(l'Jl'J; j'L) P_L(\cos\theta), \quad (1.12)$$

where L in the last sum should be taken over even values for $L \leq \min(2l, 2l', 2J)$; the rest of the symbols are as in (1.11). The angular momentum factors $Z(abcd; ef)$ are given by Blatt and Biedenharn[17] and can be expressed in terms of Clebsch–Gordan and Racah coefficients.[16] The $Z(a, b, d, d; ef)$ vanish unless $a+c+f$ is even. In our case this means that the only nonvanishing terms in the last summation are those for which

$$2l+L, \quad \text{i.e., } L \text{ is even.}$$

This has the important consequence that in Eq. (1.12), only Legendre polynomials $P_L(\cos\theta)$ of even order are present, i.e., that the angular distribution is symmetric around 90°.

It is interesting to note that the statistical assumption, in which interference terms between different states in the compound nucleus are assumed to average out leads to the fact that l and J, and l' and J' repeat in the Z symbols. Consequently, in the cross section, involving products of wave functions, only terms containing the same l and J values are retained. This same cancelation of interference term means that no polarization of emitted particles can result in compound nuclear reactions. Thus if the incident beam is unpolarized, the cross section depends only on the polar angle θ.

The integration of (1.12) over the solid angle leads to the expression (1.11) for the total cross section for the emission into a separate final state.

The cross section for the compound nuclear transition in the case when final levels are not separated should be obtained from (1.11) by summing (or integrating) over all final states. This should lead to an expression identical to (1.3), obtained in a semiclassical way.

We thus assume that the density of final states is a continuous function of energy and perform explicitly the integration of expression (1.11) over a definite range of energy. For simplicity, competing decay channels α' leading to fission or radiative transitions are neglected, and only particle channels assumed to be important. Furthermore, no parity conservation restrictions are present, since the continuum has equal population of positive and negative parity states.

With these assumptions, the cross section for the reaction induced by a particle a with energy ϵ_0 leading to a particle ν with energy in the interval ϵ, $\epsilon+d\epsilon$, is given by

$$\sigma_{a,\nu}(\epsilon_0, \epsilon)\, d\epsilon = \pi\lambda\!\!\!^{-2} \sum_{J,j,l} \frac{2J+1}{(2i+1)(2I+1)} \times \left(T^J{}_{ajl}(\epsilon_0) \cdot \sum_{J'l'I'} T^J{}_{\nu j' l'}(\epsilon) \cdot \rho_\nu(I', E)\, d\epsilon \Big/ \sum_{\nu'' j'' l'' I''} \int_0^{\epsilon_0 - Q_{\nu''}} d\epsilon\, T^J{}_{\nu'' j'' l''}(\epsilon) \rho_{\nu''}(I'', E'')\, dE'' \right). \quad (1.13)$$

The symbols are again as in (1.11) and (1.12) except that the incoming and outgoing channels, α and α' have been replaced by the notation a and ν, respectively. The sum in the denominator runs over all energetically possible emitted particles ν''. $\rho_\nu(I', E)$ is the density of levels of the residual nucleus after the emission of a particle, leaving the residual nucleus with an excitation

$$E = \epsilon_0 - \epsilon - Q, \quad (1.13a)$$

where Q is the Q value of the reaction.

To reduce Eq. (1.13) to a form similar to the Weisskopf–Ewing formula (1.3) two additional assumptions are necessary:

(i) that spin and energy dependence of the level density (I, E) can be factored into

$$\rho(I, E) = (2J+1)\rho(E)$$

(ii) that the penetrabilities T do not depend on j' or J but only on l.

With the consequent simplifications in the summations, after the enumeration of the statistical weight factors, Eq. (1.13) reduces to

$$\sigma_{a\nu}(\epsilon_0, \epsilon)\, d\epsilon = \sigma_c(a, \epsilon_0) \left((2i'+1)\epsilon \sigma_{c,\nu}{}^*(\epsilon) \rho_\nu(E)\, d\epsilon \Big/ \sum_{\nu''} (2i''+1) \int_0^{\epsilon_0 - Q_{\nu''}} \epsilon'' \sigma_{c,\nu''}(\epsilon'') \rho_{\nu''}(E'')\, dE'' \right), \quad (1.14)$$

where the combinations $\sum_l(2l+1)T_l$ have been replaced by the cross sections for compound nucleus formation, $\sigma_{c,\nu}$* to which they are proportional.

Equation (1.14) is the well-known Weisskopf–Ewing formula (1.3) derived in the preceding section.

4. *Direct Reaction Theories: General Predictions*

The other extreme in a time classification of nuclear reactions is given by the extremely fast reactions, with duration times of the order a nucleon takes to cross the nucleus. These reactions are generally known as direct reactions and comprise a number of mechanisms by which a particle can be excited in a direct collision.

In a long process during which the nucleon crosses the nucleus several times, many degrees of freedom can be excited. On the contrary, if the nucleon just crosses the nucleus, it excites only a few degrees of freedom. Thus the time scale of nuclear reactions implies a description of direct processes as those involving only a few of the many degrees of freedom of a nucleus. The minimum number of degrees of freedom that must be involved in a nuclear reaction are those required to describe the initial and final channels and direct reaction studies consider just these. Strictly speaking this kind of reasoning contains a sometimes not justifiable mixture of classical (collision time and number of collisions) and quantum concepts (number of degrees of freedom involved). Its only justification is that it provides a simple insight into the energy and angular dependence of the two main mechanisms of interaction.

It is clear that direct interaction processes take only a fraction of the incident wave function. The rest is connected with complicated excitations of many degrees of freedom and result in the gradual formation of a compound nucleus. It is however true that the direct processes, when existing, have a large cross section. The causes for such a large cross section are not yet fully understood, and the answer is probably not unique.

The reason why direct effects are, when existing, large is deeply bound with our knowledge of nuclear structure. Our attitude towards the direct interactions has been—even historically—rather parallel to that towards the shell model. This is clear, since both models rely on the assumption that, to a good approximation, the mean free path of nucleons in nuclear matter is infinite. For reactions involving nucleons, the intrinsic reason of the extraordinary magnitude of direct reactions is found in the same properties which cause the independent particle model to be a good approximation of nuclear behavior. Namely, the attractive part of the two-nucleon force is moderately weak and of long range and thus goes mostly in setting up an average potential responsible for shell model configurations. Now, the low-lying excited states which are in the same shell model configuration as the ground state have a great deal of overlap with the ground state and can be excited strongly in the very initial stages of interaction.

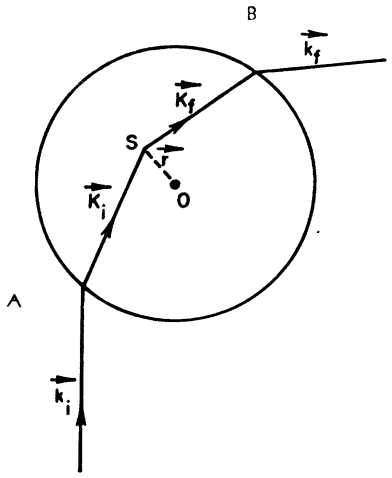

FIG. 1. The semiclassical model of direct reactions (Ref. 19).

Thus strong direct interaction excitations are expected to occur for these states in the cases of (incident) nucleon–(outgoing) nucleon reactions. For composite particles the reasons are more complex, but in general are connected to their low penetrabilities and the excitation of low-lying surface vibrational levels.[16]

The simplest direct interactions involve a three-body rearrangement collision.[19] They are known as *knock-out* scattering (a bombarding particle, which need not be a nucleon, may interact with a particle in the target nucleus, both particles being then lifted to higher states of motion), *stripping* and its inverse *pick-up* (a particle bound in one of a pair of colliding nuclei may make a transition to a bound state in the other), and *collective surface oscillations* (a bombarding particle collides with the surface of a nucleus thereby inducing a collective oscillation, which again results in inelastic scattering). The mathematical expressions governing these processes can be found in several excellent reviews, on which the following presentation is based.[18–21] We briefly review the main ideas and state, when possible, the most widely used formulas.

The treatment of direct reactions is somewhat different for the cases when final levels can or cannot be resolved. In each case a semiclassical treatment (Fig. 1) can be applied, that leads to an asymmetric angular distribution of emitted particles. However, while in the former case the asymmetry can be understood as a consequence of angular momentum conservation, in the latter case it is rather the conservation of linear momentum that causes a general forward peaking.

(*i*) *Sharp levels not resolved.* In this case the theory predicts forward peaked angular distributions and spectra composed predominantly of higher energy particles. The two results can be understood qualitatively in the following way.[19] A direct interaction process can be pictured as involving the collision of a nuclear unit a colliding with a subunit b_1 of a nucleus B, the remaining subunit b_2 of B being only a spectator to this

collision. As a result of this collision any of the three particles may emerge, the other two remaining bound together. Hence the possible reactions are:

$$a+B\rightarrow a+(b_1+b_2)\rightarrow(a+b_1)+b_2$$
$$\rightarrow a+(b_1+b_2)$$
$$\rightarrow(a+b_2)+b_1.$$

The first and third processes are stripping or pickup processes, while the second is inelastic scattering. Now, as b_2 is only a spectator of the process, it retains its original energy and momentum. Thus $(a+b_1)$ in the first and a and b_1 in the second and third processes will emerge with essentially the energy and momentum (and hence in the direction) of the incident particle a, thus giving rise to forward peaked angular distributions.

A similar argument can explain the hardening of the spectra observed in direct processes. Since the incident particle a and the interacting subunit b_1 are usually of a comparable size, the transfer of momentum will be maximal, favoring the emission of more higher energy particles. A more specific derivation of the shape of the spectra of particles emitted in direct reaction can be obtained by taking into account the fact that in a direct reaction the energy distribution is the result of two competitive processes. For a volume direct interaction the incoming nucleon first interacts with the proton and neutron Fermi sea. For a maximal transfer of energy and momentum, the reaction may take place only on the surface of the Fermi sea. Reactions with less momentum transfer can occur also deeper in the Fermi sea. Thus the maximum in the spectrum comes as a result of the interplay of two factors:

—the Pauli principle making more and more protons available for the interaction and
—the Coulomb barrier, inhibiting their emission.

The expression for the energy spectrum of direct volume reactions is thus given by[22]

$$N(\epsilon)\propto b_1(\epsilon_{\max}-\epsilon)+b_2(\epsilon_{\max}-\epsilon)^2+b_3(\epsilon_{\max}-\epsilon)^3+\cdots, \tag{1.15}$$

where $\epsilon_{\max}$ is the maximum energy transfer. The above expression is valid only for volume interactions. Qualitatively both volume direct and compound nuclear mechanisms lead to similar results for the energy spectrum of emitted particles, since in both cases the distribution is the result of two competitive processes.

(*ii*) *Sharp levels resolved.* In this case it is possible to speak only of angular distributions. The general argument from the preceding section holds again, but the forward peaked asymmetry is modified by angular momentum conservation requirements. In the semiclassical model of Butler[23] the process is pictured as a refraction of the incident ray on the surface of the nucleus followed by the main scattering inside the nucleus and a second refraction when the emitted particle leaves the nucleus. The transfer of momentum to the nucleus is

$$\mathbf{q}=\mathbf{k}_i-\mathbf{k}_f,$$

where $\mathbf{k}_i$ and $\mathbf{k}_f$ are the momenta of the incident and outgoing particles, respectively. In the semiclassical picture we shall assume that the momenta of the particles inside the nucleus are equal to the momenta outside it. Thus the transfer of angular momentum, which takes place at S is

$$\Delta\mathbf{L}=\hbar\mathbf{q}\times\mathbf{r}.$$

As the angular momentum is quantized, and restricted to integer values $l\hbar$, the reaction may proceed only at those points $\mathbf{r}$, which satisfy the equation

$$l=|\mathbf{Q}\times\mathbf{r}|.$$

These points lie all on a surface of a cylinder of radius l/Q whose axis passes through the center of the nucleus in the direction $\mathbf{q}$, the so-called *active cylinder*. A further simplification, based on the absorption of particles in nuclear matter, restricts the contributing points to the nuclear surface only ($r\geq R$). Thus the contributing points lie on the intersection between the active cylinder and the nuclear surface, and the total transition amplitude can be obtained by adding coherently all these contributions:

$$T=\int_{ac(r\geq R)}p(r)\exp(i\mathbf{Q}\cdot\mathbf{r})\,d\mathbf{r}. \tag{1.16}$$

$p(r)$ weights the probability that a reaction can take place at a given point and $\exp(i\mathbf{q}\cdot\mathbf{r})$ is a phase factor accounting for the differences in phases between outgoing rays originating from different points in the nucleus.

Performing the integration, (1.16) leads to

$$T=4\pi l\int_R^\infty rdrp(r)\cos(Q^2r^2-l^2)^{\frac{1}{2}}(Q^2r^2-l^2)^{\frac{1}{2}}. \tag{1.17}$$

The factor $p(r)$ must fall off very rapidly for $r>R$, since it is proportional to the nuclear density. Moreover only as long as $qR<l$, so that the active cylinder does in fact intersect the nuclear surface, will the transition amplitude be different from zero. When $qR<l$, the active cylinder misses the nucleus, and so there are no contributions and the cross section is zero. Combining this with the above assumption on $p(r)$, the angular distribution can be written in the form

$$\sigma(\theta)\propto\cos^2(Q^2r^2-l^2)^{\frac{1}{2}}/(Q^2r^2-l^2) \qquad \text{for } qR>l$$
$$\sigma(\theta)\rightarrow 0 \qquad \text{for } qR<l. \tag{1.18}$$

Equations (1.17) and (1.18) give all the essential features of a direct reaction angular distribution: the oscillatory behavior, seen as a typical interference effect, and the existence of forbidden regions of emission. Namely, for a reaction in which $l>0$ it may happen

that for small angles $qR<l$. For this reaction there will be no (in the extreme case) emission in the forward angles.

Despite its shortcomings the simple model gives a better than qualitative insight into the main features of the direct processes. It has, however, been almost abandoned in favor of the more sophisticated approaches, which we briefly review in the next section.

5. *Direct Reaction Theories: The DWBA Method*

The exact matrix for a direct transition between an initial state i and a final state f is given by

$$T_{if}=\langle\phi_f \mid V \mid \psi_i\rangle, \tag{1.19}$$

where ϕ_f and ψ_i are the wave functions of the final and initial states, and V the interaction that causes the transition. The interaction V is usually the nucleon–nucleon interaction, or, in the case of more complex particles, some mathematically solvable prescription. To the present time we are not able to evaluate (1.19) exactly. It can be shown, however,[21] that the exact expression (1.19) can be approximated by

$$T_{if}\doteq\langle\chi_f^{(-)} \mid V \mid \chi_f^{(+)}\rangle, \tag{1.20}$$

where $\chi_i^{(+)}$ and $\chi_f^{(-)}$ are simple wave functions obtained by factoring the state wave functions into their components:

$$\chi_{i,f}^{(\pm)}=\psi_{i,f}^{(\mathrm{el})}\phi_{i,f}^{(\mathrm{int})}\xi_{i,f}^{(\mathrm{spin})}\Psi(\text{target, residual}), \tag{1.21}$$

where $\psi^{(\mathrm{el})}$, $\phi^{(\mathrm{int})}$, and $\xi^{(\mathrm{spin})}$ stand for the elastic scattering, internal, and spin wavefunctions of the incident (i) viz. outgoing (f) particle, respectively, and $\Psi^{(\mathrm{target})}$ and $\Psi^{(\mathrm{residual})}$ represent the target and the residual nuclei wave functions, respectively.

Up to this point we have not made any physical assumption about the nature of the process. Now we take into account the physical nature of the transition, and appropriately decompose the final state wave function. It is most convenient to consider a (d, p) stripping process, as representative of direct reactions.[21] In this case we decompose the wave function of the residual nucleus on a basis exhibiting the target+stripped neutron,

$$\Psi^{(\mathrm{residual})}(A, \mathbf{r}_n, \mathbf{s}_n)=\sum_{l,j,J_c}\beta_{jl}(J_c, J_f)\Phi(J_c, j, l), \tag{1.22}$$

where Φ is a wave function constructed by vector coupling the extra nucleon in the spin–orbit state $\phi_{l,j}$ to a target wave function with angular momentum J_c. The expansion coefficients β_{jl} represent the degree to which the final state has the configurations indicated by Φ, and are directly related to the reduced widths of the corresponding states.

With the necessary rearrangements,[21] the square of the transition amplitude, i.e., the stripping cross section is given by

$$\frac{d\sigma}{d\Omega}=\frac{m_d^*m_p^*}{(2\pi\hbar^2)^2}\frac{k_p}{k_d}\frac{2J_f+1}{2J_i+1}\sum_{j,l,m}\beta_{jl}^2 \mid B_l^m \mid^2, \tag{1.23}$$

where

$$k_p^2=2m^*p\epsilon_p/\hbar^2,$$

$$k_d^2=2m_d^*\epsilon_d/\hbar^2,$$

$$\epsilon_p=\epsilon_\alpha+Q=\epsilon_d+B_n-B_d,$$

m^* are the reduced masses, while ϵ's and B's are kinetic energies in the center of mass system and binding energies respectively. Equation (1.23) holds—*mutatis mutandis*—for any direct process and represents the general form of direct reaction cross sections.

Aside from multiplicative constants, the cross section (1.23) has been decomposed into two factors: the already defined expansion coefficients β_{jl} and the quantities B^m that in essence represent the overlap integrals between the elastic scattering wave functions of the incoming and outgoing particles:

$$B_l^m=i^{-l}(2l+1)^{-\frac{1}{2}}\int\psi_p^*\xi_pV_{np}(r)\psi_d\xi_d\,dr, \tag{1.23a}$$

where ψ_p and ψ_d are elastic scattering proton (outgoing) and deuteron (incoming) wavefunctions and ξ_p and ξ_d are corresponding spin functions. The quantities B_l^m depend sensitively on l, and this is the root of the spectroscopic value of stripping and direct reactions in general.

The effect of antisymmetrization deriving from the fact that the nucleons in the nucleus are indistinguishable modifies the expression (1.23) into

$$\frac{d\sigma}{d\Omega}=\frac{a}{4}\frac{m_f^*m_i^*}{(2\pi\hbar^2)^2}\frac{k_f}{k_i}\frac{2J_f+1}{2J_i+1}C^2\sum_{l,m}S(l) \mid B_l^m \mid^2, \tag{1.24}$$

where

$$S(l)=\sum_j S(l,j)$$

$$S^{\frac{1}{2}}(l,j)=(A+1)^{\frac{1}{2}}\beta_{lj}$$

$$=(A+1)^{\frac{1}{2}}\int\Phi^*(J_c, j, l)\Psi_{J_f}\,d(A+1). \tag{1.24a}$$

a and A are the masses of the incident and target particles in the process, so that the equation (1.24) holds for any transfer reaction

$$A(a, a\mp1)A\pm1.$$

The rest of the symbols used have already been defined.

The importance of Eqs. (1.23) and (1.24) lies as already mentioned in the possibility of factorization. The first factor $S(l)$, called also the *spectroscopic factor*, is connected with the β_{jl}, i.e., with the overlap of the wavefunction Ψ_{J_f} of the residual nucleus and $\Phi_{J_c,j,l}$, the wave function constructed by vector coupling the

extra particle (nucleon, in general) in the spin orbit state ϕ_{lj}. This factor depends only on the nuclear structure. Vice versa, nuclear structure information can be obtained from knowledge of it. The second factor $|B_l^m|^2$ contains the angular distribution and the incident and outgoing wave functions. The difference between (1.23) and (1.24), introduced by the antisymmetrization does not affect the angular distribution but only the absolute value of the cross section. Hence it is important in obtaining spectroscopic information.

We end this presentation of direct reactions by discussing the elastic scattering wave functions $\psi_{i,f}$ of the incident and outgoing particles. In the plane wave Born approximation (PWBA) we assume that there is no interaction either between the incident particle and the target nucleus or between the outgoing particle and the residual nucleus. Thus the two particles satisfy the field free Schrödinger equation and are represented by plane waves.

Obviously this approximation is too crude. The effect of the optical and the Coulomb potentials of the nucleus distorts the wave functions of the incident and outgoing particles. These wave functions are now solutions of the Schrödinger equation including the nucleon–nucleus interaction. The presence of the distortion affects the B_l^m factors. However, the effect of the distorted wave Born approximation (DWBA) on the angular distribution itself is rather small; it rather changes the absolute value of B_l^m thus influencing the reliability of spectroscopic information obtained.

The potential that distorts the wave functions is the potential determined from the best fit of elastic scattering data. Thus in principle the DWBA method is an exact method which does not allow for any free parameters. In practice there is still considerable ambiguity in the values derived from the DWBA calculations.

6. *Intermediate Processes*

Between the two extremes in nuclear reaction mechanisms—the compound nucleus and the direct interaction—there certainly exists a wide spectrum of intermediate stage processes, characterized by a partial equilibrium resulting from the sharing of the incoming energy among a small number of particles.

Ideas of partial equilibrium were first introduced a long time ago by Bethe as spot heating. Bethe assumed that the nuclear interaction takes place in a rather restricted region of the nucleus, which is excited to a high temperature, and the evaporation takes place only in this region. A new approach to this problem has been given by Izumo.[24] Although Izumo uses the same concept of partial equilibrium, the essentially new idea in this approach is the supposition that the interacting nucleons need not be localized, but can very well be distributed over the whole nuclear volume. In this model the reaction is understood as taking place after a state of partial equilibrium is achieved. In other words, based on the experimental fact of rather broad resonances in the energy dependence of the cross section for a given final state (100–400 keV) Izumo envisages a partial (intermediate) equilibrium taking place after a time τ_μ, several orders of magnitude shorter than the time necessary for a complete equilibrium and yet much longer than the nucleon transit times in the nucleus. The total equilibrium is attained after a time

$$\tau_{CN}=\hbar/\Gamma\doteq 10^{-16}\text{ sec} \qquad (\Gamma=\text{level width})$$

while the nucleon transit time is equal to

$$\tau_{DI}=R/v\sim 10^{-22}\text{ sec.}$$

The intermediate partial equilibrium time should be of the order of

$$\tau_\mu=\hbar/\Gamma_\mu\sim 10^{-20}\text{ sec.}$$

One sees that

$$\tau_{CN}\gg\tau_\mu\gg\tau_{DI}.$$

These considerations lead to the assumption that the reaction proceeds through a certain partial equilibrium, in which only a fraction of the nucleons takes part. One divides the nucleons into two groups: the inert core nucleons and the outer nucleons. Izumo's assumption states that only outer nucleons interact strongly with the incident particle, while the inert core remains in its ground state and produces only an average potential for the incident particle.

The essential part of the theory is that the transition amplitude T, although calculated analogously as for the core nucleons, uses a different density of residual states. As these states stem from the interaction of fewer particles, their density is smaller. The result is the same as having the same number of particles in a large potential well (the density of states decreases with R^{-2}). In calculating, therefore, the partial equilibrium transitions we select from all the possible levels of the residual nucleus only those, which one can reach through a partial equilibrium (compound state) process. The density of these states is smaller than for the whole compound nucleus which is accounted for by a smaller value of the parameter a entering in the formula

$$\rho(E)=\text{ const } E^{-2}\exp\left[2(aE)^{\frac{1}{2}}\right].$$

The associated physical picture implies that, as the energy is shared among fewer particles, the temperature is higher, and consequently, a is smaller ($E=aT^2$). Following our argument, this excitation E_0 gives the same level density as an excitation E of a classical compound nucleus given by

$$E_0=\left[(A+n)/(N+n)\right]^{\frac{3}{2}}E, \qquad (1.25)$$

where A, N, and n are the masses of the target nucleus, the interacting fragment inside the nucleus, and the incident particle, respectively. The factor $\left[(A+n)/(N+n)\right]^{\frac{3}{2}}$ shows the R^{-2} dependence. The level density $\rho(E)$ for a compound nucleus process is

then related to the intermediate state level density ρ_μ as

$$\rho(E)=[(A+n)/(N+n)]^{\frac{3}{2}}\rho_\mu(E_0). \quad (1.26)$$

As the factor in brackets is greater than one, the intermediate state level density is less than the corresponding compound nucleus level density. A good fit for particles of medium energy is obtained with

$$N+n=6,$$

i.e., the interaction is spread over 6 particles.

A different approach has been taken by Feshbach and collaborators,[25] although again the same basic idea of sharing the energy among a smaller number of particles is present. Feshbach considers the different stages of creation of the compound nucleus, that takes part when the degree of complexity of the excitations gradually rises.

(i) The simplest interaction is when the incident particle interacts with what is essentially the real part of the shell model potential of the target nucleus, in elastic scattering, this interaction would correspond to the so-called potential scattering.

(ii) The next step is a two-body interaction between the incident particle and a nucleon from the target nucleus. This interacting particle is raised to higher state and leaves a hole behind. In this way a 3 quasi-particle (two particles–one hole) state has been created that may exhibit some of the features of a resonant state. This state, appropriately called a doorway state consists of two particles (usually two nucleons) the incident one and the excited one, raised to unbound (or bound) states in the nucleus and a hole that is left behind the excited particle.

(iii) This 3 quasi-particle configuration leads either to more complicated 5-, 7-, etc. quasi-particle configurations or dissolves back to a single-particle state in a potential well. In the former case, the gradual rise in complexity of the configurations (ultimately) leads to the creation of a compound nucleus. Hence the name of doorway states.

There is no question that such or similar processes take place. The question is whether this doorway state lives long enough to give rise to resonant structure narrow enough to be observed, or the lifetime of the state is so small that the related structure in the excitation functions is undetectable.

Feshbach has suggested that doorway states having a finite lifetime would give rise to intermediate structure in neutron total cross-section excitation functions. The estimated width of these resonances is 50–100 keV, and they would reveal themselves as a characteristic structure within a single giant (optical model) resonance.

A quantitative estimate of the width of doorway states has been suggested by Le Couteur.[26] The argument of Le Couteur is based on the fact that the total energy of excitation E, present in the process is partitioned between the excitation E_1 of one particle above the Fermi level and the excitation E_2 of the particle above the hole it previously occupied. The corresponding number of states within the range dE of excitation is

$$\tfrac{3}{4}g^2E\cdot dE,$$

where g is the average single-particle spacing,

$$g=(6a/\pi^2)\doteq\tfrac{1}{8}A \text{ MeV}^{-1}.$$

Hence[26] for a nucleus with atomic number A, the average spacing of doorway states is

$$\Delta=\tfrac{4}{3}(6A/8\pi^2)^{-2}E^{-1}=230A^{-2}E^{-1} \text{ MeV}. \quad (1.27)$$

This average distance is modified when considerations of angular momentum are taken into account. For a nucleus with small target spin the spacing is given by

$$\Delta_0=1.7A^{\frac{1}{3}}\Delta. \quad (1.27a)$$

The formula of Le Couteur gives a strong A dependence of the spacing of doorway resonances, contrary to possible experimental evidence.

B. Energy Spectra and Angular Distributions

Although we believe that, globally speaking, at least 80% of interactions of fast neutrons with atomic nuclei proceed via the compound nucleus formation, the investigation of the compound nucleus–direct interaction competition in neutron induced reactions is far from being exhausted. This concerns especially the presence of possible intermediate mechanisms.

There are several means of investigating reaction mechanisms, energy spectra and angular distribution studies being the most popular one. It has, however, been often pointed that none of these methods, taken *per se* provides sufficient information as to ascertain unambiguously the reaction mechanism.[27] Moreover, the determination of parameters connected with different models usually requires more than single-information-type experiments. Several complete experiments have been performed recently or are in progress.

1. Very Light Elements ($A<20$)

A few measurements of neutron reactions on very light elements ($A<20$) have been performed in the last two years. The easy obtainable combination C–N–O, present in nuclear emulsions has been investigated by Sen[28] with 14.3-MeV neutrons. The obtained spectra of alpha particles, although experimentally somewhat uncertain, show typically direct features with unresolved levels. The angular distribution of alpha particles from 14-MeV neutron bombardment of emulsions is shown in Fig. 2. A fit in terms of the three familiar direct interaction mechanisms, namely the pick-up (of He^3), knock-out of (He^4), and heavy-particle stripping has been attempted. For all the three mechanisms, the differential cross sections are given by the spherical

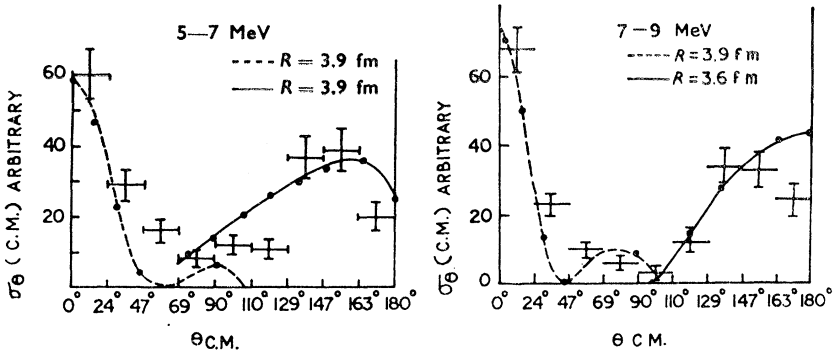

FIG. 2. Angular distribution of alpha particles from 14-MeV neutron bombardment of nuclear emulsion (C–N–O). The dotted line represents a fit with the pick-up mechanism; the full line is heavy-particle stripping (Ref. 28).

Bessel function of order l:

$$\sigma(\theta) \propto f j_l^2(QR), \tag{1.28}$$

where f is the form factor, and the distinction of the three reaction mechanisms comes only in the definition of the momentum transfer $\mathbf{Q}$:

pick-up:

$$\mathbf{Q} = (M_R/M_T)\mathbf{k}_n - \mathbf{k}_\alpha \tag{1.28a}$$

knock-out:

$$\mathbf{Q} = [(M_T - M_\alpha)/M_T]\mathbf{k}_n - [(M_T - M_\alpha)/M_R]\mathbf{k}_\alpha \tag{1.28b}$$

heavy-particle stripping:

$$\mathbf{Q} = \mathbf{k}_n + (M_n/M_R)\mathbf{k}_\alpha. \tag{1.28c}$$

(This is purely a consequence of the different kinematics of the three processes.) A reasonable fit for forward angles with the pick-up process and with heavy-particle stripping for backward angles has been attained. Thus it appears that a better approach to the understanding of the reaction mechanism is to assume a He^3 pick-up than a He^4 knock-out mechanism, in contrast with the results of several other authors. In fact in a later article Chatterjee *et al.*[29] found that the angular distribution of ground-state alphas from C^{12} could be fitted equally well by either [(pick-up, knock-out)+heavy-particle stripping mechanisms]. Furthermore, Al Kital *et al.*[30] found evidence for clearly knock-out processes in the emission of alpha particles from C^{12} (Figs. 3–5). In their results the strongly forward angular distributions of ground state alphas and alphas from the excited states up to 5 MeV of excitation (it is believed that no alphas are emitted below this energy region, a point that experimentally has yet to be verified) of the residual nucleus are again equally well fitted by the pick-up and knock-out mechanisms. However, an additional argument in favor of the knock-out mechanism—in C^{12} *a priori* more likely—is given by the reduced widths of the ground and first excited states. The ratio of the reduced widths of these states for α emission amounts to 1.5. The knock-out mechanism gives 1.1 while the pure pick-up mechanism yields a ratio of 6.5. Thus our *a priori* guess seems well endorsed by the experimental evidence.

Further data about the $O^{16}(n, \alpha)C^{13}$ reaction are presented by Chatterjee,[31] who measured the angular distribution of alpha particles emitted up to an excitation of 4 MeV of residual nucleus C^{13}. The distribution is peaked in the backward direction and heavy-particle stripping gives an excellent fit. This and the preceding

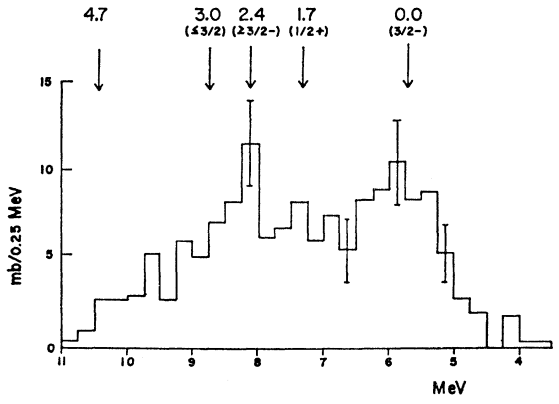

FIG. 3. Energy spectrum of alpha particles emitted from the reaction $C^{12}(n, \alpha)Be^9$; $E_n = 14$ MeV. The ordinate is the total cross section between 0° and 90° in the laboratory system, and the abscissa is $-Q$. Arrows show the known levels of Be^9 labeled with excitation (MeV), spin and parity (Ref. 30).

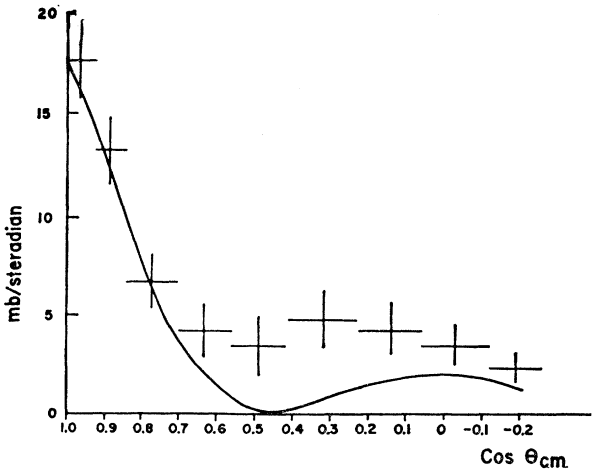

FIG. 4. Angular distribution for the transition to the ground state ($-6.2 < Q < -5.2$) of the reaction $C^{12}(n, \alpha)Be^9$. The solid curve is a theoretical Butler curve with $l = 1$ and $R = 5$ F. A knock-out mechanism has been assumed (Ref. 30).

results seem to establish heavy-particle stripping as an exchange process in the (n, α) reactions on light nuclei. This process accounts for most of the backward peaking. The presence of strong heavy-particle stripping contributions in the backward angles for the reaction $O^{16}(n, \alpha)C^{13}$ favor implicitly the presence of knock-out rather than the pick-up process at forward angles (see also Sec. IIIB).

The problem of reaction mechanism on very light nuclei has been also studied by measuring the angular distribution of gamma rays following the inelastic scattering of 14.1-MeV neutrons with C^{12} and Mg^{24}.[32] The angular distributions for both the 4.43-MeV gamma ray in C^{12} and the 1.37-MeV gamma ray of Mg^{24} were symmetrical around 90°, in agreement with the statistical model theory predictions of Satchler,[33] although it is well known that the corresponding inelastic scattering processes are well described by a direct mechanism. Although it is possible that both the direct and statistical theories of gamma emission give similar angular distributions, these results remain open to further speculations.

The interaction of neutrons with very light nuclei has been employed to study a different aspect of reaction mechanisms, more familiar to those working in few nucleon problems, namely the distinction between sequential decay and simultaneous disruption into many bodies. Jeremie[90] has measured the spectra and angular correlations of the two neutrons resulting from the $(n, 2n)$ reaction on Be^9. This reaction can proceed in several ways, the one most in accordance with the experiment being the simultaneous decay into three or four bodies:

$$n+Be^9 \rightarrow (n+n)+Be^8 \rightarrow 2n+2He^4.$$

On the other hand, the results of Batchelor and Towle[34] and Valković[35] on the interaction of fast neutrons with Li isotopes and B^{10} are rather inconclusive as far as the particular direct reaction mechanism is concerned. Only in the case of the $Li^7(n, t)$ reaction Valković[35] reports strong final state interaction of the neutron

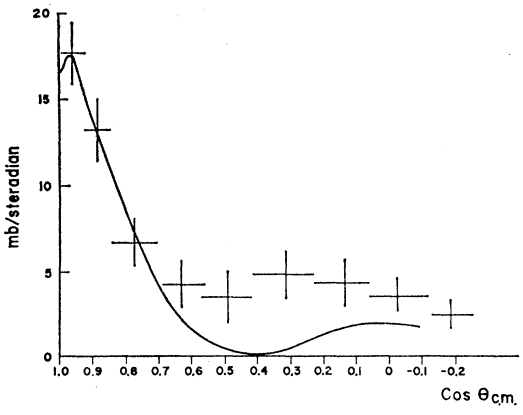

FIG. 5. Same as Fig. 4, with pick-up curve $l=1$, $R=4.45$ F (Ref. 30).

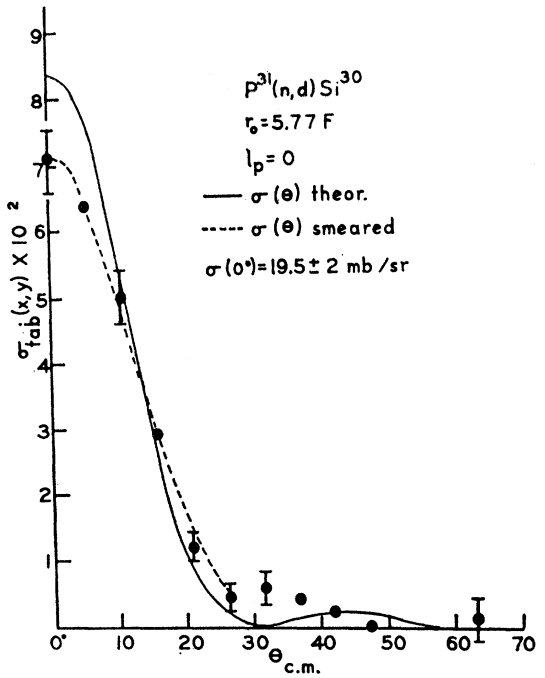

FIG. 6. Angular distribution of deuterons from the reaction $P^{31}(n, d_0)S^{30}$ (ground state). The ordinate values are those from the numerical tables of Lubitz.[37] They are proportional to the square of the Wronskian and contain the whole angular dependence of the cross section. The error flags show statistical counting errors only. Measurements have been extended to 150° lab., but no significant yield has been obtained. The energy of the neutrons was $\epsilon_0=14$ MeV (Ref. 36).

and the alpha particle, giving rise to a strong ground-state peak of tritons, while the continuous part of the triton spectrum is presumably due to sequential decay and not to the simultaneous three-body break-up. We shall again turn to (n, d) and (n, t) reactions when speaking of the cluster structure in light nuclei. A measurement of $N^{14}(n, d)C^{13}$ ground and first excited state distributions shows no appreciable cross section at backward angles.[36] Hence heavy-particle stripping seems to be rather unimportant in (n, d) reactions at 14 MeV. Good fits to these angular distributions have been obtained with plane wave Butler curves, showing that either both Coulomb and nuclear distortions are small or they cancel in a peculiar way (see also Sec. IB2 for results on P^{31} and S^{32}).

2. *Intermediate Elements* $(20<A<100)$

This is a region where, at least in its lower part, the statistical assumptions of the compound nucleus model should not necessarily be fulfilled. In spite of this, the model works surprisingly well in all this region, both for emission of charged particles and neutrons. In fact, direct reactions in this region of nuclei can be traced only for some $(n,$ charged particle) reactions leading to low-lying states in the residual nuclei, e.g., in the case of $P^{31}(n, d)Si^{30}$ ground and first excited states and $S^{32}(n, d)P^{31}$ ground state at 14 MeV[36] (Fig. 6).

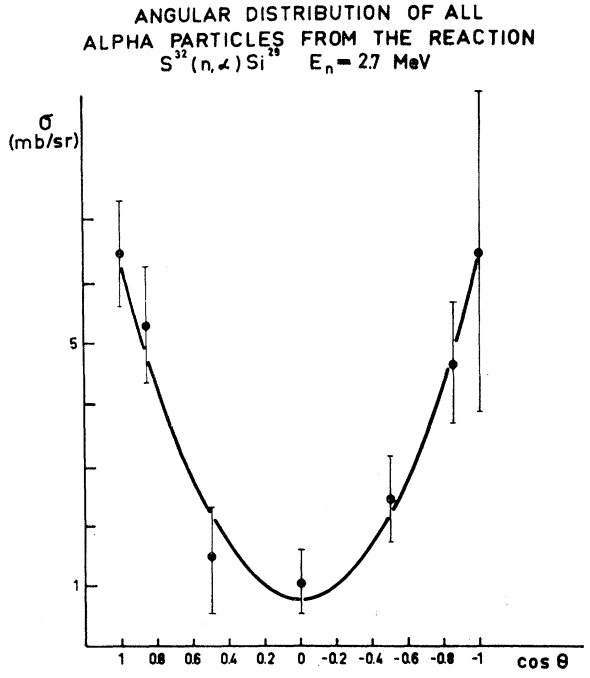

FIG. 7. Angular distribution of ground-state alpha particles from 2.7-MeV neutron bombardment of S^{32} (Ref. 38).

Most of the other results could be interpreted in terms of the compound nucleus mechanism. Even some ground state (n, α) transitions on elements like S^{32} (Ref. 38) for lower energy neutrons show a shape symmetrical around 90° that can be fairly well fitted by a polynomial of the type (Fig. 7).

$$P(A)=a+b\cos^2\theta.$$

Calvi *et al.*[39,40] measured angular distributions from the reaction $Ca^{40}(n, \alpha)A^{37}$ ground state and first excited state measured at neutron energies of 3.6, 4.0, and 4.5 MeV. While the earlier result at 3.6 MeV showed a symmetrical angular distribution for ground state alphas [Fig. 8(a)], the two recent ones at 4.0 and 4.5 MeV showed marked asymmetry both for ground state and first excited state alphas [Fig. 8(b)]. The strong dependence of the angular distributions on neutron energy shows that the results cannot be explained simply, neither in terms of the statistical model nor in terms of the simple direct interaction theory. It is again an example of the inadequacy of judging the reaction mechanism from angular distributions solely.

Actually the direct reaction mechanism could even account for angular distributions practically symmetrical around 90° as, e.g., in the work of Massot *et al.*[41] Using a plane wave approximation and both a zero range and Gaussian potential of interaction these authors obtained differential cross sections for pick-up and knock-out processes in terms of the respective momentum transfers. As shown in Figs. 9(a) and (b), quasi-symmetrical angular distributions could be fitted with a mixture of (pick-up+knock-out) processes. It seems that the range of the assumed interaction does not play an important role [cf. Figs. 9(a) and (b)].

A new field of experimental investigation has been opened by methods employing the targets simultaneously as detectors. This is an illustrative example on how physicists find ingenious devices to circumvent the inherent difficulties of fast neutron work. From the early work of the Milan group[42,43] physicists have discovered that they can use this same technique for a number of other targets: scintillators, gases, and semiconductors. This has proven to be fruitful especially when more subtle techniques, like pulse-shape discrimination and others are added. In this way charged-particle spectra of silicon,[44,45] potassium,[46] and argon[47] have been measured for neutron bombarding energies up to 14 MeV. Figure 10 shows cross sections for (n, α) disintegration of Ar^{40} obtained in this way.[47]

More classical techniques have been used to study spectra and angular distributions of (n, α) reactions on Al^{27} and Co^{59}, (Ref. 48) and P^{31}, S^{32}, and Ca^{40} (Refs. 49, 50), all with 14-MeV neutrons. Both energy spectra and angular distributions (Figs. 11–13) are consistent with an evaporative process provided one does not take into account a slightly excessive emission of higher energy alpha particles.

An extensive study of energy spectra of (n, α) reactions on light and medium weight elements has been performed by Saetta *et al.*[51] They have analyzed a number of spectra in terms of the statistical model using the Weisskopf–Ewing formula (1.3) derived in Sec. IA2. The maximum energy of integration in the denominator of (1.3) was computed from the bombarding energy ϵ_0, the values Q_n and the corresponding pairing energies δ_n for the particular reaction involved. The pairing energies were taken from the calculations of Cameron.[12] The other parameters involved in the analysis were as follows:

—the inverse cross sections σ_c^* were taken from Huizenga and Igo[9] for alpha particles, from Campbell *et al.*[51] for neutrons and from Shapiro[52] for protons, taking a nuclear radius of $1.6A^{\frac{1}{3}}$ F.

—the energy dependence of the level density was assumed to be a modified version of the high energy limit of the Fermi gas model [Eq. (1.8)].

$$\rho(E)\propto(E+t)^{-2}\exp[2(aE)^{\frac{1}{2}}], \qquad (1.29)$$

where t is the thermodynamic temperature defined in (1.4a) and (1.7).

Under the above assumptions the value of the level density parameter a was deduced employing the usual reduced spectra plots technique. This technique is based on the Weisskopf–Ewing formula (1.3), which gives the logarithm of the "reduced spectra" in simple pro-

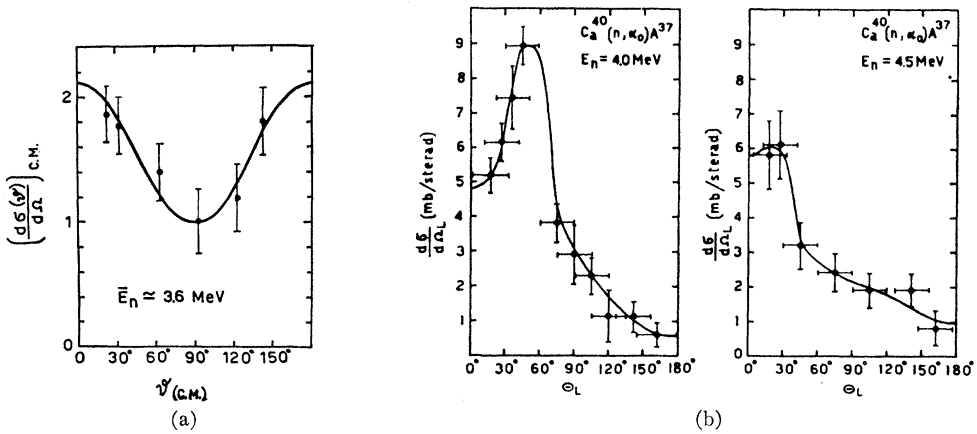

FIG. 8. (a) Angular distribution of alpha particles from the reaction $Ca^{40}(n, \alpha_0)Ar^{37}$ for the bombarding energy $\epsilon_0 = 3.6$ MeV (Ref. 39). (b) Angular distributions of alpha particles from the reaction $Ca^{40}(n, \alpha_0)Ar^{37}$ for bombarding energies $\epsilon_0 = 4.0$ MeV and 4.5 MeV, respectively (Ref. 40).

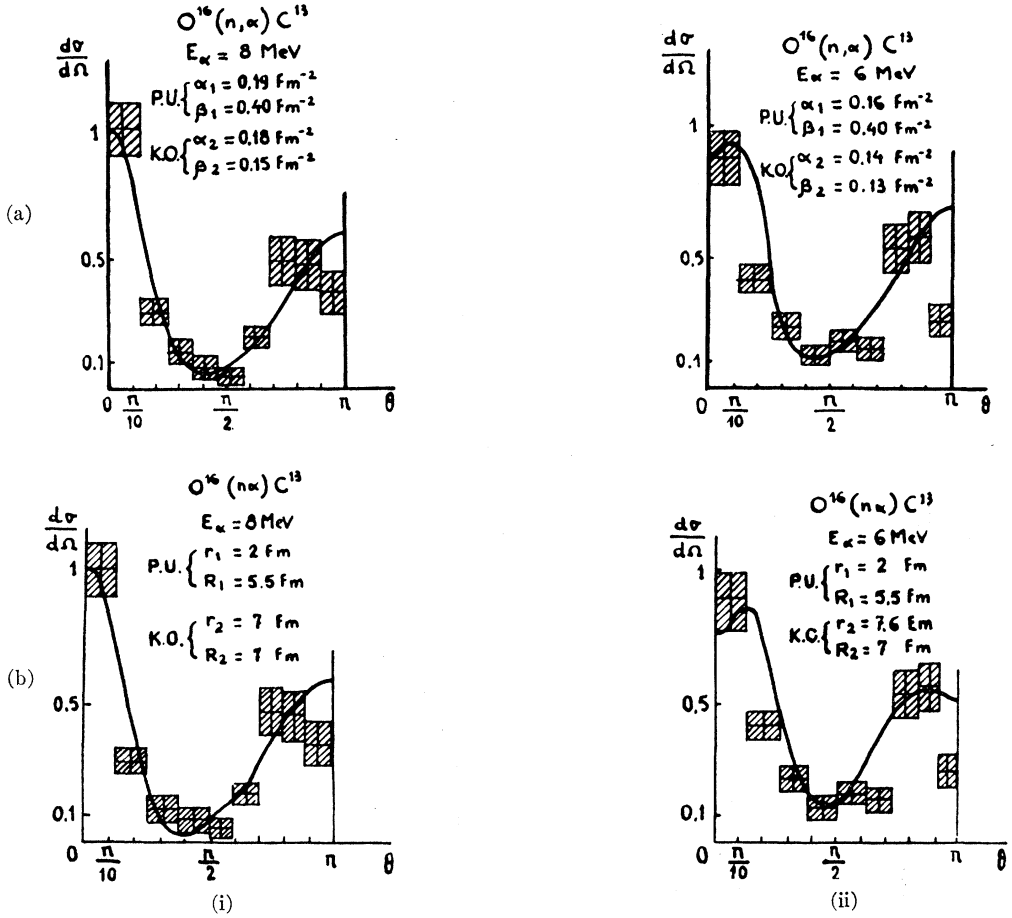

FIG. 9. (a) Angular distribution of alpha particles from the reaction $O^{16}(n, \alpha)C^{13}$ ($\epsilon_0 = 14$ MeV) with a zero range interaction potential for (i) alpha-particle energy $\epsilon = 8$ MeV; (ii) alpha-particle energy $\epsilon = 6$ MeV (Ref. 41). (b) Angular distribution of alpha particles from the reaction $O^{16}(n, \alpha)C^{13}$ ($\epsilon_0 = 14$ MeV) with a Gaussian interaction potential for (i) alpha-particle energy $\epsilon = 8$ MeV, (ii) alpha-particle energy $\epsilon = 6$ MeV (Ref. 41).

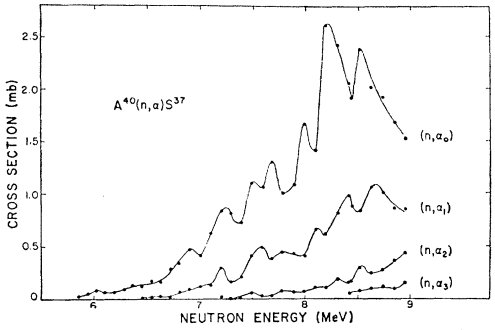

FIG. 10. Cross section for (n, α) disintegrations of Ar^{40}, leaving S^{37} in its ground and three lowest excited states; $\epsilon_0 = 14$ MeV (Ref. 47).

portionality to the level density exponential dependence:

$$N(\epsilon)\, d\epsilon \propto \sigma(\epsilon)\, d\epsilon \propto \sigma_c^*(\epsilon)\rho(E)\, d\epsilon,$$

hence

$$\ln \rho(E) \propto \ln [N(\epsilon)/\epsilon\sigma_c^*(\epsilon)]. \qquad (1.30)$$

The quantity $N(\epsilon)/\epsilon\sigma_c^*(\epsilon)$ is often called the reduced spectrum. If the assumption of the level density as given by (1.29) holds the plots of

$$\ln\left[\frac{N(t)}{\epsilon\sigma_c^*(\epsilon)}\,(E+t)^2\right] \text{ vs } E^{\frac{1}{2}} \qquad (1.31)$$

should be represented by straight lines as shown in Fig. 14. The slope of this line gives the value of the level density parameter a. The values of a obtained in this way are shown in Fig. 15 together with the values obtained from the analysis of slow neutron resonances.

TABLE I. The a value used for various nuclei in excitation function calculations compared to values deduced from the spectra (a_s) and slow neutron resonances (a_D).

Residual nucleus	N	a $(\text{MeV})^{-1}$	a $(\text{MeV})^{-1}$	a $(\text{MeV})^{-1}$
Na^{24}	13	4.9		5.5
Al^{27}	13	4.9		
Mg^{27}	15	4.9		
Al^{28}	15	4.6		4.5
P^{31}	16	5		
Si^{31}	17	5		
K^{42}	23	7		
Sc^{45}	24	7		
Ca^{45}	25	7		
Mn^{56}	31	9	8.3	8.6–10
Co^{60}	32	9		
Fe^{60}	33	9		
Ga^{72}	41	13	12.1	13
As^{75}	42	13		16.5
Ge^{75}	43	13		
As^{76}	43	13	12.8	
Br^{79}	44	12.6		
Se^{79}	45	12.6		
Sr^{89}	51	10.5		
Y^{90}	51	10	9.8	
Zr^{92}	52	11.8		
Nb^{93}	52	11.8		
Y^{92}	53	12.5		
Zr^{93}	53	12.5		

Several conclusions can be drawn from this analysis:

(1) The over-all agreement of statistical model calculations with α-particle spectra for nuclei $20 < A < 80$ is fairly good.

(2) The logarithms of the reduced spectra (1.30)

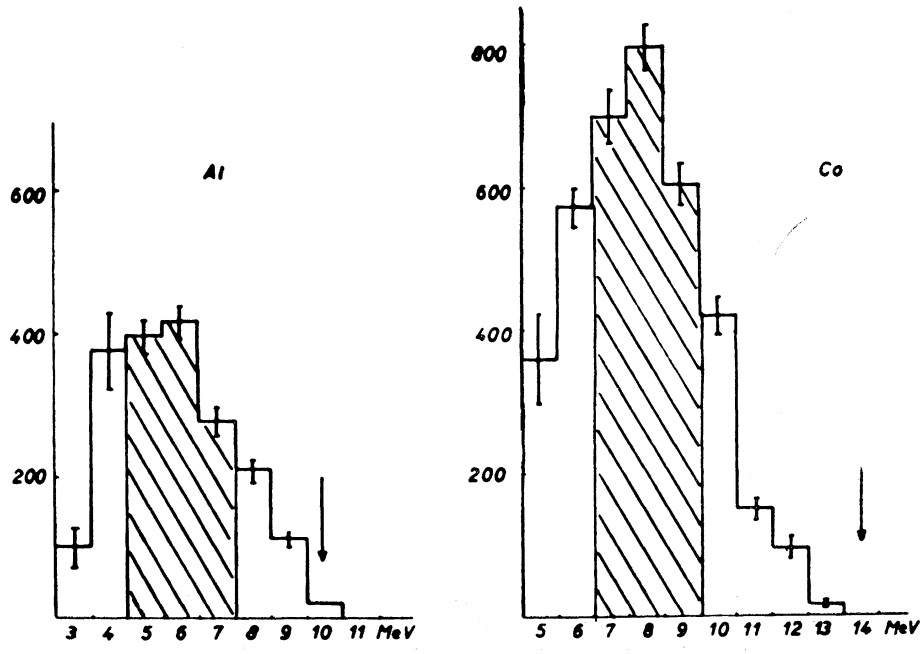

FIG. 11. Energy spectra of alpha particles from 14-MeV neutron bombardment of Al^{27} and Co^{59}. The arrows correspond to maximal energies calculated from Q values (Ref. 48).

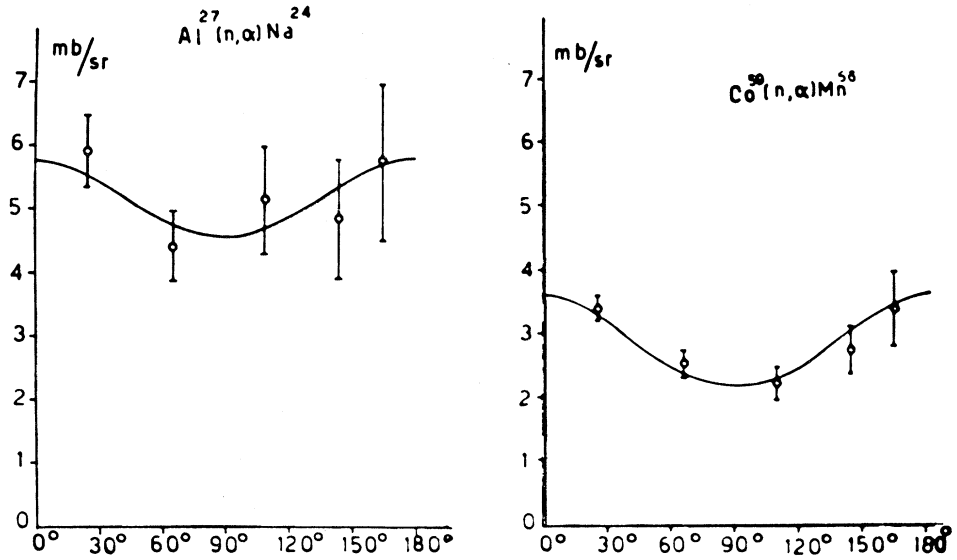

FIG. 12. Angular distribution of alpha particles from 14-MeV bombardment of Al^{27} and Co^{59} (experimental points and theoretical curves) (Ref. 48).

are linear with $E^{\frac{1}{2}}$ up to about 8 MeV; later, they curve up.

(3) The parameters a employed to obtain fits with experimental spectra are, globally speaking, linear with A and agree well with values obtained from other experiments (Table I).

Thus the over-all conclusion from this work is that the statistical theory, using the Fermi gas model for the level densities can account fairly well for the energy spectra of (n, α) reactions for lighter and medium weight nuclei.

Seebeck *et al.*[53] have done a thorough study of the reactions $Al^{27}(n, \alpha)Na^{24}$ and $Ni^{58}(n, \alpha)Fe^{55}$ using a pulse shape discrimination technique. The spectra of alpha particles emitted at 103° c.m. from Al^{27} and Ni^{58} bombarded with 14.1-MeV neutrons are shown in Fig. 16. While the spectrum of Al^{27}, besides a maximum at about 5 MeV, exhibits also some gross structure at higher energies, the spectrum from Ni^{58} has the typical evaporation shape, with a maximum at about 8 MeV. The angular distributions of all alpha particles from neutron bombardment of Al^{27} and Ni^{58} are shown in Fig. 17.

As these data, together with the existing experimental excitation functions, represent a complete set of data, it is instructive to discuss them in terms of the statistical model, in order to check whether this analy-

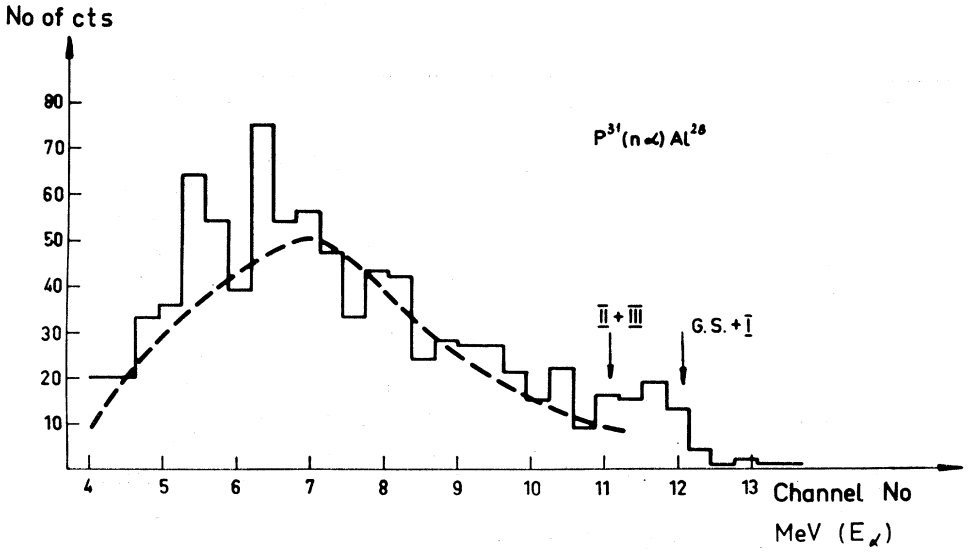

FIG. 13. Energy spectrum of alpha particles from 14.6-MeV neutron bombardment of P^{31} and evaporation calculation (Ref. 50).

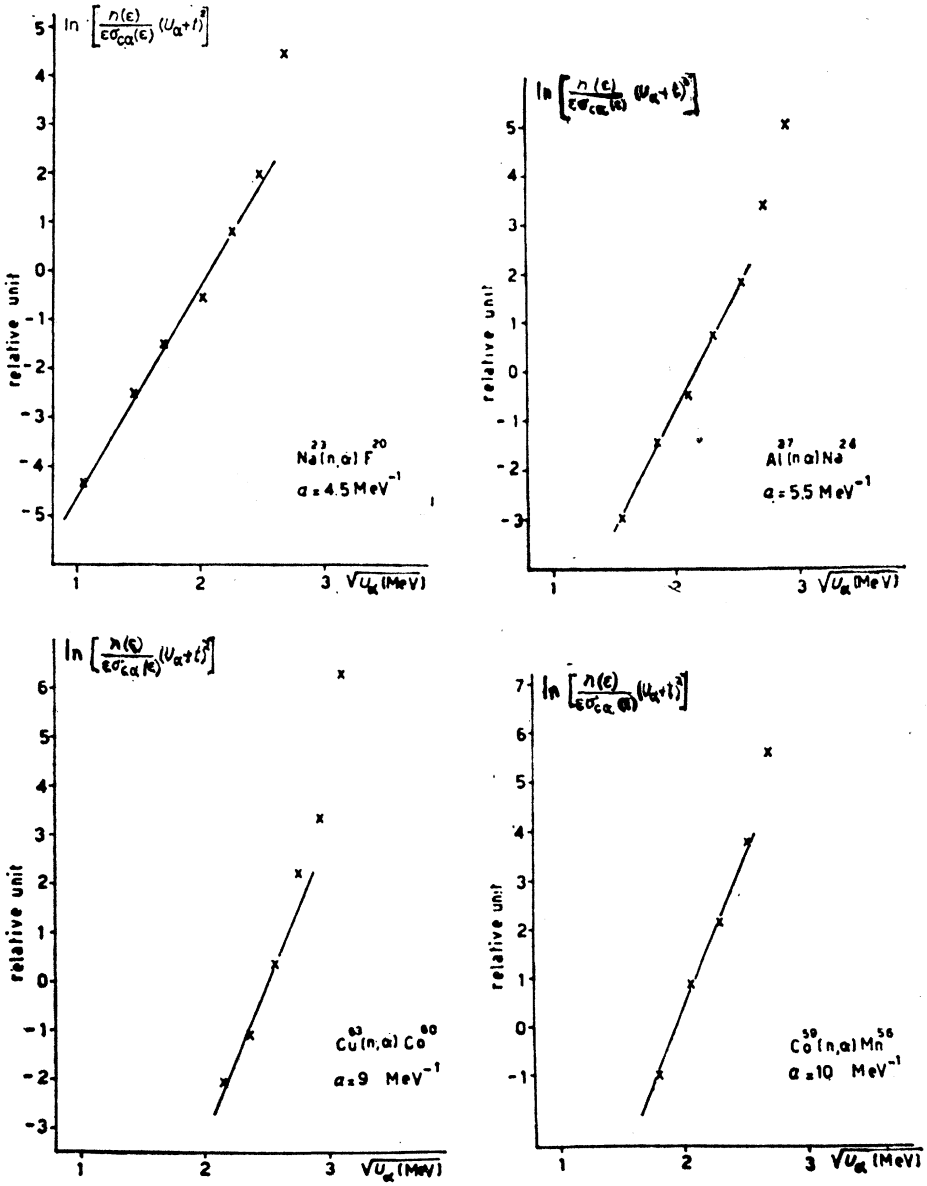

FIG. 14. Values of the parameter a from reduced spectra plots of (n, α) reactions at 14 MeV (Ref. 51).

sis is consistent in itself. Seebeck *et al.* have applied the analysis outlined in Sec. IA2 and given by Eq. (1.30) and (1.31) using for the energy dependence of the level density

$$\rho(E) \propto E^{-2} \exp\left[2(aE)^{\frac{1}{2}}\right] \tag{1.8}$$

instead of (1.29). Then the plot of the logarithm of the reduced spectra

$$\ln\left[N(\epsilon_\alpha)E^2/\sigma_c^*(\epsilon_\alpha)\epsilon_\alpha\right] \tag{1.31a}$$

plotted against $E^{\frac{1}{2}}$ should give a straight line with the slope equal to a. Actually, as one sees from Fig. 18, the experimental points for Al^{27} define a straight line on the average. The deviation from this line for high energy alpha particles can be due to several reasons, one of them being the fact that the level density at such low excitations of the residual nucleus cannot be fairly fitted with a continuous formula like Eq. (1.8). Figure 16 does, in fact, show individual groups in this region. For Ni^{58} most of the experimental points also define a straight line. There is a systematic deviation at higher excitations (above 8 MeV) which can be attributed to alpha particles from the reactions $Ni^{58}(n, n'\alpha)Fe^{54}$ and $Ni^{58}(n, \alpha n')Fe^{54}$. [$Q = -6.41$ as compared to $Q = +2.89$ for (n, α).]

Neglecting these deviations, the calculated average slope for the two cases considered are

$$a(Na^{24}) = (4.8 \pm 0.3)\ MeV^{-1}$$

$$a(Ni^{55}) = (7.0 \pm 0.4)\ MeV^{-1}.$$

This compares well to the values of Table I.

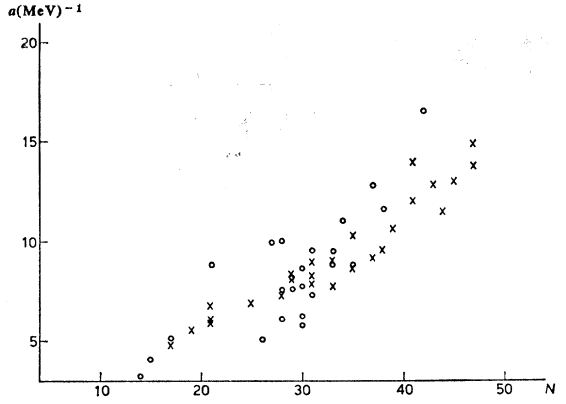

FIG. 15. Value of the level density parameter a obtained from slow neutron resonances (crosses) and from the statistical model analysis of (n, p), (n, n'), and (p, α) energy spectra (circles) plotted vs the neutron number N for $13<N<50$ (Ref. 51).

Using these values for the level density parameter a, one calculates the predicted shape of the energy spectra. The results are shown as dotted lines in Fig. 16 and as expected, appear to be quite satisfactory. Using the excitation energy of the product nucleus corresponding to the maximum of the spectra, and the above level density parameters, one obtains the nuclear temperature T

$$1/T=[d \ln \rho(E)/dE] \mid_{E=E\,(n_{max})}$$

equal to (1.52±0.15) MeV for Na^{24} and (1.39±0.14) MeV for Fe^{55}.

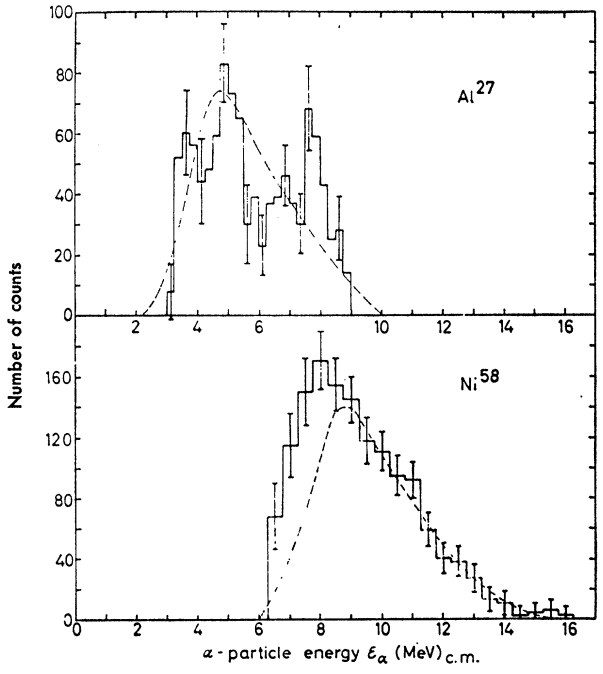

FIG. 16. Energy spectra of alpha particles from 14.1-MeV neutron bombardment of Al^{27} and Ni^{58}. Dotted lines are theoretical curves obtained from statistical model calculations (Ref. 53).

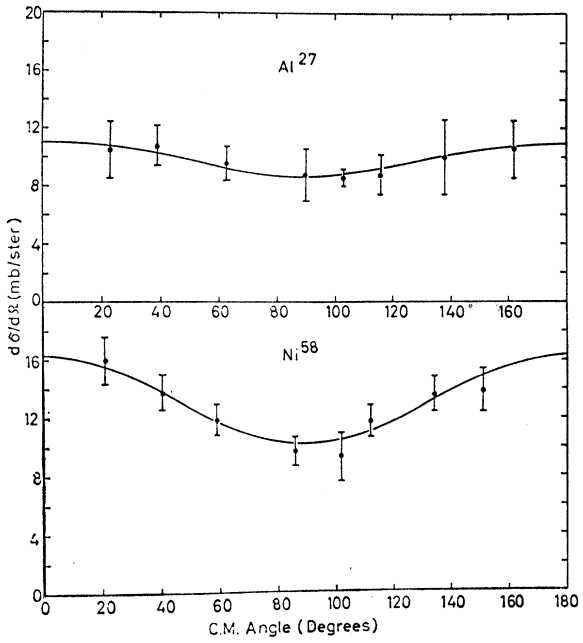

FIG. 17. Angular distribution of all alpha particles from 14.1-MeV neutron bombardment of Al^{27} and Ni^{58}. Dotted lines are theoretical curves obtained from statistical model calculations (Ref. 53).

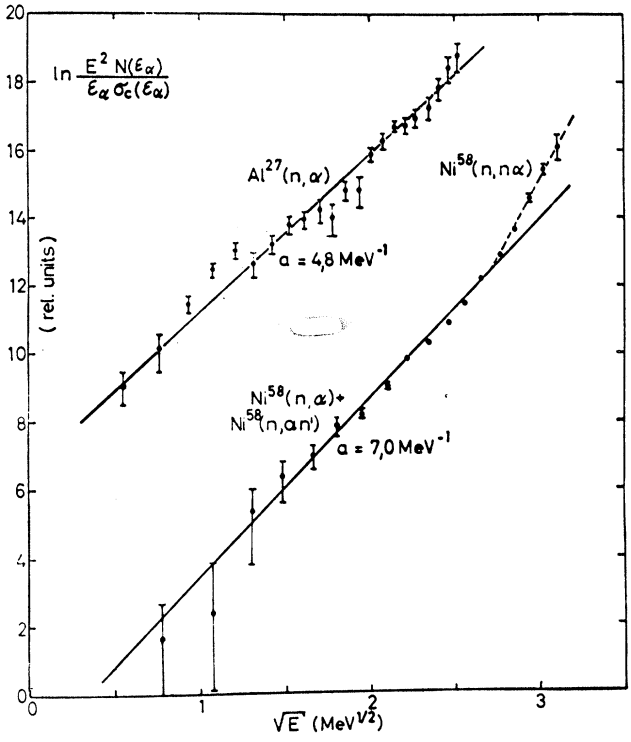

FIG. 18. Reduced spectra plots $\ln N(\epsilon) E^2/\epsilon\sigma_c^*(\epsilon)$ vs $E^{\frac{1}{2}}$ for alpha particles from 14.1-MeV neutron bombardment of Al^{27} and Ni^{58} (Ref. 53).

TABLE II. Values of parameters a obtained from 14-MeV (n, α) spectra in two different experiments. (Refs. 50 and 53).

Nucleus	a_{exp} $(MeV)^{-1}$	x in A/x (see text)
Na^{24}	4.5	5.4
Al^{28}	3.7	7.6
Si^{29}	4.0	7.2
Ar^{37}	3.5	10.5
Ni^{55}	7.0	7.8

The values obtained by Seebeck *et al.*[53] can be compared to those obtained by Turkiewicz *et al.*[50] on P^{31}, S^{32} and Ca^{40}, i.e., for the corresponding residual nuclei Al^{28}, Si^{29}, and Ar^{37}. The values are listed in Table II. Although the analyses have not been performed in an identical way [$(E+t)^{-2}$ instead of E^{-2} factor used in level densities] the agreement is satisfactory. This can be seen especially in the third column of Table II which requires some more comments. According to the Fermi gas theory the level density parameter a is proportional to the mass number A [Eq. (1.5)]. Hence the number x in Table II presents the factor of proportionality. Theoretically, the value of x depends only on the radius of nucleons. Taking this radius as $r_0=1.15$ one obtains $a=A/7.4$, i.e. $x=7.4$ in agreement with the values in Table II. The relative decrease of a in Ar^{37} ($x=10.5$) can be easily explained by the near magicity of this nucleus (smaller number of levels) while Na^{24} is probably on the lower limit of applicability of the statistical model.

According to Ericson[1] the angular distribution of particles evaporated from a compound nucleus is, in first order, given by

$$[d\sigma(\theta)/d\Omega]=1+(\bar{J}^2\bar{l}^2/12\sigma^4)P_2(\cos\theta) \quad (1.32)$$

provided the spin J of the compound nucleus and the orbital angular momentum l of the emitted particle are only weakly coupled. Thus, in first order, the zeroth-order isotropy has been corrected by an angle-dependent term including a Legendre polynomial $P_2(\cos\theta)$. The spin cutoff factor σ^2 defined by Eq. (1.4) is connected to the nuclear temperature T by

$$\sigma^2=(IT)/\hbar^2 \quad (1.33)$$

where I has been interpreted as the moment of inertia of the nucleus.

Fitting the experimental angular distributions in Fig. 17 by the above formula with a calculated value of 105 and 108 for the product $\bar{J}^2\bar{l}^2$ for Al and Ni, respectively, leads to the following spin cutoff parameters

$$\sigma=2.6^{+1.0}_{-0.4} \quad \text{for } Na^{24}$$

and

$$\sigma=2.2^{+0.4}_{-0.2} \quad \text{for } Fe^{55}.$$

The values of statistical parameters a, σ, and T obtained by Seebeck *et al.* are in agreement with similar results for several neighboring nuclei and with the systematic trend of these parameters throughout the periodic table. This is worthwhile to point out since these analyses, especially those of angular distributions are not always mutually consistent, as can be illustrated by the case of the reaction $Al^{27}(n, \alpha)Na^{24}$.

This reaction has been studied with particular thoroughness by many authors (and for obvious reasons). To about 30 determinations of the cross section added now are about half a dozen of angular distributions and energy spectra measurements.[48,53–58] Not all of these measurements and the respective analyses are mutually consistent. While energy spectra show a more or less consistent shape (see Figs. 11 and 16), the angular distributions vary from nearly isotropic[48,53,54] to strongly curved, with a deep minimum around 90°.[55–57] As we have already seen the angular distribution in the evaporation model is connected to the so-called spin cutoff factor by the expression (1.32),[1] which can be calculated accordingly. A more isotropic distribution will give rise to a larger value of σ^2 [smaller angular-dependent term in (1.32)]. In fact, Patzak *et al.*[46] Cindro *et al.*,[54] Jarwis *et al.*,[57] and Seebeck *et al.*[53] give values of

$$2\sigma^2=13,\ 15,\ 16,\ \text{and } 14,$$

respectively, while Irfan *et al.*[56] obtain

$$2\sigma^2=5$$

in accordance with the result of Csikai *et al.*[57] and earlier results of Kumabe[50] of $2\sigma^2<5$. Turkiewicz[50] reports a value of $2\sigma^2=7$ for the residual nucleus Al^{28}. Thus even this reaction, at first glance very well studied and understood, does not lend itself to a straightforward interpretation. One important point that can be made that there is little doubt of the evaporation nature of the process of the (n, α) reaction on Al^{27}. The same conclusion has been drawn by Debertin *et al.*[60] for (n, p) reactions on the same element. Although some ambiguity remains as to the exact value of some parameters it can be concluded from the preceding section that there is little doubt that the statistical process is the main contributing mechanism to fast neutron induced reactions in this region of nuclei.

The improved experimental technique in measuring neutron spectra (use of nanosecond system) and the availability of high flux monoenergetic fast-neutron beams from Van de Graaff accelerators has resulted in a number of extensive measurements of inelastic neutron spectra in the region of intermediate and heavy elements. Since most of these measurements treat both medium and heavy elements, we shall present all the results in this section.

Papers by Thomson,[61] Huber *et al.*,[62] Buccino *et al.*,[63] Seth *et al.*,[64] and Wilenzick *et al.*[65] give an extensive review of the neutron inelastic scattering on several energies and many nuclei. The results have been ana-

lyzed with the aim of establishing the reaction mechanism and obtaining the related parameters. As most of the results are concordant in singling out the statistical process as the predominant mechanism, the usual procedure of plotting the logarithm of the reduced spectra has been applied in order to obtain the energy dependence of the level density.

The data of Thomson[61] comprise energy spectra of more than 20 elements from Al to Pb at an incident energy of 7 MeV while some spectra and angular distributions have been taken at 4, 5, and 6 MeV, respectively. The data of Seth *et al.*[64] and Wilenzick *et al.*[63] contain measurements of spectra and angular distributions of 6-MeV neutrons in the energy region of 0.5–4 MeV (scattered neutrons). As these results are rather complementary, we discuss them together.

The spectra obtained by Thomson[61] were analyzed in terms of an incomplete Fermi gas model and the exponential (constant temperature) model of level densities:

$$\rho(E) \propto \exp\left[2(a'E)^{\frac{1}{2}}\right] \quad \text{and} \quad \rho(E) \propto \exp\,(E/T).$$

The pre-exponential E-dependent factor ($E^{-\frac{5}{4}}$ or E^{-2}) in the Fermi gas model has not been included. Actually, Thomas reports that the inclusion of the latter showed no noticeable influence on the shape of the spectra, contrary to the experience of several other investigations. For this reason the comparison of Thomson's data to other data is not always straightforward since the a's corresponding to the Fermi gas model are introduced in an indirect way. Some of the reduced spectra plots of Ref. 61 are shown in Figs. 19 and 20. The reduced spectra here mean only the log of $N(\epsilon)/\epsilon$, since the inverse cross sections have been assumed constant.

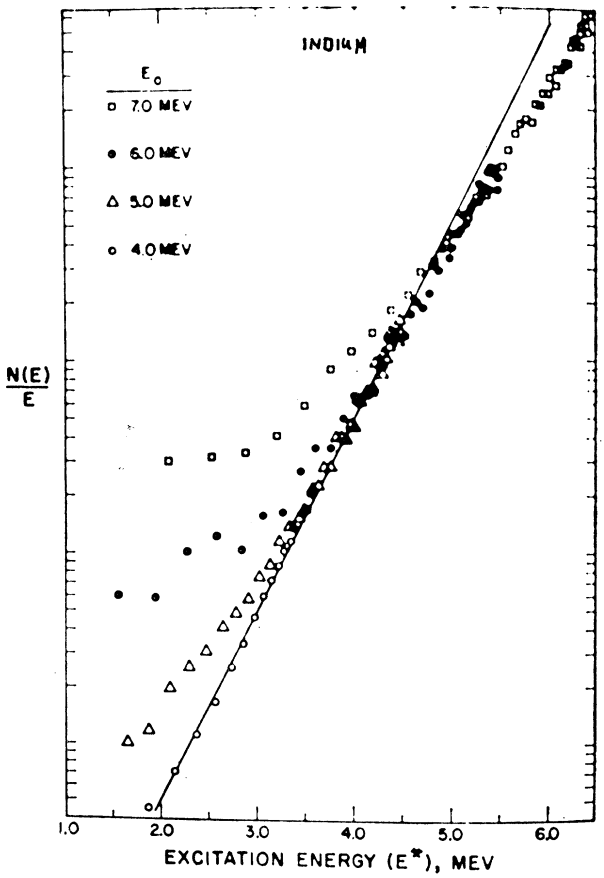

FIG. 19. Plots of $\ln N(\epsilon)/\epsilon$ vs excitation energy E for neutrons scattered inelastically by indium (Ref. 61).

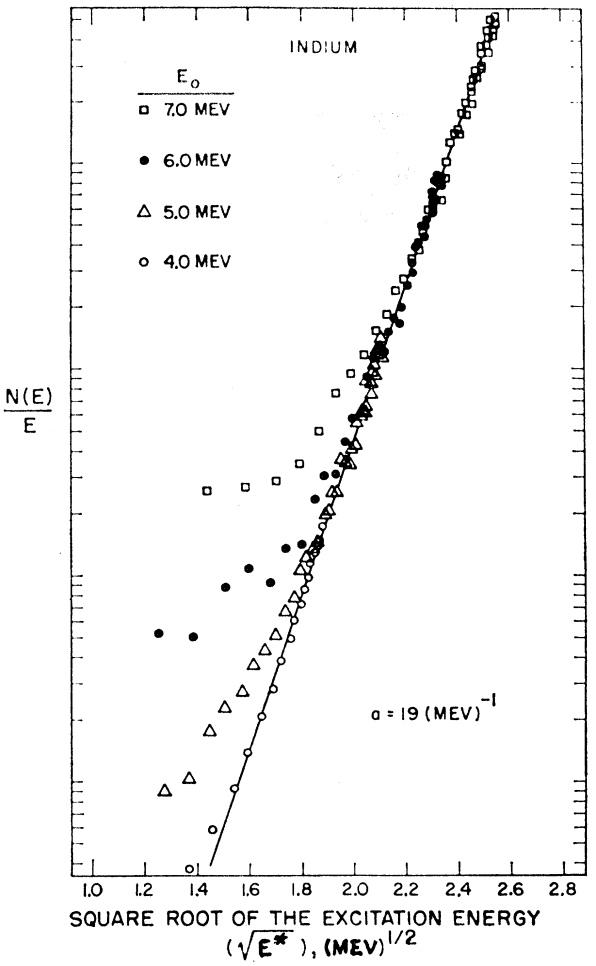

FIG. 20. Plots of $\ln N(\epsilon)/\epsilon$ vs the square root of the excitation energy, $E^{\frac{1}{2}}$, for neutrons scattered inelastically by indium (Ref. 61).

No clear statement in favor of either of the two models employed $\{\exp[2(a'E)^{\frac{1}{2}}]$ vs $\exp\,(E/T)\}$ could be obtained from Ref. 61. The constant temperature model fits the reduced spectra curves for several elements (Fe, Tl, Bi) and so does the exponential model (In). The experimentally obtained values for the nuclear temperature T increase with the bombarding energy, while the reduced spectra plotted vs $E^{\frac{1}{2}}$ give the same value of the parameters a' for all bombarding

TABLE III. Level density parameters obtained from inelastic neutron scattering (Ref. 61). The meaning of the different values for a is explained in the text.

Element	(MeV)	T (MeV)	a' (MeV^{-1})	a (MeV^{-1})	a_p' (MeV^{-1})	a_p (MeV^{-1})
Al	7.0	0.96±0.15	5.5	10.5	3.2	8.7
V	7.0	0.90±0.09	6.4	11.7	4.6	10.1
Mn	7.0	1.00±0.10	5.0	9.8	3.7	8.8
Fe	7.0	0.95±0.06	5.7	10.7	2.6	8.5
Cu	7.0	0.79±0.06	8.7	14.6	6.4	12.4
Cu	5.0	0.72±0.07	6.9	13.5	4.1	11.5
As	7.0	0.67±0.06	12.6	19.3	9.3	16.3
Se	7.0	0.62±0.05	15.0	22.1	8.0	15.7
Sr	7.0	0.80±0.08	8.4	14.2	4.6	11.0
Nb	7.0	0.59±0.03	16.7	24.2	14.9	22.5
Nb	6.0	0.49±0.05	20.9	29.9	18.3	27.4
Nb	5.0	0.48±0.05	17.5	26.2	14.8	24.3
Nb	4.0	0.33±0.03	30.7	44.0	24.9	38.6
In	7.0	0.56±0.02	18.8	26.2	14.6	22.7
In	6.0	0.52±0.03	18.3	26.8	13.6	22.4
In	5.0	0.48±0.04	17.6	26.9	11.9	21.7
In	4.0	0.40±0.03	20.0	31.3	11.9	24.0
Sb	7.0	0.58±0.05	17.4	24.9	13.5	21.3
Sb	4.0	0.40±0.04	20.0	31.3	12.0	24.1
I	7.0	0.60±0.05	16.1	23.5	12.8	20.3
I	4.0	0.41±0.04	18.9	29.9	11.8	23.6
La	7.0	0.68±0.06	12.2	18.8	11.0	17.7
La	5.0	0.69±0.07	7.6	14.5	6.5	13.6
La	4.0	0.65±0.07	6.4	14.0	5.1	13.1
Ce	7.0	0.60±0.06	16.2	23.5	11.3	18.9
Ce	5.0	0.60±0.07	10.6	18.3	5.7	14.3
Ta	7.0	0.52±0.04	22.1	30.4	18.5	27.0
W	7.0	0.50±0.05	24.0	32.6	15.4	24.5
Au	7.0	0.60±0.06	16.1	23.5	14.4	21.9
Au	4.0	0.47±0.04	13.9	23.7	11.1	21.2
Tl	7.0	0.78±0.06	8.9	15.0	8.1	14.0
Tl	6.0	0.80±0.05	6.9	12.8	6.1	12.1
Tl	5.0	0.81±0.05	5.2	11.3	4.4	10.7
Tl	4.0	0.76±0.05	4.3	11.2	3.4	10.7
Bi	7.0	1.05±0.07	4.5	9.1	3.7	8.5
Bi	5.0	0.68±0.09	7.9	14.9	6.1	13.4
Pb^{206}	7.0	0.92±0.09	6.1	11.2	4.5	9.9

energies. The constant temperature model predicts a faster increase of the level densities with excitation and it has sometimes been interpreted as a sign of a second-order phase transition or "melting" of the nucleus.

The variation of the parameters a and T with the mass number A is shown in Table III. In the column labeled T the value of the nuclear temperature is given. The values a' (fourth column) have been calculated from the relation

$$a'=E_{Av}/T^2, \tag{1.34}$$

where the average excitation has been calculated from the evaporation model as

$$E_{Av}=\epsilon_{inc}-2T. \tag{1.35}$$

The values of a' calculated in this way (1.34) correspond to the incomplete Fermi gas model $\{\rho(E)\propto \exp[2(a'E)^{\frac{1}{2}}]\}$. If, instead, one takes the high-energy limit of the Fermi gas model

$$\rho(E)\propto E^{-2}\exp[2(aE)^{\frac{1}{2}}] \tag{1.8}$$

the relation (1.34) takes the form

$$a=E_{Av}(1/T+2/E_{Av})^2. \tag{1.34a}$$

The values of a are listed in column 5 of Table III. The average values are:

$$a'=A/10.9$$

$$a=A/7.2. \tag{1.36}$$

As mentioned earlier the theoretical value predicted by the Fermi gas model is $A/7.4$ for a nucleon radius $r_0=1.15$ F. A similar result has been obtained also for

(n, α) spectra, speaking of the reliability of the Fermi gas model.

The reduced spectra analysis of inelastic scattering of 6-MeV neutrons from many nuclei has been performed by Seth *et al.*[64] using, however, optical model values for the inverse cross section σ_c*. After having established that the sets of values σ_c* obtained from the volume local optical potential and the nonlocal optical potential of Perey *et al.*,[66] do not differ appreciably, Seth *et al.* compare the experimental reduced spectra to several forms of level densities:

$$\rho(E) \propto (E+t)^{-n} \exp\left[2(aE)^{\frac{1}{2}}\right] \qquad n=\tfrac{5}{4}, 2 \qquad (1.36a)$$

$$\rho(E) \propto \exp\left[E/\langle t\rangle\right] \quad \text{or} \quad \exp\left[-\epsilon/T\right], \qquad (1.36b)$$

where T is the nuclear temperature defined by (1.7). Equation (1.36a) derives from the Fermi gas model while (1.36b) is valid under the extreme supposition

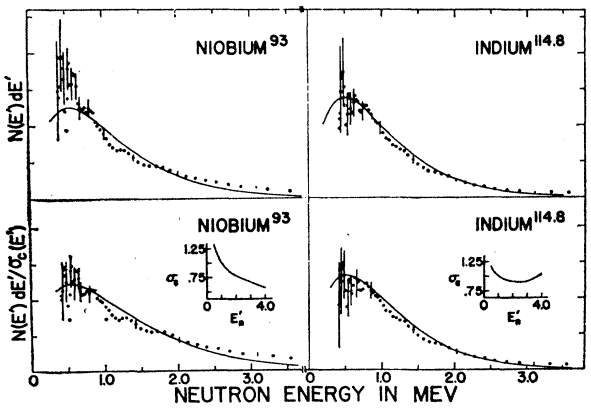

FIG. 21. Energy spectra of neutrons inelastically scattered by niobium and indium. Solid lines present the statistical fits assuming constant (upper figure) and optical model cross sections (lower figure). The little insert represents the optical model cross sections σ_c used in the calculation (Ref. 64).

of $\langle\epsilon\rangle \ll \epsilon_0$. a and T are related by Eq. (1.35). The inelastic scattering data in Ref. 64 are not too well fitted either by (1.36a) or (1.36b). (See Fig. 21.) Actually (1.36b) always fits the data somewhat better. The obtained temperatures are angle-dependent, which can be explained by the inclusion of 5–10% direct contribution at forward angles. (cf. Fig. 22). The temperatures also decrease monotonically from 1.22 MeV (Fe^{56}) to 0.55 MeV (U^{238}) as expected on general grounds, since in heavy nuclei the excitation energy is spread over a greater number of nucleons. The results are shown in Table IV.

It is of interest to compare the a values obtained by Seth,[64] listed in Table IV to those obtained by Thomson,[61] listed in Table III, although, as mentioned earlier, the comparison is not straightforward. In this respect we compare Thomson's a values in column 5 of Table III. The two last columns in Table III have been obtained by including the pairing effects[12] in calculat-

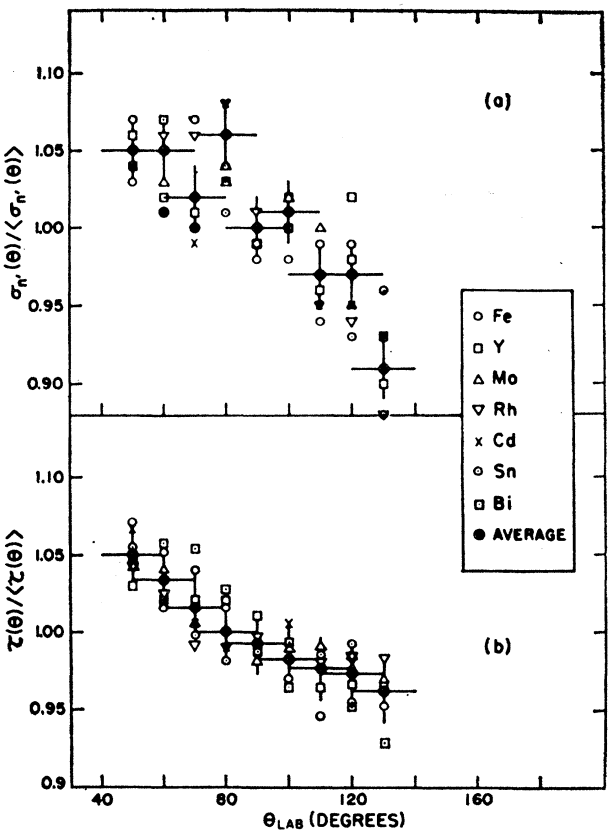

FIG. 22. Forward peaking in inelastic scattering of 6-MeV neutrons: (a) $\sigma_n(\theta)/\langle\sigma_n(\theta)\rangle$ and (b) $T(\theta)/\langle T(\theta)\rangle$ for several elements studied and their averages. The averages of differential cross sections $\langle\sigma_n(\theta)\rangle$ and nuclear temperatures $\langle T(\theta)\rangle$ have been performed for each element over all the studied angles (Refs. 64 and 65).

TABLE IV. Nuclear temperatures and Fermi gas coefficients for E_n=6 MeV (Ref. 64).

Element (at. weight)	T (MeV) ±10% using σ_c=const	T (MeV) ±10% using σ_c(opt. model)	a (MeV)$^{-1}$ ±20%, using σ_c(opt. model) δ_p=0
Fe (56)	0.87	1.22	2.4
Y (89)	0.56	0.66	10.9
Nb (93)	0.55	0.65	11.2
Rh (193)	0.54	0.64	11.7
Pd (106.4)	0.51	0.58	14.7
Ag (107.9)	0.54	0.60	13.6
Cd (112.4)	0.52	0.56	15.9
In (114.8)	0.49	0.51	19.2
Sn (118.7)	0.55	0.56	16.0
Te (127.6)	0.61	0.59	14.1
W (183.9)	0.46	0.46	23.8
Pt (195.1)	0.52	0.51	19.0
Au (197)	0.55	0.54	17.1
Hg (200.6)	0.62	0.58	14.7
Pb (207.2)	0.69	0.66	11.0

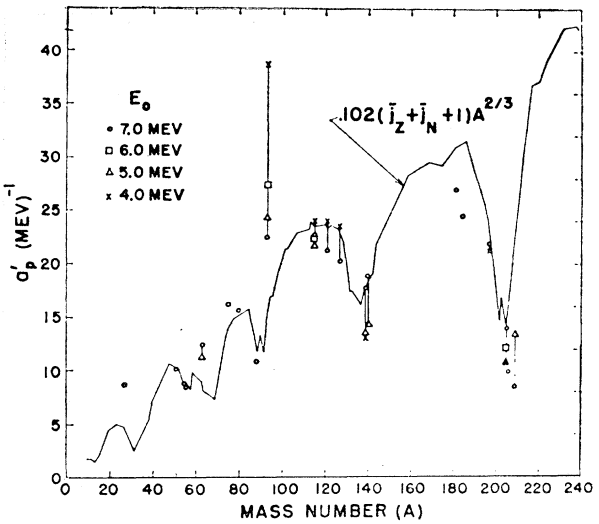

FIG. 23. The corrected level density coefficient a_p defined by the Fermi gas model (1.34a) with Cameron's pairing energy corrections[12] plotted vs mass number for each nucleus and neutron energy observed in Ref. 61. The solid line is a plot of (1.37), using Newton's value[67] for $\bar{\imath}_Z$ and $\bar{\imath}_N$ with $2\alpha=0.102$ (Ref. 61).

ing the excitation energies (see Sec. IA2). In the case of Thomson's results, this means expression

$$E_{Av}=\epsilon_0-2T+P(Z)+P(N) \qquad (1.35a)$$

replacing (1.35) in Eqs. (1.34) and (1.34a). Thus only the values in column 5 of Table III (Ref. 61) and the a values in the Table IV (Ref. 64) are suitable for comparison, since they use an approximately equal form for the energy dependence of the level density and no pairing corrections. Considerable differences can be found in absolute values, but the main trends are similar. The pairing-dependent a values of Thomson[61] (a_p) and Seth *et al.*[64] should be compared to the theoretical values given by Newton[67]

$$a=2\alpha(\bar{\jmath}_Z+\bar{\jmath}_N+1)A^{\frac{1}{3}}, \qquad (1.37)$$

where $\bar{\jmath}_Z$ and $\bar{\jmath}_N$ are defined as the effective values of proton and neutron angular momenta in the outermost shell of the nucleus.[67,68] A good fit for the values of Thomson[61] is achieved with $2\alpha=0.102$, (Fig. 23) while the same excellent agreement for Seth *et al.*[64] is obtained by using $2\alpha=0.075$. (Fig. 24). The difference is obviously due to the incomplete form of the energy dependence employed and to different values for the inverse cross sections. The theoretical value for the parameter 2α given by Lang[69] is

$$2\alpha=0.0784 \qquad (1.37a)$$

almost identical to the experimental value of Seth.[64] Although this identity should not be taken too seriously, alpha particle spectra obtained from 14-MeV neutron bombardment of Nb^{93} yield a value of $2\alpha=0.062$ close to the theoretical value.[70]

Further light on the shell dependence of the level densities in atomic nuclei has been shed by the investigations of Huber *et al.*[62] and Buccino *et al.*[63] Huber *et al.* have investigated the inelastic neutron energy spectra for 15 elements near and at closed shells. The bombarding energy was 14 MeV and the elements ranged from molybdenum to uranium. The analysis of the energy distribution $N(\epsilon)$ was carried out in the range of 0.5–4.7 MeV. The nuclear temperature T was obtained by using the Le Couteur formula,[71] which takes into account that at 14-MeV incident energy nuclei may emit more than one nucleon:

$$N(\epsilon)\propto\epsilon^{5/11}\exp[-12\epsilon/11T]\,d\epsilon \qquad (1.38)$$

for the number of neutrons emitted with energy ϵ. From the reduced spectra plots the nuclear temperatures T were obtained, the values of the level density parameters a calculated [using expression (1.34)]

$$a=E_{Av}/T^2 \qquad (1.39)$$

with E_{Av} calculated from (1.35a) with the inclusion of pairing effects. The a values are again well fitted by the Newton formula (1.37) with

$$2\alpha=0.065$$

close to the theoretical value of Lang[69] (Fig. 25).

Energy spectra of neutrons inelastically scattered by 23 medium and heavy nuclei at 90° have been reported by Buccino *et al.*[63] The bombarding energies were 4.0, 5.0, 6.0, and 6.5 MeV. Although it was not possible to distinguish unambiguously between the Fermi gas and constant temperature models, straight reduced spectra

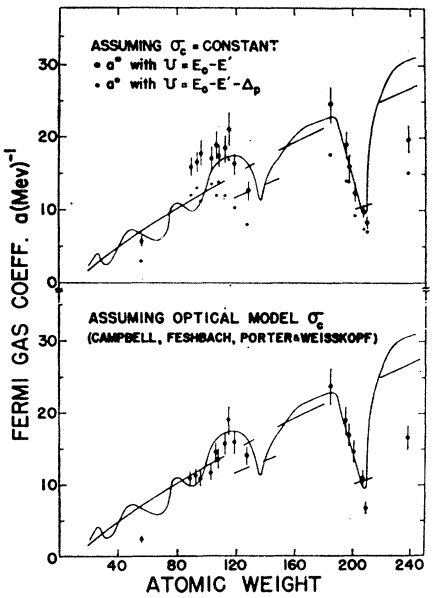

FIG. 24. Fermi gas coefficients determined under the assumptions: (i) σ_c=const, no pairing ($\delta_p=0$); (ii) σ_c=const, pairing included (upper picture); and (iii) σ_c=optical model, no pairing ($\delta_p=0$) (lower picture) (Ref. 64).

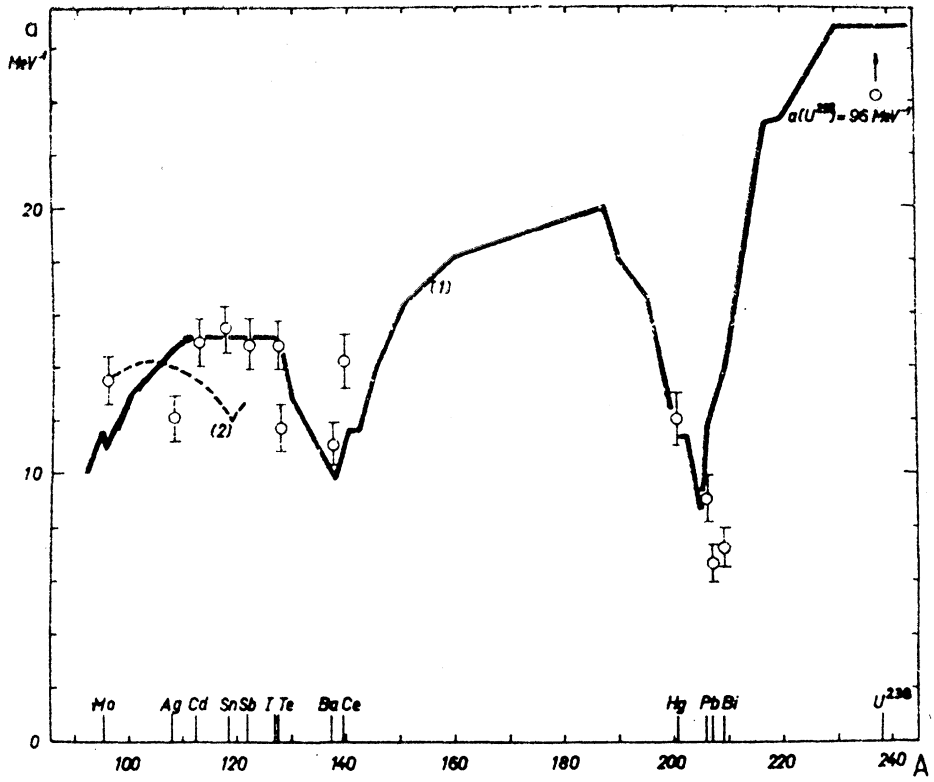

FIG. 25. Values of the level density parameter a derived in Ref. 62 (see text) compared to the Newton formula[67] with $2\alpha=0.065$ (Ref. 62).

plots vs $E^{\frac{1}{2}}$ have been obtained in all cases with the inclusion of the preexponential factor E^{-2} in the level density (cf. Fig. 26). The omission of E^{-2} leads to different values of a for different excitation energies. For nuclei between closed shells the value of a was independent of the bombarding energy, while for nuclei near or at shell closures of $N=82$ and 126 and $Z=82$, the nuclear temperatures were nearly constant over the range of excitations studied. In an overall picture, a general agreement between the experimentally determined values of a and the theoretical values was found, although the average increase of the level density coefficient with mass number A appears to be slower than predicted by a simplified equidistant model.

Results on angular distributions of inelastically scattered neutrons obtained by Thomson[61] (Fig. 27) and Wilenzick *et al.*[65] corroborate the results obtained from the analysis of the spectra. The angular distributions are either symmetric or show an unperceptible but systematic forward peaking, which is more clear if one takes the average of all elements at a given angle. A similar plot of relative nuclear temperatures shows the same behavior. (Fig. 22).

We have purposedly devoted much space to analyzing the neutron inelastic scattering data, since these data for several reasons (absence of Coulomb effects etc.) represent the most reliable source of information about the statistical model parameters, notably the level densities. It appears from the above discussion that the Fermi gas model is a solid base of our treatment of level densities. The use of more accurate expressions for level densities brings the value of the parameter a close to theoretical predictions, and the inclusion of shell and pairing effects accounts for the deviations from the average value. The ever present Fermi gas—constant temperature dilemma appears to be more due to the fact that *both* models satisfy, indicating that the evaporation picture is a better approximation than one would expect at first glance. Anyway as the Fermi gas model for level densities is based on more physical grounds (notably with the success of many-body calculations of nuclear spectra) it is our opinion that it should be used throughout in the analysis of spectra.

In all experiments discussed so far we have tacitly omitted angular momentum effects. At the same time, we have not accounted for the energy variation of the nuclear level density parameters a and T observed in some experiments.[72–74] This variation is a serious problem, since it may imply that the level density expressions chosen are not adequate to describe the actual level density over a wide range of energies. Bodansky[75] has reviewed some of the possible reasons for this variation:

(i) as the incident energy increases, there is an increasing probability of direct processes with a consequent hardening of the spectra;

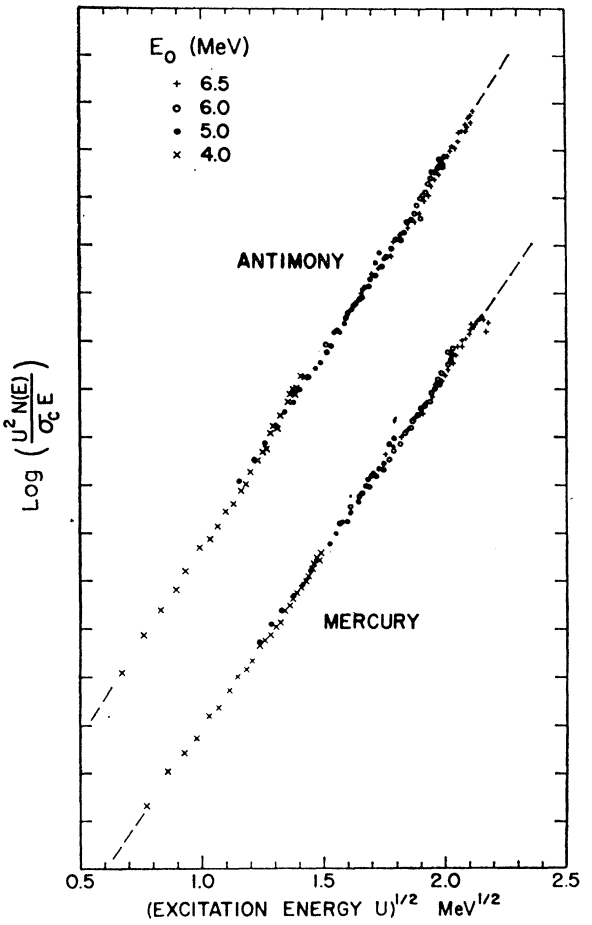

FIG. 26. Plots of $\ln N(\epsilon)E^2/\epsilon\sigma_c^*(\epsilon)$ vs $E^{\frac{1}{2}}$ for antimony and mercury. The dashed lines are drawn along the average slopes (Ref. 63).

(ii) since higher energies produce higher angular momenta in the compound nucleus, there may be an angular momentum effect producing the variation.

Although the first assumption is rather obvious, Thomas[76] has discussed this last possibility in terms of the Fermi gas model, using different degrees of approximation. In terms of the exact Fermi gas model, the number of levels with a given energy E and angular momentum J (level density) is given by Eq. (1.4) which for the high energy limit reduces to (1.8). According to Thomas[76] it is questionable whether this high energy limit is reached in most of the neutron experiments analyzed.

The rate of emission $R\,dE_f$ of a particle with a channel energy ϵ from a compound nucleus with an energy E_c and angular momentum J that leaves a residual nucleus with an energy E_f and angular momentum j is given by

$$R(E_f,j)\,dE_f=h^{-1}[\Omega(E_f,j)/\Omega(E_c,j)] \times \sum_{s=|j-s|}^{j+s}\sum_{l=|J-s|}^{l=J+s} T_l\,dE_f, \quad (1.40)$$

where S is the channel spin $S=s+j$, and T are the penetrabilities of the emitted particle [cf. Eq. (1.13)]. The spectrum of the emitted particles is then obtained by summing over all j and averaging over J.

Several approximations to this formula are possible:

(1) For an infinite moment of inertia ($c\hbar^2=\infty$) the level density is proportional to $(2J+1)$. Carrying out the summation in (1.40) one obtains:

$$R(E_f)\propto\frac{\epsilon\sigma_c^*\exp[2(aE_f)^{\frac{1}{2}}]}{(E_f+t_f)^{-\frac{5}{4}}T^{\frac{3}{2}}} \quad (1.40a)$$

which for high excitations reduces to

$$R(E_f)\propto\frac{\epsilon\sigma_i^*\exp[2(aE_f)^{\frac{1}{2}}]}{E^2} \quad (1.40b)$$

in accordance with the preceding discussion. Formula (1.40b) is the familiar evaporation formula.

(2) We arrive at a similar result assuming that only S-wave neutrons are emitted, i.e., that

$$T=1 \quad \text{for} \quad l=0$$
$$T=0 \quad \text{for} \quad l\neq 0.$$

Thus the expressions (1.40a) and (1.40b) hold, strictly

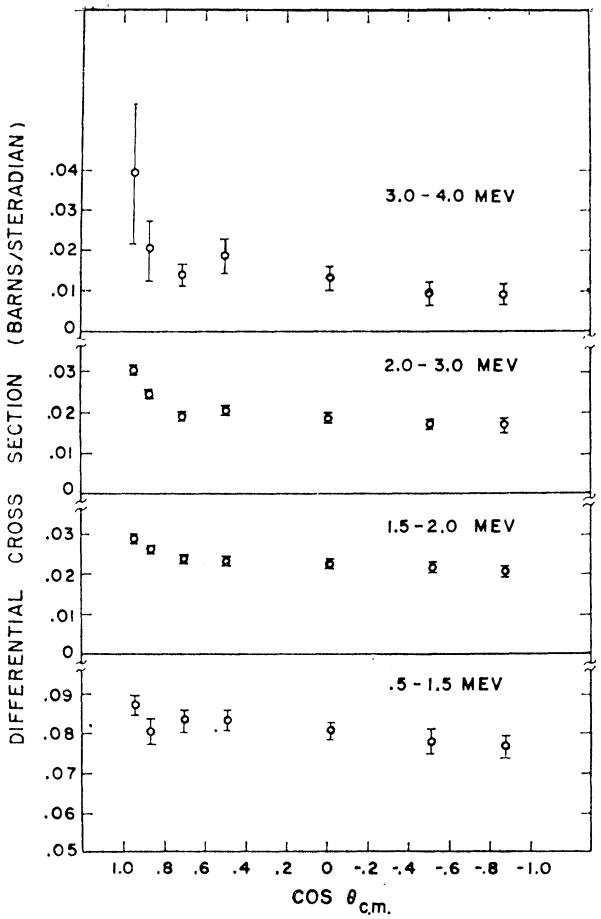

FIG. 27. Angular distributions for inelastic scattering of 5-MeV neutrons from indium (Ref. 61).

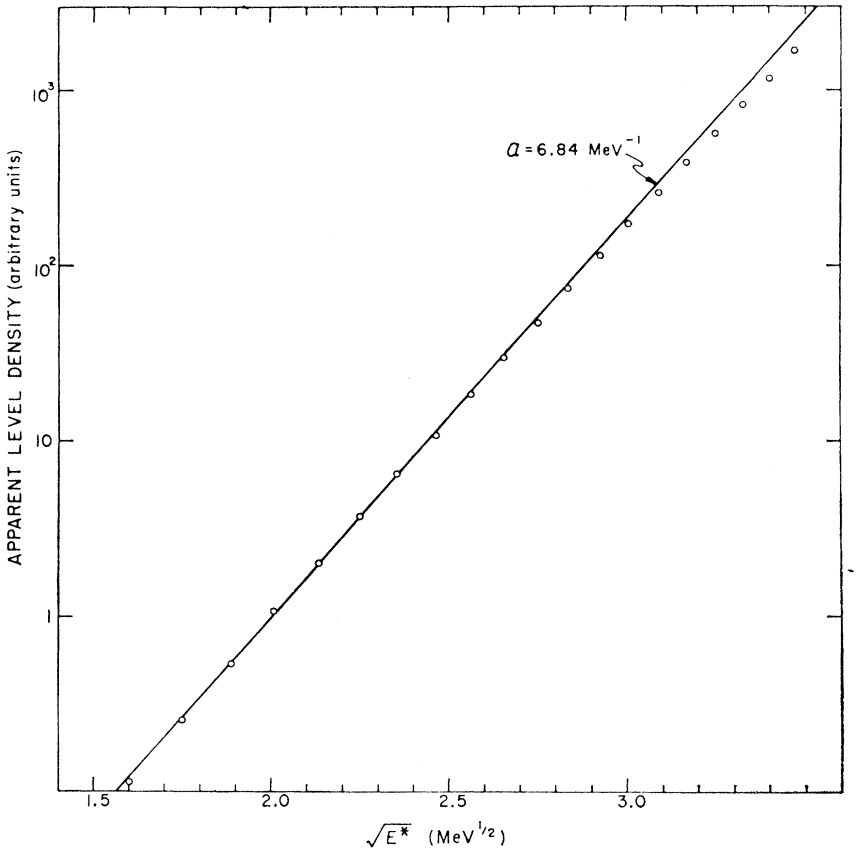

FIG. 28. Apparent level density plot based on the analysis of a calculated evaporating spectrum. The compound nucleus is taken to be Mn^{55} formed by irradiation of V^{51} with 16-MeV alpha particles. For this analysis it has been assumed that the level density is proportional to E^{-2} exp $[2(aE)^{\frac{1}{2}}]$ (Ref. 76).

speaking, only when either (1) the spin cutoff factor $2\sigma^2$ becomes infinite or (2) when only S-wave neutrons are emitted. It is thus possible that the energy variation of the level density parameter a observed when analyzing experimental spectra by the use of (1.40a) or (1.40b) can be connected to angular momentum effects.

To test this assumption Thomas has calculated several theoretical neutron evaporation spectra using the correct formula (1.40) summed over the final angular momenta and averaged over initial angular momenta. The assumed level density was (1.4) and (1.4a). The *same* value of a was used for different bombarding energies.

Afterwards, each calculated spectrum was analyzed, as if it were an experimental one, in terms of the expression (1.40b) to derive an apparent value of a. The result of an analysis of this kind is shown in Fig. 28.

If the supposition on the influence of angular momentum effects on the energy variation of a was correct, one should get the same variation of a with ϵ_{bomb} as in the experimental work. However, *no variation of a with* ϵ_{bomb} has been observed in the range of ϵ_{bomb} 12–20 MeV (for incident alpha particles). However, the a values obtained were about 40% higher than the input a values. Hence, angular momentum effects could not be responsible for the energy variation of a. The value of a obtained from the "experiments" was, however, considerably larger than the one from the Fermi gas model partly for angular momentum effects ($\doteq 50\%$) and partly because of the inadequacy of the expression (1.4) for the actual level density ($\doteq 50\%$).

These results are corroborated also by the analysis of Hurwitz *et al.*[77]

3. *Heavy Elements* ($A > 100$)

Except for neutron inelastic scattering, most of which has been analyzed in the preceding section, results of neutron induced reactions in this region are still scarce and no systematic search has been done so far. It is characteristic of this region of nuclei that the predominant part of the cross section for charged particle production is composed of nonequilibrium (direct) processes, due to the regulating effect of the Coulomb barrier.

The difference between direct and equilibrium processes is that the former are single-stage processes while the latter are multistage ones. Thus the energy and momentum transfer to the reaction product in the case of direct interactions is large, giving rise to particles with energies close to the maximum possible; on the contrary, statistical processes will favor the emission of lower energy particles. The Coulomb barrier, which for nuclei of $A = 100$ is about 10 MeV for protons and deuterons and the double of this value for α particles

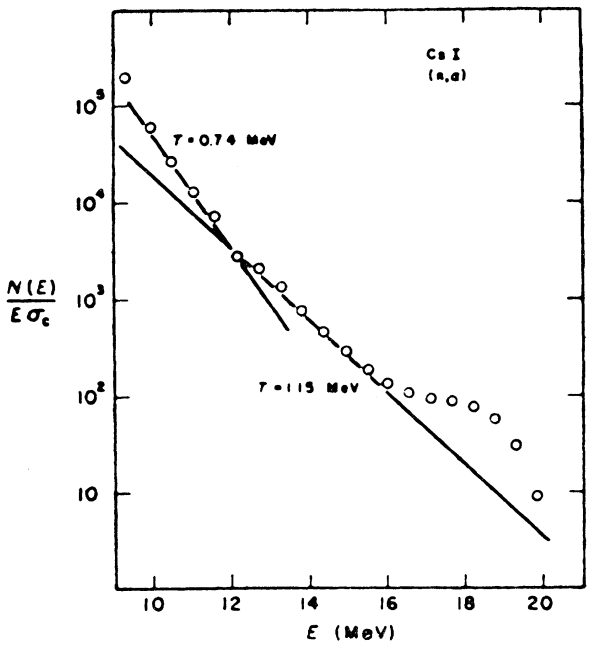

FIG. 29. Reduced spectra of protons from 14-MeV bombardment of CsI (Ref. 78).

prevents the emission of all low energy charged particles, thus inhibiting more strongly the charged products of statistical decay.

The prevalence of direct interaction products should be seen also in the spectra and angular distributions of charged particles emitted from heavy nuclei. Dixon[78] using the pulse-shape discrimination method has measured spectra of protons, deuterons and alpha particles from 14-MeV bombardment of a CsI crystal. It has been noted that Cs^{133} and I^{127} are close in mass number and $Q_{n,\text{charged part}}$ values and that both are odd Z–even N nuclei. Thus it is expected that their spectra are similar and it is meaningful to speak about the spectrum of CsI.

The reduced spectra plot vs the particle energy for protons from 14-MeV bombardment of CsI is shown in Fig. 29. No single straight line could be drawn, and the curve itself can be broken into three sections. The low-energy section, corresponding presumably to admixtures of the reaction (n, np) is characterized by a low nuclear temperature ($T=0.74$ MeV), which corresponds to the low residual excitation of a nucleus after the emission of the fast particle. The medium and higher energy part correspond presumably to prevalently compound and direct processes. The above division gives about $\frac{1}{3}$ statistical and $\frac{2}{3}$ direct emission of protons, as exhibited in Fig. 30, where a possible decomposition of the proton spectrum is shown. As already noted in Sec. IA4 the shape of the spectra for volume direct and statistical processes are rather similar, the main difference being in the shifting of direct spectra toward higher energies. As mentioned, the theory of Brown *et al.*,[22] gives the following expression for the energy spectrum of volume direct reactions:

$$N(\epsilon)=b_1(\epsilon_{\max}-\epsilon)+b_2(\epsilon_{\max}-\epsilon)^2+b_3(\epsilon_{\max}-\epsilon)^3+\cdots, \tag{1.15}$$

where $\epsilon_{\max}$ is the maximum energy transfer. For 14-MeV neutrons a potential well of 40 MeV and a Fermi energy of 33.6 MeV, the ratios b_2/b_1 and b_3/b_1 have been calculated to be 10^{-2} and 10^{-4}, respectively. The volume direct interaction spectrum should be in essence linear in energy and its peak should come at higher energies, as shown in Fig. 30.

The same experiment as the one discussed above[78] has been performed independently by Robertson[79] who, in addition gives also total cross sections (see Sec. IC3). Also, similar results have been obtained by Hans *et al.*[80] by a telescopic method. These authors measured the spectra for $In^{115}(n, p)$ and $Au^{197}(n, p)$. The experimental results agree fairly well with a calculated compound nucleus+volume direct interaction energy distribution.

(n, α) reactions on heavy elements have a very small cross section. Thus their experimental investigation is rather difficult. The first extensive search of spectra of these reactions on heavy elements has been performed by Marcazzan *et al.*[44] They used the experimental fact that (n, α) reactions on heavy elements have a highly positive Q value, while the Coulomb barrier prevents the emission of alpha particles below 12 MeV. Thus a simple method of sticking the targets to a silicon counter (Q_n in $Si^{28}=-2.8$ MeV) has been used to obtain forward and backward spectra. Some of their results are shown in Fig. 31. A clearly direct mechanism for these reactions has been inferred from the rather large forward to backward ratio in the angular distributions.

The same method was used by Cuzsocrea *et al.*[81] to measure alpha-particle spectra from molybdenum isotopes up to several MeV of excitation. (Bombarding energy $\epsilon_n=15$ MeV.) The results obtained suggest also a direct process. Where it was possible, the ground-state transition has been separated and the relative

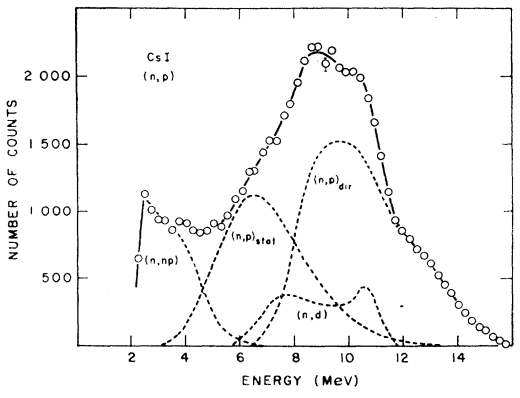

FIG. 30. Full curve: experimental distribution of protons and deuterons from 14-MeV neutron-induced reactions in CsI. Dashed curves: a possible decomposition into four components, as described in the text (Ref. 78).

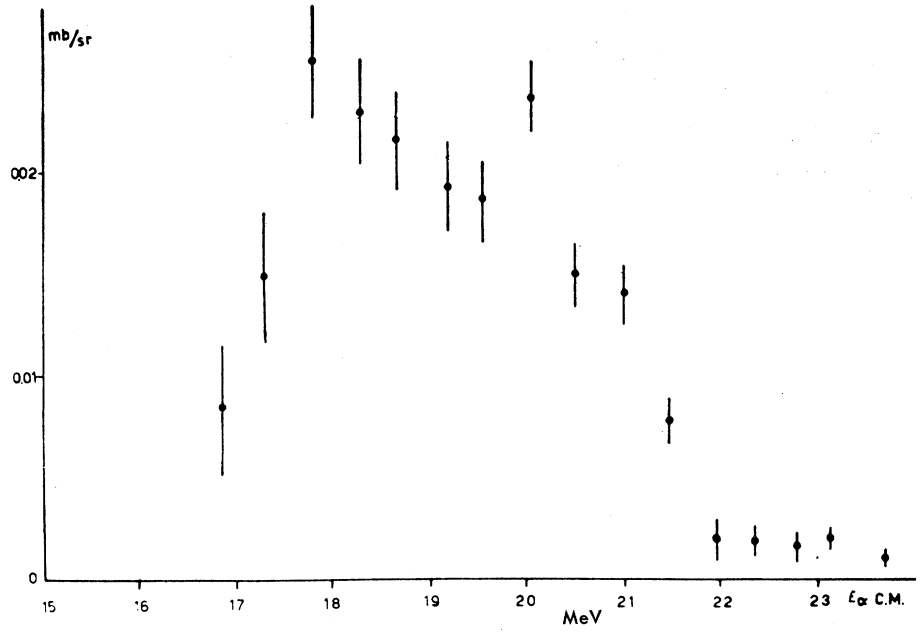

FIG. 31. Energy spectrum of alpha particles emitted in the $Lu^{175}(n, \alpha)Tm^{172}$ reaction; $\epsilon_0 = 14$ MeV (Ref. 44).

intensities of the α_0 groups compared to spectroscopic factors in order to establish which of the two main direct mechanisms—the knock-out and the pick-up processes—is responsible for this transition. In a pick-up process, the transition probability between an initial and a final state is proportional to the spectroscopic factor describing the removal of the various nucleons from the target nucleus. In the case of an (n, α) pick-up process,

$$S = S_n S_{2p}.$$

Considering the ground-state transitions only, the factor S_{2p} should be equal for all the molybdenum isotopes, and hence the transition probability is proportional to S_n. This quantity can be calculated assuming a shell model configuration for molybdenum and zirconium isotopes and should reproduce the relative cross sections. The comparison of calculated S_n values and α_0 group intensities is shown in Table Va. The agreement with pickup mechanism for ground state transitions is striking.

A recent preliminary result of Veselić *et al.* on (n, α) ground-state transitions on zirconium isotopes (Zr^{90}, Zr^{91}, and Zr^{93}) does not seem to confirm the above conclusions. In fact a glance on Table Vb shows that the values of spectroscopic factors S and the relative intensities of the α_0 group do not agree completely. Although the results of Veselić have been taken with a telescopic technique that seems to be more suitable for experiments of this kind, so far they are only preliminary.

Using an elaborate telescopic technique Kulišić *et al.*[70,83] and Lalović *et al.*[84] have measured energy and angular distributions of alpha particles emitted by 14-

TABLE V(a). Comparison of calculated values of the spectroscopic factor S_n and experimental values α_0 of group intensities for molybdenum isotopes. (Ref. 81).

Reaction	Transition	S_n	Group intensity
$Mo^{92}(n, \alpha)Zr^{89}$	$\left(\frac{9}{2}\right)_0^{10} \rightarrow \left(\frac{9}{2}\right)_{9/2}^{9}$	10	10±1.0
$Mo^{94}(n, \alpha)Zr^{91}$	$\left(\frac{5}{2}\right)_0^{2} \rightarrow \left(\frac{5}{2}\right)_{5/2}^{1}$	2	3±1.0
$Mo^{95}(n, \alpha)Zr^{92}$	$\left(\frac{5}{2}\right)_{5/2}^{3} \rightarrow \left(\frac{5}{2}\right)_0^{2}$	0.67	1±0.5
$Mo^{98}(n, \alpha)Zr^{95}$	$\left(\frac{5}{2}\right)_0^{6} \rightarrow \left(\frac{5}{2}\right)_{5/2}^{5}$	6	6±0.5
$Mo^{100}(n, \alpha)Zr^{97}$	$\left(\frac{5}{2}\right)_0^{6} \rightarrow \left(\frac{5}{2}\right)_{5/2}^{5}$	6	6.3±1.3

TABLE V(b). Comparison of calculated values of the spectroscopic factor S_n and experimental values of α_0 group intensities for zirconium isotopes (Ref. 82).

Reaction	Transition	S_n	α_0 group intensity
$Zr^{90}(n, \alpha)Sr^{17}$	$\left(\frac{9}{2}\right)_0^{10} \rightarrow \left(\frac{9}{2}\right)_{9/2}^{9}$	10	2.3
$Zr^{91}(n, \alpha)Sr^{88}$	$\left(\frac{5}{2}\right)_{5/2}^{1} \rightarrow \left(\frac{5}{2}\right)_0^{10}$	1	1
$Zr^{92}(n, \alpha)Sr^{89}$	$\left(\frac{5}{2}\right)_0^{2} \rightarrow \left(\frac{5}{2}\right)_{5/2}^{1}$	2	1.1

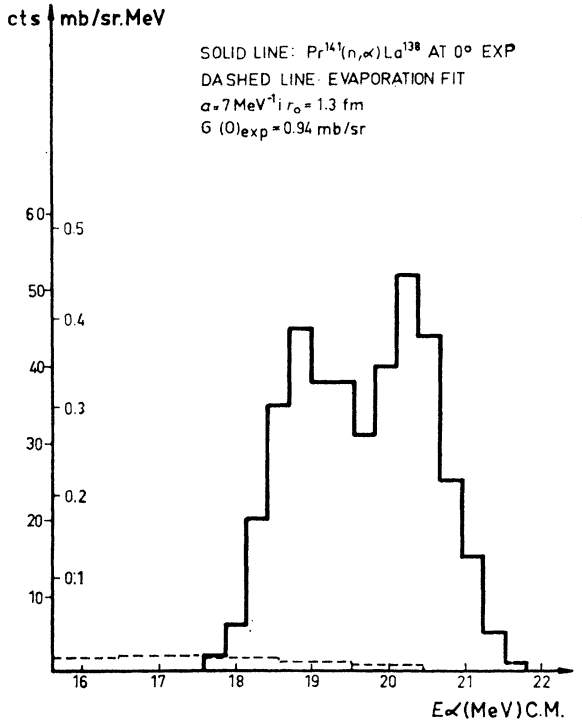

FIG. 32. The energy spectrum of alpha particles from 14-MeV neutron bombardment of Pr^{141}. Dotted lines represent statistical model calculations. (Ref. 70).

MeV neutron bombardment of several heavy nuclei from Nb^{93} to Bi^{209}. Their results, shown in Figs. 32 and 33(a) and (b), have been obtained by a telescopic technique combined with a two-dimensional analysis in dE/dx and E. Except for Nb^{93}, all the spectra and angular distributions are clearly direct. A statistical fit to the spectra could not be obtained even by using unreasonable values of the level density parameter a such as $A/25$. Thus some doubt is cast on the meaning of statistical model fits of (n, α) total cross sections for heavy elements that will be discussed in the next section.[85] The shape of the spectra and angular distributions show a clear surface process, and, contrary to the previously discussed results of Cuzsocrea *et al.*[81] several indications exist that the reactions proceed via a knock-out mechanism. Inferences from this supposition are discussed in Chapter 3.

An outstanding feature of the spectra is the constant position of the peak in the spectrum for the elements studied. The constancy with change in excitation energy is present also in the results of Marcazzan *et al.*[44] Its meaning has not yet been fully understood, although some attempts have been done.[83]

Spectral and angular distributions of alpha particles from 14- and 22-MeV neutron bombardment of silver have been studied by Rössle *et al.* using a gas scintillation telescope described by Mausberg *et al.*[87] (see Chap. 4). Angular distributions of portions of alpha-particle spectra are given; a remarkable feature of these distributions is the perseverance of forward peaking up to rather high residual excitations (lower energy alpha particles). Thus the nuclei around $A=100$ seem to be the turning point where the direct processes start to predominate.

Most of the information concerning the inelastic scattering of fast neutrons has been already discussed in the previous section. Actually, inelastic scattering data for the very heavy nuclei are rather difficult to obtain, since in this region the neutron spectrum is contaminated by contributions from fission neutrons. Batchelor *et al.*[88] have measured inelastic neutron spectra in U^{238} and Th^{232} and eliminated the post-fission contribution by assuming an appropriate spectral shape for fission neutrons,

$$N_{\text{fission}}(\epsilon)=A\epsilon^{\frac{1}{2}}\exp(-b\epsilon), \qquad (1.41)$$

and subtracting this part to the total spectrum. The difference was then analyzed by the usual method of reduced spectra. Best fits were obtained using the Fermi gas model for level densities. The values of the parameter a were independent of incident neutron energy.

Using 14-MeV neutrons, Adam *et al.*[89] have measured the angular correlation of the two neutrons from the reaction $(n, 2n)$ on bismuth in order to check the evaporation assumption of uncorrelated directions of emission. Their results suggest that the pure compound nucleus contribution (uncorrelated events) account for at most 70–80% of the $(n, 2n)$ cross section, which is somewhat surprising (see next section), and in contrast to the results of Jeremie,[90] who found no correlation at all between the two outgoing neutrons from the reaction $Bi^{209}(n, 2n)Bi^{208}$.

C. Total Cross Sections and Excitation Functions

In the earlier years, the bulk of information about neutron induced reactions came from total cross section measurements. Only recently, the improvement of detection methods, especially the introduction of telescopic techniques and multiparameter analysis, has shifted the peak of interest to angular and energy distributions. Nevertheless a large amount of data concerning total cross sections has been collected, from which valuable information can still be outlined. Several excellent compilations of total cross sections exist,[91] mostly around 14 MeV and we refer the reader to them, since we will not be able to review all the results.

1. Total Cross Sections of Neutron Induced Reactions up to 14 MeV

Most of the total cross sections have been measured by the activation method. Globally speaking, they corroborate and complement the information obtained from results of spectra and angular distributions dis-

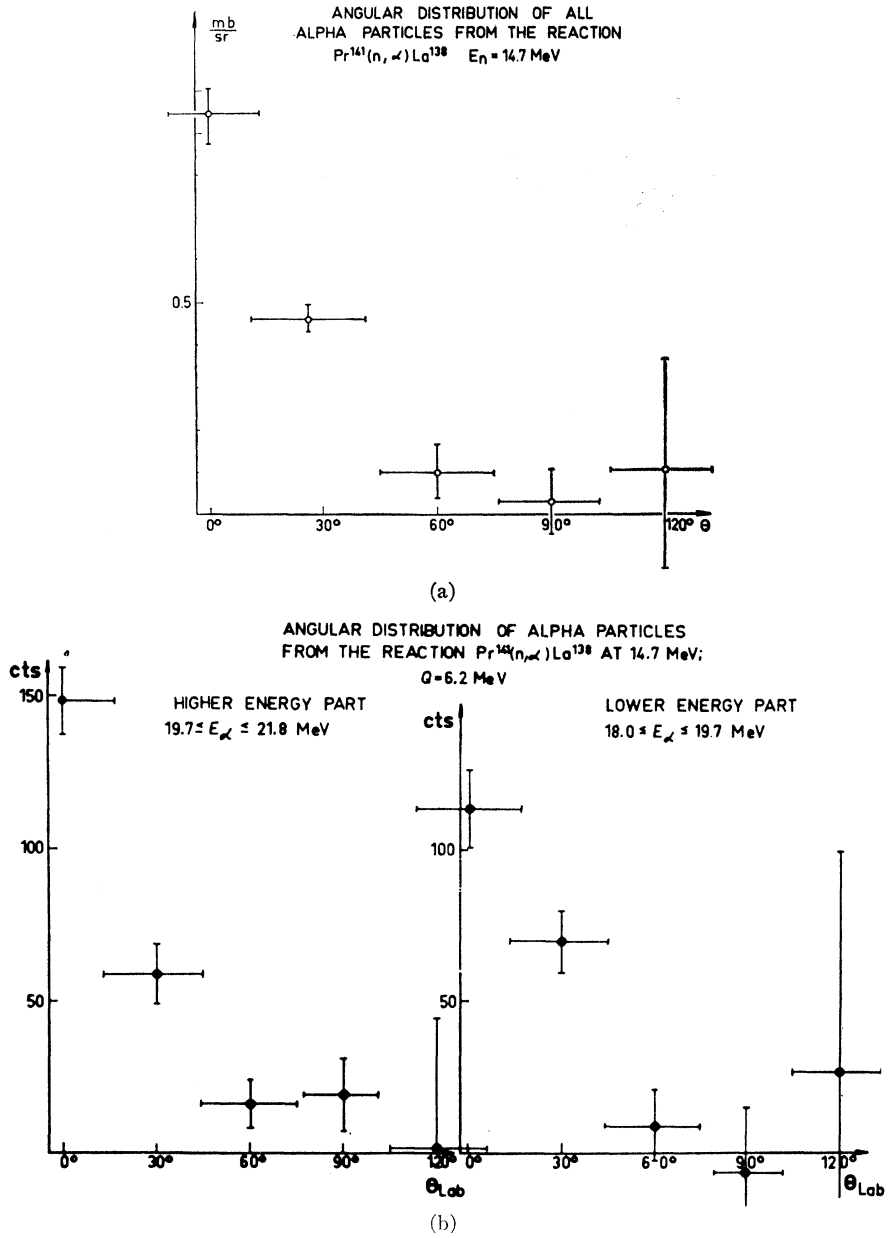

FIG. 33. (a) Angular distribution of all alpha particles from 14-MeV neutron bombardment of Pr^{141} (Ref. 70). (b) Angular distribution of higher and lower energy alpha particles from 14-MeV neutron bombardment of Pr^{141} (Ref. 70).

cussed in the previous sections and add valuable data on statistical and optical model parameters.

In the very low energy range (up to about 1 MeV) only (n, γ) reactions are important in the total cross section.[92] Cross-section measurements at lower energies are reported also by Cuzzocrea *et al.*[93] and Potenza *et al.*[94] However, the bulk of the total cross-section measurements lies, for obvious reasons, around 14 MeV. In these measurements usually the comparison technique was used, with $Al^{27}(n, \alpha)Na^{24}$ taken as a standard with 112–118 mb around 14 MeV. The measurements are reported in the references,[96] and we present here compilation of available data on total cross sections of (n, p) and (n, α) reactions taken from the work of Jeronimo *et al.*[95] (Fig. 34) and Facchini *et al.*[85] (Fig. 35).

It is our opinion that the analysis of total cross sections of neutron induced reactions is meaningful only in the case when a systematic search of many elements in a given region has been done. The underlying philosophy in the analysis should not be to obtain excellent fits for particular cases by an irregular variation of parameters, but to get fair overall fits varying sys-

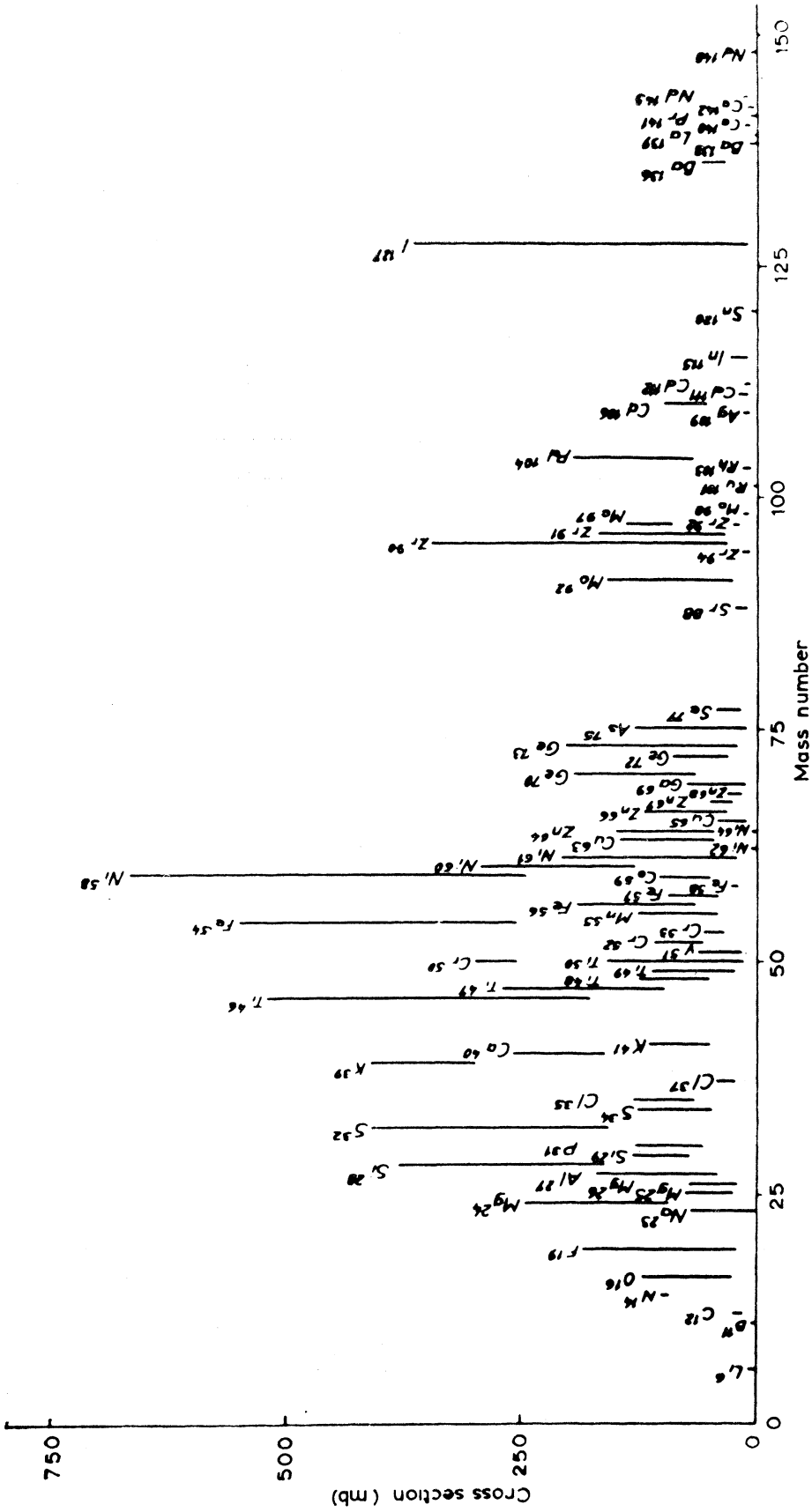

FIG. 34. Total cross sections for (n, p) reactions at 14-MeV neutron energy obtained by various laboratories. The full line for each nucleus is the total dispersion in the experimental values found in literature (Ref. 95).

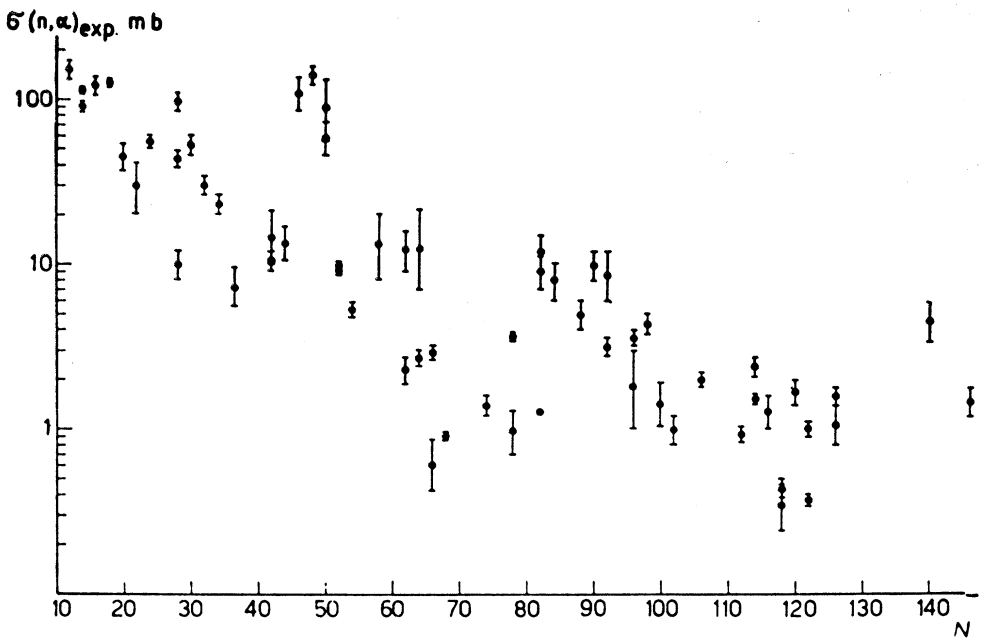

FIG. 35. Total cross sections of (n, α) reactions at 14-MeV neutron energy obtained by various laboratories for $A<150$. The full line for each nucleus is the total dispersion in the experimental results found in the literature (Ref. 85).

tematically the parameters within reasonable limits. If this is not possible, then the conclusion that the model does not apply is meaningful and well established.

Most of the analyses of total cross sections yield information about the reaction mechanisms, although some attempts to check the level density models through fitting the cross sections has been done.[97] The usual procedure has been to calculate the total cross section through the statistical model and compare it to the experimental value. The merits of such a comparison have been analyzed before[27] and are only briefly summarized here. It has been noted that:

(i) the statistical model cross sections are rather parameter-dependent; this concerns especially the level density parameter a;

(ii) thus a system of statistical parameters used in the analysis should be simultaneously tested through a set of other experiments;

(iii) calculations of total cross sections in terms of direct interaction theories are necessary in order to get a more complete insight into the reaction mechanism of neutron-induced reactions.

Very few calculations of direct interaction total cross sections are available. Robertson[79] has calculated the total cross section of the (n, p) reaction on I^{127}. Using both the volume direct theory of Brown and Muirhead[22] and the statistical theory, Robertson has obtained the total cross section for the reaction $I^{137}(n, p)$ as:

$$\sigma_{\text{direct}}=16 \text{ mb},$$

$$\sigma_{\text{comp}}=1 \text{ mb}.$$

This compares fairly well with the experimental cross section of about 12 mb. A similar measurement and calculation has been reported by Dixon[78] but with a considerably worse agreement. The experimental (n, p) cross section for a mixture of Cs and I was measured to be 8 mb, compared to a 16-mb value obtained from the volume direct theory.

2. *Excitation Functions of Neutron-Induced Reactions*

Valuable information about the reaction mechanisms and related parameters can be obtained from excitation function studies. Jeronimo *et al.*[95] have measured excitation functions of (n, p) and (n, α) reactions for some lighter (Mg^{26}, Al^{27}, Si^{28}) elements and medium weight elements in the range $E_n=6$–20 MeV and compared the results with the statistical theory [Figs. 36(a), (b), and (c)]. They used the optical model penetrabilities of Mani *et al.*[8,10] and Huizenga *et al.*[9] obtained from elastic scattering data and the level densities of Cameron.[12] The meaning of the over-all good fit obtained lies in the fact that it was obtained with *no adjustable* parameters. Thus in this region the compound nucleus model generally reproduces trends in the total cross sections.

Concurring results have been obtained by Bormann *et al.*,[98] the only difference being that these authors allowed a variable energy parameter η which essentially adjusted the excitation energy, replacing the neutron separation energy S_n by an effective value

$$S_n^{\text{eff}}=S_n+\eta.$$

Varying η within a couple of MeV excellent fits have been obtained for a number of excitation functions.

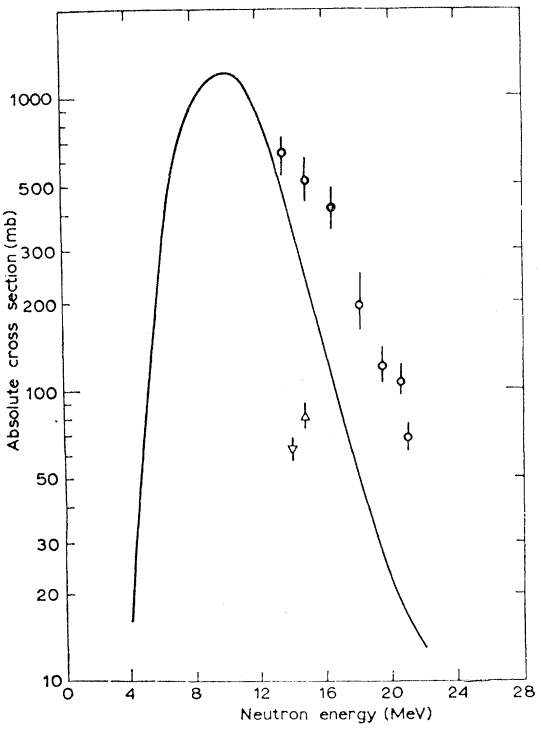

(a)

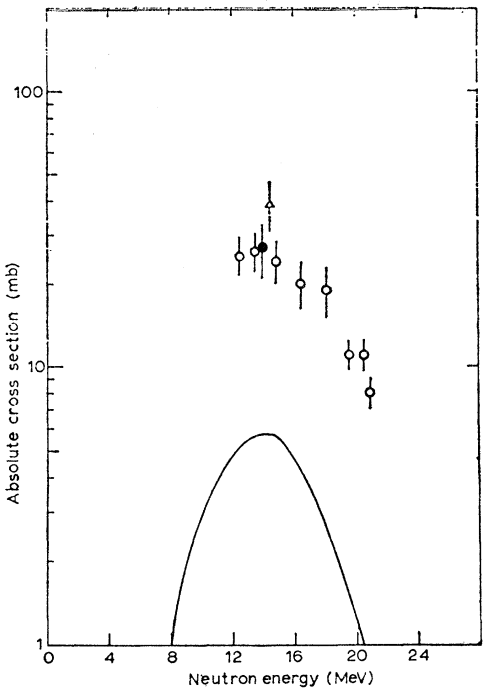

(b)

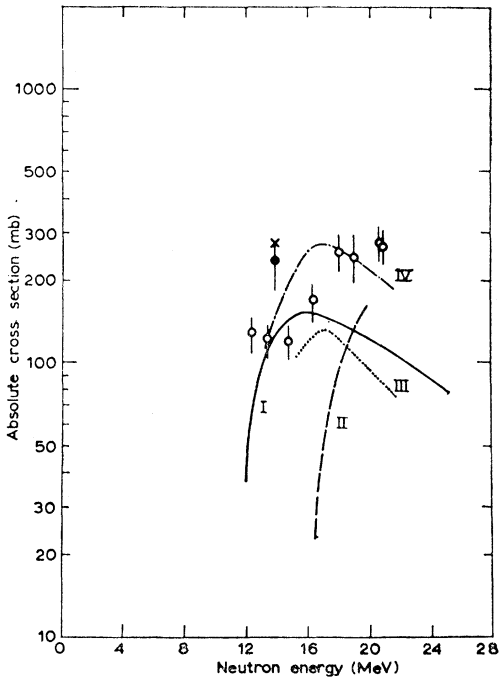

(c)

FIG. 36. (a) Total cross section for the $Co^{59}(n, p)Fe^{59}$ reaction. Experimental points: ○ (Ref. 95), ▽ (Ref. 99), △ (Ref. 100). The full curve is the calculation of Mani *et al.*[101] (Ref. 95). (b) Total cross section for the $Co^{59}(n, \alpha)Mn^{56}$ reaction. Experimental points: ○ (Ref. 95), ● (Ref. 102), △ (Ref. 103). The full curve is the calculation of Mani *et al.*[101] (Ref. 95). (c) Total cross sections for $Ni^{58}(n, np)Co^{57}+N^{58}(n, d)Co^{57}+Ni^{58}(n, pn)Co^{57}$ reactions from Refs. 100 and 104. The curves I, II, III, and IV have been obtained from calculations of Mani *et al.* [101]and represent excitation functions for these reactions and their sum, respectively. (Ref. 95).

The underlying argument was that the neutron bombarding energy for which particular (n, p) and (n, α) reactions attain their maxima (in the excitation functions) follow closely, in their Z dependence, the respective Q values.

An extensive analysis of excitation functions of (n, α) reactions in terms of the statistical model has been performed by the Milan group[51] (see Sec. IB2). Using the same values of optical penetrabilities as in the analysis of spectra, they obtained a set of values for the level density parameter a in complete agreement with the values obtained from the analysis of the

spectra. Thus the applicability of the compound nucleus model for (n, α) reactions in the region of nuclei up to $A \leq 100$ has again been confirmed. An exception are the recent results of Liskien *et al.*[105] on the excitation functions of the reactions $Cu^{63}(n, \alpha)Co^{60}$, $Ni^{60}(n, p)Co^{60}$, $Ti^{46}(n, p)Sc^{46}$, and $Na^{23}(n, 2n)Na^{22}$ in the neutron range of 12.5–16.5 MeV. Statistical model calculations are off by a factor of 2–4 in all the reactions studied (cf. Fig. 37). It can, however, be hardly expected that the statistical model, being a model of average nuclear properties can account for every particular reaction. Moreover, it is possible that a different set of parameters could lead to better agreement with experiments.

The excitation functions of $(n, 2n)$ reactions on Cu^{63}, Zn^{64}, Ag^{107}, and Sb^{121} have been measured by Rayburn[106] in the energy range from 12–20 MeV. The results have been compared to the simple statistical formulas[6] and the formulas of Barr *et al.*[107] These formulas reproduce the shape of the curves fairly well, but both give too large cross sections. Recently Büttner *et al.*[108] have calculated the cross section for the statistical emission of two particles taking into account the emission of gamma rays as a competing process. It is found that the competition of gamma emission is only important near the threshold of the considered reaction, where the level density formula fails to give a reliable result. Using their formula Büttner *et al.*[108] have obtained satisfactory agreement with $(n, 2n)$ excitation functions for nuclei around $A=60$ over a wide range of energies.

3. *Trends in* (n, p), (n, α), *and* $(n, 2n)$ *Cross Sections at 14 MeV*

For obvious reasons the bulk of total neutron reaction cross sections has been measured around 14 MeV. As mentioned before these results have been compiled,[91] and excellent reviews about the physical inferences from these measurements have appeared in the last few years. Facchini *et al.*[85] and Gardner *et al.*[109] have analyzed the 14-MeV (n, α) cross sections in terms of the statistical model, while in a series of articles Chatterjee *et al.* have analyzed the compound nucleus and shell effects in (n, α)[110] and (n, p)[111] cross sections. The same effects in $(n, 2n)$ reactions have been analyzed by Bormann.[112] Rather than presenting individual measurements we discuss these survey articles in some more detail.

The statistical model analysis of Facchini *et al.*[85] is based on compound nucleus calculations of the (n, α) cross section in terms of the cross section for the emission of inelastic neutrons, based on Eq. (1.3),

$$\frac{\sigma(n,\alpha)}{\sigma(n,n)}=\left(\frac{a_\alpha}{a_n}\right)^{1/2}\left(\frac{A}{A+3}\right)^{-5/2}\frac{g_\alpha m_\alpha}{g_n m_n} \times \frac{\int_{\epsilon_{\min}}^{\epsilon_{\alpha\,\max}} \epsilon_\alpha \sigma_{c\alpha}^*(\epsilon_\alpha)\exp\left[2(a_\alpha E_\alpha)^{\frac{1}{2}}\right]/(E_\alpha+t)^2\,d\epsilon}{\int_{\epsilon_{\min}}^{\epsilon_{n\,\max}} \epsilon_n \sigma_{cn}(\epsilon_n)\exp\left[2(a_n E_n)^{\frac{1}{2}}\right]/(E_n+t)^2\,d\epsilon},$$

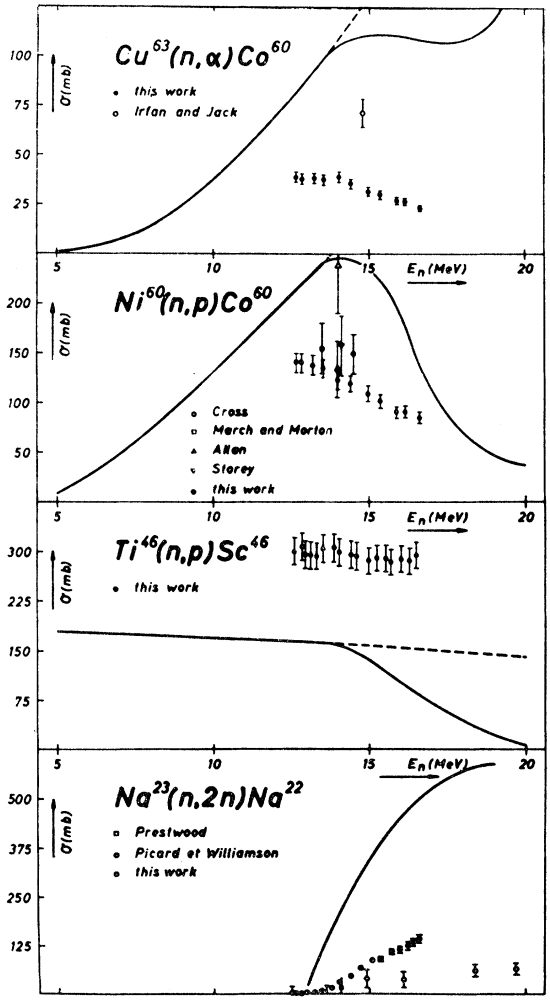

FIG. 37. Statistical model calculations together with the experimental cross sections for various neutron reactions. The dashed line represents theoretical cross sections without regarding second particle emission. Notice that in all the cases statistical model calculations are off by at least a factor of two. (Ref. 105).

where the cross section for inelastic neutron scattering is given by

$$\sigma(n, n)=\sigma_{\text{in}}-\{\sigma(n, p)+\sigma(n, \alpha)\}$$

and σ_{in}, the total inelastic cross section (all outgoing channels), has been computed from experimental data. The lower limit $\epsilon_{\min}$ in the integral in the numerator has been inserted to eliminate possible contributions from the region where $(n, n\alpha)$ and $(n, \alpha n)$ reactions became energetically possible. The other symbols are already familiar to the reader.

The a values used in the computation are shown in Table VI. They yield the same relationship between a and the neutron number N as those of Erba[113] shown in Fig. 38.

The interesting feature of this relationship is the presence of shell effects corresponding to closed neutron shells of $N=50$, 82, and 126 (for the corresponding proton shell effect see below). As the decrease of a

TABLE VI. Values of level density parameter a used in computing the (n, α) cross sections at 14 MeV.

Residual nucleus	a	Residual nucleus	a	Residual nucleus	a	Residual nucleus	a
F^{20}	4.5	Ga^{72}	13	Cd^{114}	17.5	Dy^{162}	23.6
Ne^{23}	4.5	As^{75}	13	Cd^{115}	18.6	Dy^{164}	22.8
Na^{23}	4.5	As^{76}	13	In^{115}	16	Dy^{165}	20.2
Na^{24}	4.9	As^{78}	13	Sn^{118}	16.4	Dy^{167}	23.5
Mg^{26}	4	Br^{79}	12.6	Sn^{127}	17.5	Er^{168}	21.4
Al^{27}	4.9	Br^{81}	12	Sb^{124}	18	Er^{170}	24
Al^{28}	4.6	Br^{82}	14	Te^{130}	17	Yb^{175}	22
Si^{31}	5	Br^{84}	14	I^{127}	18	Hf^{178}	23.5
P^{31}	5	Kr^{85}	14	I^{130}	17.5	Ta^{184}	30.6
P^{34}	5	Rb^{85}	10	Cs^{133}	17.4	W^{187}	23.5
S^{34}	5.5	Rb^{87}	8	Cs^{136}	15.5	Re^{187}	27
Cl^{37}	6	Sr^{88}	8	Ba^{137}	15.5	Re^{188}	23.5
Cl^{38}	6	Sr^{89}	10.5	Ba^{139}	17	Os^{190}	27.7
K^{41}	7.2	Sr^{91}	13	La^{139}	13.5	Os^{191}	24
K^{42}	7	Y^{90}	10	Ce^{139}	13.5	Os^{193}	25
Ca^{47}	8	Zr^{92}	11.8	Ce^{140}	12.5	Ir^{191}	23.7
Sc^{45}	7	Zr^{94}	13.5	Ce^{142}	15	Ir^{194}	24
	8	Zr^{97}	15.7	Ce^{145}	25	Pt^{194}	23
Ti^{50}	7	Nb^{93}	11.8	Nd^{142}	11.5	Pt^{196}	20
V^{51}	7.3	Mo^{100}	15.7	Nd^{148}	21	Pt^{197}	20
V^{52}	8.5	Ru^{105}	16.5	Nd^{149}	24	Au^{197}	20
Cr^{51}	7.5	Ru^{107}	16.5	Nd^{151}	23	Hg^{200}	19
Mn^{55}	8	Rh^{106}	17.6	Sm^{152}	23	Tl^{206}	10.3
Mn^{56}	9	Pd^{108}	17	Sm^{153}	23	Bi^{209}	11.2
Fe^{54}	7	Pd^{109}	17.6	Sm^{154}	24.5	Ra^{227}	24.8
Co^{59}	9	Pd^{110}	17.5	Sm^{157}	22.5	Th^{230}	27.3
Co^{60}	9	Pd^{111}	17.8	Gd^{156}	24.5	Th^{235}	30
Co^{62}	9.5	Ag^{109}	17	Gd^{159}	21.6	U^{238}	29
Cu^{63}	9.5	Ag^{112}	19	Gd^{160}	21.4		
Cu^{65}	9.5	Cd^{112}	17.5	Gd^{161}	18.2		

near the closed shells hinders more the emission of neutrons than the emission of alpha particles (the Coulomb barrier anyway prevents the emission of low-energy alphas corresponding to high excitation of the compound nucleus), the relative cross sections for alpha emission increase near the closed neutron shells.

The comparison between compound nucleus theory and experimental cross sections is shown in Fig. 39. The results can be briefly summarized as follows:

—a fair agreement can be obtained for nuclei up to about the middle of the periodic table ($A \leq 80$);

—nuclei with closed neutron shells ($N=50$ and 82) have a cross section an order of magnitude higher than for neighboring nuclei; there is good agreement between experimental and theoretical values;

—for nuclei with neutron number N in between the two closed shells 50 and 82 the agreement becomes gradually worse, and often the experimental cross section becomes 5–10 times larger than the theoretical (compound nucleus) one. A different choice of parameters may sometimes reduce the disagreement;

—for heavy nuclei ($N>82$) the experimental cross sections are of the order of 1 mb and the disagreement between the experimental and theoretical values becomes at times catastrophic (ratio of 100–1000). No variation of parameters could eliminate this discrepancy. Other reaction mechanisms have to be taken into account (see below).

While very light nuclei have not been included in the survey in Ref. 85, in a recent article Gardner *et al.*[109] have tried to establish trends in (n, α) total cross sections for nuclei with $6 \leq Z \leq 30$. Using a suitable form for the Coulomb barrier, the fractional probability of alpha particle emission F_α has been obtained in a simple form, particularly applicable to ratios of cross sections for neighboring isotopes:

$$\sigma(Z, A+1)/\sigma(Z, A) \doteq [F_\alpha(Z, A+1)/F_\alpha(Z, A)] \doteq \exp 2\{[a(\epsilon_{\max}-\beta_\alpha)]_{A+1}^{\frac{1}{2}}-[a(\epsilon_{\max}-\beta_\alpha)]_A^{\frac{1}{2}}\},$$

where $\epsilon_{\max}$ is the maximum energy of emission for alpha particles and β_α the corresponding Coulomb barrier. However, in this region of nuclei the experimental results are rather scanty, and a meaningful comparison with experiment was not possible.

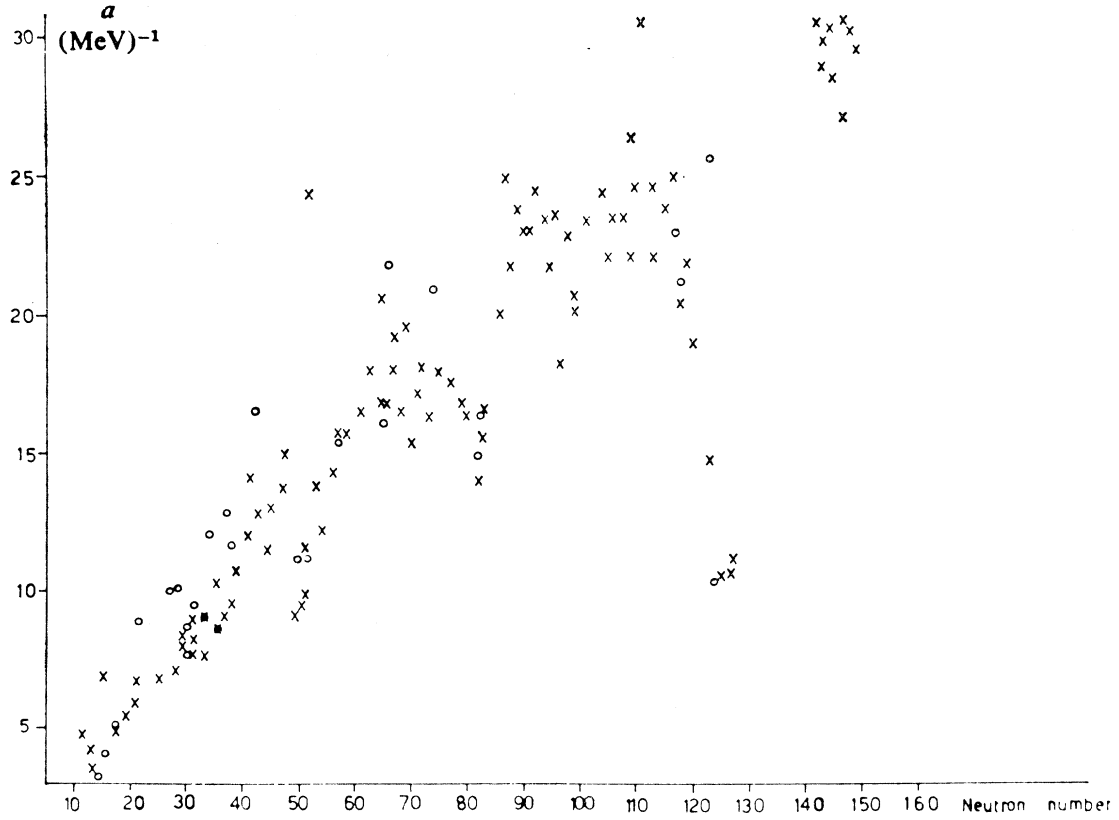

FIG. 38. Values of the level density parameter a from neutron resonances (*) and from energy spectra (O) plotted vs the neutron number N (Refs. 85 and 113).

In a series of articles Chatterjee[110,111] has discussed various aspects of trends in (n, α) and (n, p) reactions, especially shell effects. Shell effects in neutron induced reactions have been observed before[114] and in (n, α) reactions can be observed clearly by plotting the cross sections against the proton number Z and the neutron number N of the target nucleus (Figs. 40 and 41). Chatterjee reports dips at Z values of 10, 22, 30, 40, 52, and 84 and N values of 38 and 78. In all these cases the residual nuclei had closed proton shells. It is true that although in drawing the solid lines in Figs. 40 and 41 especially for large values of Z and N some freedom could have been employed, nevertheless the location of the dips near the closed shell numbers can

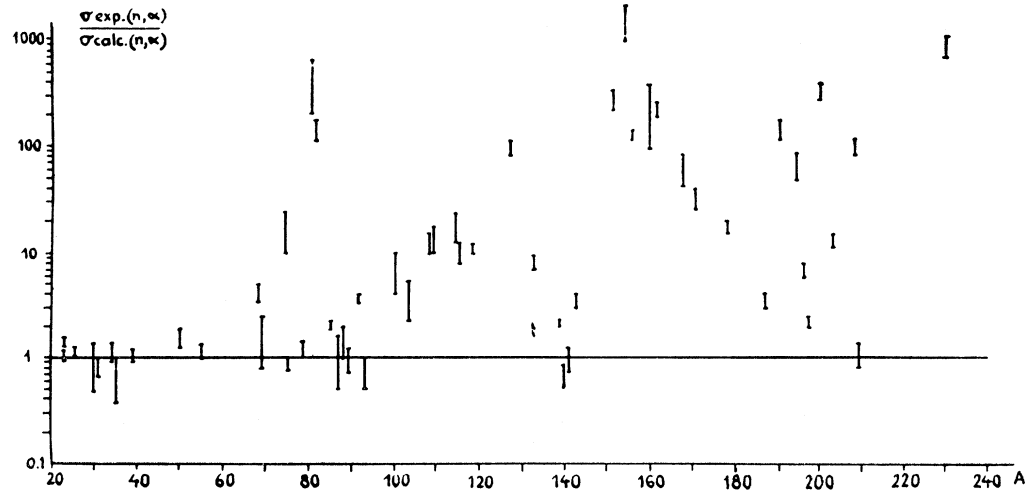

FIG. 39. Ratio of experimental cross sections and theoretical calculations of Facchini *et al.*[85] for (n, α) reactions at 14 MeV (Ref. 41).

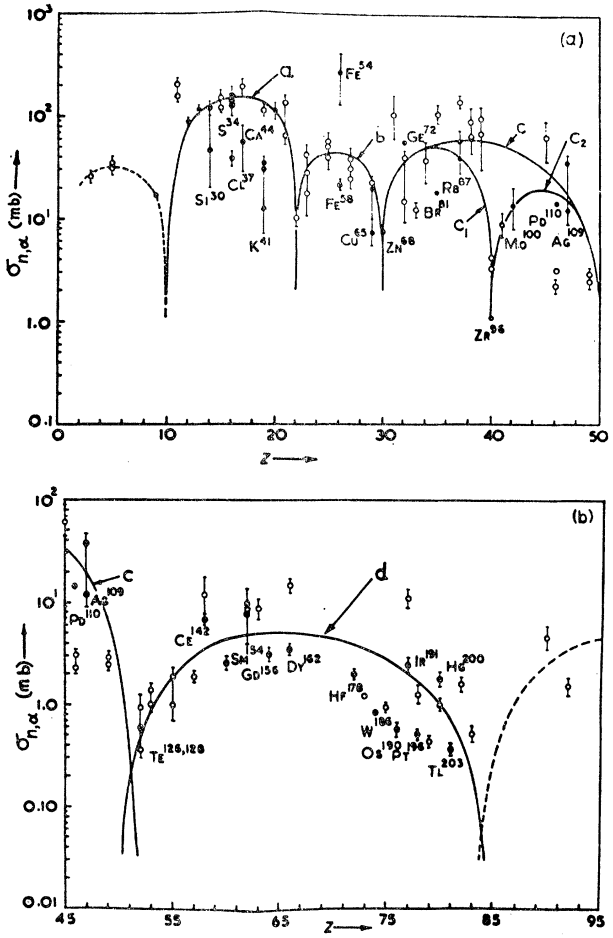

FIG. 40. Plot of the observed (n, α) cross sections against the proton number Z of the target nucleus. (a) the observed values between $Z=0$ and 50; (b) the values between $Z=45$ and 95. The scale of the ordinates has been shifted in the two cases. The isotopes of lesser natural abundance have been marked with black circles and have also been identified in the two plots (Ref. 110).

be hardly considered coincidental. This is confirmed by plotting the cross sections vs the number of protons of the residual nucleus Z_R.[110] The positions of the minima correspond exactly to the positions of proton shell closure of the residual nuclei. Also, the so-called Levkovski effect[115] has been observed in some cases for (n, α) reactions too.

The same effects have also been observed for (n, p) total cross sections,[111] however, only for residual filled proton shells, while no effect of closed neutron shells has been clearly observed. These results are shown in Fig. 42.

The observed shell effects have been discussed in terms of the compound nucleus model. The analysis starts from the standpoint that while no appreciable odd–even fluctuations in the cross sections are observed, distinct proton and neutron shell and subshell effects are present. The question is whether these effects can be understood from the statistical theory. Using the Weisskopf–Ewing evaporation formula (1.3) and a very crude expression for the inverse cross section and the level density distribution, Chatterjee obtains the following expression for the total (n, α) viz. (n, p) cross sections:

$$\sigma(n, \nu)=\sigma_c(n)[g_\nu\mu_\nu\rho_\nu(E, j)/\sum_i g_i\rho_i(E, j)], \quad (1.42)$$

which gives the cross section in terms of the residual level densities $\rho_i(E, j)$. It is clear that shell effects will give rise to differences in excitation values, and that this will be eventually transposed to the level density. The level density in the Fermi gas model can be expressed as a product of two factors:

$$\rho(E, j)=K[(2j+1)/A^2]P_j(E, A), \quad (1.43)$$

where K is a constant depending only on the Fermi energy ζ and P_j is given by

$$P_j(E, A)=\rho(E, A) \times\{\exp[(1/2\pi)j(j+1)A^{-5/3}(AE/\zeta)^{1/2}]\}. \quad (1.43a)$$

$\rho(E, A)$ is the familiar energy dependence of the level density,

$$\rho(E, A)=E^{-2}\exp[\pi(AE/\zeta)^{\frac{1}{2}}]. \quad (1.43b)$$

We now study the effect on $\rho(E, j)$ of a shift in

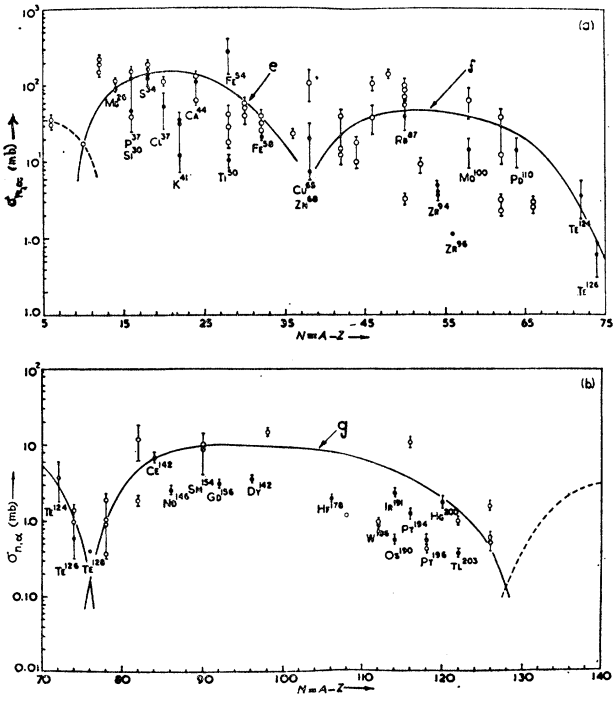

FIG. 41. Plot of observed (n, α) cross sections against the neutron number $N=A-Z$ of the target nucleus. (a) the N values between 5 and 75; (b) the N values between 70 and 140. The scale of the ordinates has been shifted in the two cases. The black circles are values for the identified isotopes of lesser abundance; the isotopes of higher abundance are marked as white circles and unidentified (Ref. 110).

excitation energy from E to E',

$$E'=E+\Delta E, \qquad \Delta E \ll E. \tag{1.44}$$

Thus, to first order,

$$(E')^n=E^n(1+\Delta E/E) \tag{1.44a}$$

and

$$P_j(E', A)=P_j(E, A)\frac{\exp\left[(1/2\pi)(A/\zeta E)^{\frac{1}{2}}\Delta E\right]}{1+2\,\Delta E/E}. \tag{1.45}$$

It is now interesting to explore whether a shift due to shell effects could explain the trends in the cross sections. According to Rosenzweig[117] this shift is given by

$$\Delta E=\tfrac{1}{12}N^2d_n+\tfrac{1}{12}P^2d_p-\tfrac{1}{2}d_n(n-\tfrac{1}{2}N)^2-\tfrac{1}{2}d_p(p-\tfrac{1}{2}P)^2. \tag{1.46}$$

Here it is assumed that the nucleons have occupation number n and p in neutron and proton shells with maximum occupancy N and P, equal, respectively, to $2j_N+1$ and $2j_P+1$, and d_n and d_p are the equidistant

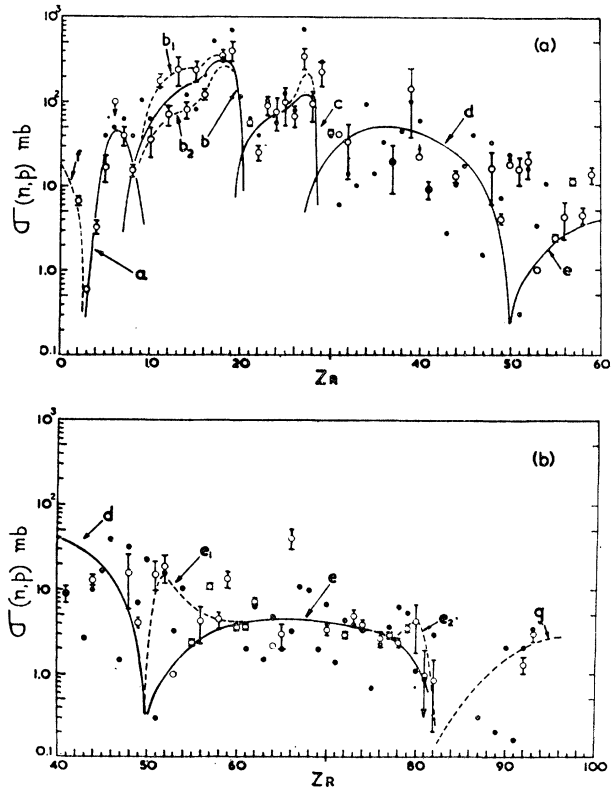

FIG. 42. Plot of the~14-MeV total (n, p) cross sections against the residual nuclear charge Z_R. (a) values between $Z_R=0$ and 60; (b) values between $Z_R=40$ and 100. Reaction cross sections for only the most abundant target elements have been shown as white circles; the "errors" are the spread in the nominal values. Gardner's predicted values[116] are shown as black dots (Ref. 111).

fermion-level spacings for neutrons and protons. This gives the following shell-dependent level density:

$$\rho(E_s,j)=\rho_0\frac{\exp\left[-(\pi/36)(\zeta/\Delta E)^{\frac{1}{2}}(N^2+P^2)(1+x)\right]}{1-\left[\zeta(N^2+P^2)/9AE\right](1+x)} \tag{1.47}$$

with

$$\rho_0=K(1/A^2)2(j_N+j_P+1)P_j(E, A) \tag{1.47a}$$

and

$$x=12\frac{n^2+p^2-nN-pP}{N^2+P^2} \tag{1.47b}$$

($x=0$ for completely filled or empty shells, while $x=-3$ for half-filled shells $N/2$, $P/2$).

Figure 43 shows the results of this computation for (n, α) and Fig. 44 for (n, p) reactions. The full curve on both figures represents the relative level densities (E_s, j) calculated from (1.47), in terms of the normalizing factor ρ_0 (1.47a). The cross sections, according to Eq. (1.42), are roughly proportional to the level density of the residual nuclei. Thus the full curves should follow the trends in experimental (n, α) and (n, p) cross sections as, indeed, appears to be the case. For a very crude calculation, the agreement shown in Figs. 43 and 44 is rather remarkable. It should not, however, be pushed too far, since for heavy nuclei the dips in the cross sections are far from being certain. It is nevertheless clear that two important structure effects, the pairing and the shell effects, can be suitably described in terms of the statistical model. In fact, nothing has been said about the contribution of direct reactions to analyze the shell effects. The shell effects are comparable in energy to the pairing effects, but usually are less clearly seen because (i) more attention is usually given to the behavior within a shell than to that across the shells and (ii) no neutron shell effects have been observed.

This last problem has been discussed by Rubbino *et al.*,[118] in an attempt to explain the anomalies in (n, α) cross sections. In particular, it has been observed that (i) experimental cross sections show *maxima* around closed shells of *neutrons*, and *minima* around closed shells of *protons*; (ii) for $A>70$ the disagreement with compound nucleus theory is *stronger* where $\sigma_{\exp}(n, \alpha)$ are relatively *small*, and *less pronounced*, where the cross sections are *large*. According to Rubbino, the anomaly (i) could be explained in terms of the decrease of the compound nucleus (n, α) cross section for the larger values of a in the region near the closed shells of neutrons and far away from closed shells of protons, while (ii) may be interpreted as a Q value effect. The explanations of Chatterjee and Rubbino are not quite consistent.

Analyses like the ones discussed in this section could be criticized from the standpoint[116] that through the uncertainty of the bombarding energy (it is, however,

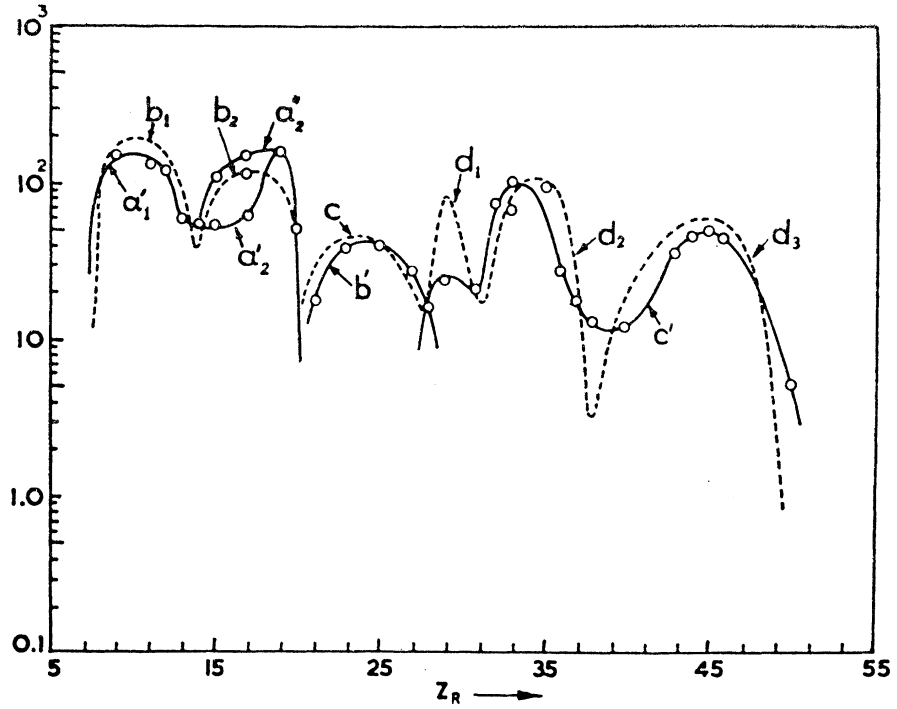

FIG. 43. The computed curves of (n, α) total cross sections (full lines) against Z_R $(9 \leqq Z_R \leqq 55)$ obtained using the shell-dependent level density (1.47). The regions of the three major proton shells *a*, *b*, *c*, use different normalizing factors ρ_0. The ordinate is $\rho(E_{s,i})/\rho_0$. The dotted curves, superimposed for comparison, present trends in experimental (n, α) cross sections (Ref. 110).

true that several measurements[45,119–121] have shown only small variations of $\sigma_{n\alpha}$ with the bombarding energy around 14.5 MeV), the unrealistic error limits, and lack of thorough standardization one can hardly perform a judicious selection of data for such systematic studies. As already mentioned, this concerns especially the (n, α) data for heavy nuclei, where most of the cross sections are of the order of 1 mb, and the presumed dips are far from being clearly discernible.

Nevertheless the analyses of Facchini *et al.* and Chatterjee *et al.* give a fair picture of the trends in (n, α) and (n, p) reactions at 14 MeV and it is hard

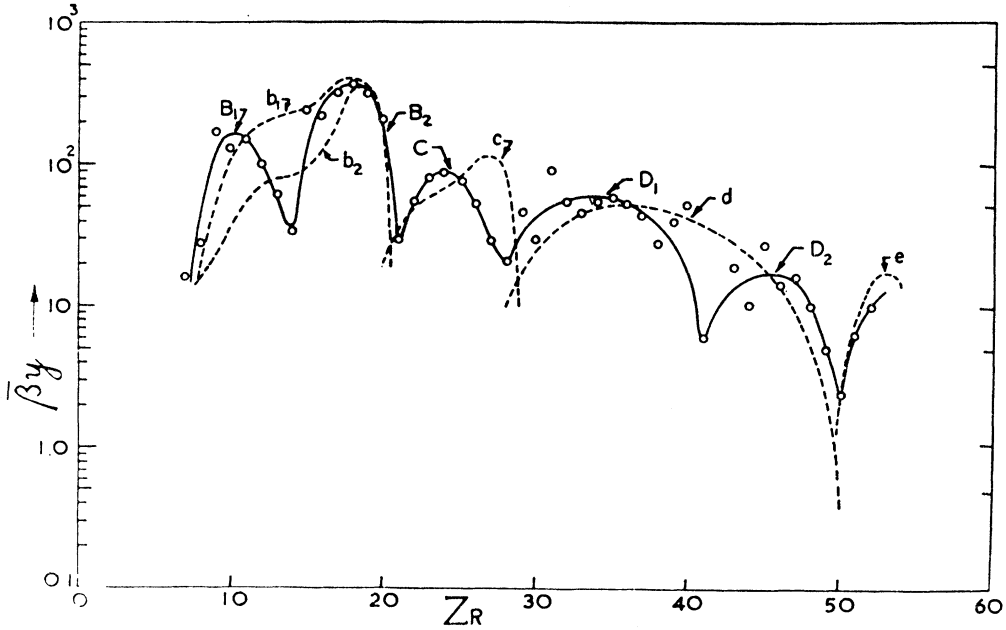

FIG. 44. Plot of the calculated (n, p) total cross sections $(\bar{\beta}_y)$ obtained using the shell-dependent level density (1.47) against the residual nuclear charge $Z_R (0 \leqq Z_R \leqq 60)$. The solid curve is drawn through the calculated values shown as white circles. Note the shell dips between the regions B_2 and *C*, *C* and D_1, and D_2 and *e*, and the subshell dips between B_1 and B_2, and D_1 and D_2. The dotted curves b_1—*e* present smooth curves drawn through the experimental points and have been shown here for comparison (Ref. 111).

to believe that new results can radically alter this picture. The interplay of compound nucleus and direct processes for these reactions can be described as follows:

For elements in the lighter half of the periodic table (up to $A=100$) the main contribution to the reaction mechanism comes from compound nucleus processes and the explanation of the dips in the cross sections as a consequence of the shell effects in the level density is quite plausible. While the direct contribution, stemming mostly from the nuclear surface, remains more or less constant throughout the periodic table, the compound contribution falls down sharply for heavy nuclei due to the effect of the Coulomb barrier. The compound nucleus cross section falls practically to zero for nuclei with $Z=60$–70. Thus the (n, α) cross sections for very heavy nuclei come from purely direct surface effects and is constant up to highest Z values. In fact, Fig. 40 shows a slight increase for $Z=70$ to 90 that could be expected from the increase of the nuclear surface, consistent with the above interpretation.

$(n, 2n)$ reactions have always been considered as evaporative processes *par excellence*. In fact, in this case even the most modest approximations gave satisfactory results. Nevertheless, structure effects in these reactions have been observed several years ago[114] and recently Bormann[122] has discussed the shell model effects in $(n, 2n)$ reactions on even-neutron target nuclei against the background of the statistical theory. Minima in the $(n, 2n)$ cross sections at the magic neutron numbers for $N=28$ and 50 for even-proton nuclei and $N=20$ for odd-proton nuclei can be explained by a similar trend in Q values. However, cross section maxima at $N=82$ and 126 for even and $N=28$, 50, 82, and 126 for odd proton nuclei can be understood as an effect of shell closure on the nuclear level density, the relative decrease of which on passing across a closed shell is larger for higher excitation energies. Now the $(n, n'\alpha)$ reaction is the principal one competing with the $(n, 2n)$ processes at 14 MeV in the medium and heavy mass region. The $(n, n'\alpha)$ reaction leaves the residual nucleus with an excitation energy up to 12 MeV whereas for the $(n, 2n)$ reaction the excitation does not exceed 4 MeV. Since the relative change in the level density is greater at higher energies, the competition between $(n, n'\alpha)$ and $(n, 2n)$ reactions favors the latter one in the region of closed neutron shells (smaller level density parameter a) and may account for the observed maxima in the $(n, 2n)$ cross sections. The effect is similar to the one observed in (n, α) and (n, p) cross sections.

4. *"Rare" Nuclear Reactions*

The "rare" nuclear reactions, including (n, d), (n, np), (n, pn), (n, t), (n, dn), $(n, 2p)$, (n, He^3), (n, γ), $(n, n\alpha)$, and $(n, \alpha n)$ and $(n, 3n)$, have been measured by the activation technique.[123,124] These reactions are important for the understanding of spectra and angular distributions, since the "rare" reactions often interfere in the region of highly excited residual states. They also give information about the clustering of particles.

In general, the upper limit for most of the above reactions at 14–20-MeV neutron energy is below 1 mb. Exceptions are the (n, pn), (n, np), and (n, d) reactions, whose total sum may exceed several hundreds millibarns (e.g., 520 mb for Ni^{58}) and some $(n, n\alpha)$ reactions. As far as this latter reaction is concerned, a search has been done to establish whether the process

$$n+X\rightarrow Y+\alpha+n$$

proceeds via the direction $(n, \alpha n)$ or $(n,\alpha n)$. This reaction might be supposed to proceed mainly via the n, n' process followed by α emission: the emission of neutrons is easier than that of alphas due to the Coulomb barrier. However, for an alpha particle to compete successfully with the emission of a proton or a second neutron *after* a first neutron has been emitted, the separation energy S must be much less than the corresponding energies S_n and S_p. This, actually, is always the case for S_n, but not for S_p. Thus $(n, n\alpha)$ cannot successfully compete with the (n, np) process and we must turn the $(n, \alpha n)$ reaction as the predominant mechanism for the emission of a neutron and an alpha particle. Indeed, the formula

$$\sigma(n, \alpha n)=\sigma(n, \alpha)P(n) \tag{1.48}$$

with

$$P(n)=\frac{\int_0^{\epsilon_n+Q_{n,\alpha}-S_n}\epsilon_\alpha\sigma_\alpha^*(\epsilon_\alpha)\rho(E)\,d\epsilon_\alpha}{\int_0^{\epsilon_n+Q_{n,\alpha}}\epsilon_\alpha\sigma_\alpha^*(\epsilon_\alpha)\rho(E)\,d\epsilon_\alpha} \tag{1.48a}$$

which is obtained under the supposition that if the residual nucleus has an energy excess of at least S_n, then a neutron is always emitted, gives excellent agreement up to Nb. For higher A values there are no $(n, n\alpha)$ or $(n, \alpha n)$ reactions, since these reactions can hardly arise as a consequence of direct processes.

5. *Fluctuations in Total Cross Sections*

In this section we review briefly some of the recent experimental information concerning the presence of intermediate structure in reaction excitation functions.

Feshbach[25] has suggested (see Sec. IA6) that structure due to effects of intermediate processes could be expected in excitation functions of neutron total cross sections. Seth[125] has measured average total cross sections for many nuclei from Cu to Tl in the energy range 3–650 keV, with an energy resolution of 8–10 keV. His results can be summarized as follows:

(i) The excitation functions on all elements show a characteristic structure. The structure is not random

in character, has widths of 75±25 keV over the whole region and amplitudes 10–20 in the $\langle\sigma_t\rangle$ (3–10 times the statistical error);

(ii) the structure is most prominent for monoisotopic elements and small for elements containing many isotopes.

As the known level density for most of the nuclei is of the order of $\langle D\rangle$=10–100 eV, the average width

$$\langle\Gamma_{\text{exp}}\rangle\gg\langle D\rangle$$

and the observed structure cannot be due to Ericson fluctuations. Seth[125] suggests that they represent evidence of Feshbach's doorway states.

The width of doorway states has been calculated in the region of lead[25] to be of the order of 100 keV. However the mentioned result of Le Couteur[26] (see Sec. IA6) that the width of intermediate states varies as $A^{-5/3}$ [Eqs. (1.27) and (1.27a)] is not confirmed by the experimental evidence in Ref. 125.

Results that could be interpreted along the same lines have been presented by Csikai,[126] and Cabe[127] who have measured $(n, 2n)$ total cross sections in the region around 14 and 17 MeV, respectively. Here the energy resolution of the neutron beam was considerably worse than in the preceding experiments (25–50 keV). Nevertheless, the structure of 50–100-keV width could be seen for all the nuclei studied except the lightest ones.[128] Now for medium weight and heavy nuclei the $(n, 2n)$ cross section accounts for most of the total cross section above 14 MeV, and an interpretation in terms of doorway states is feasible.

The structure in the excitation functions is not confined solely to total cross sections. Characteristic peaks 100–200 keV wide and separated by energy intervals of 300–400 keV have been observed in both the polarization and the differential cross sections of neutrons scattered by F, Na, Al, and P in the energy range 0.2–2.2 MeV.[129] The optical model of Perey *et al.* reproduced the average behavior of the energy dependence of the cross sections and the polarization, but not the fine structure. It is suggested[129] that the resonances are due to doorway states. The supposition is enhanced by the fact that the observed structure is correlated at different scattering angles as a function of energy.

The structure in total cross sections need not, however, be interpreted uniquely in terms of doorway states or intermediate structure in general. Calvi *et al.*[39] have suggested that the resonances found in total cross sections could be interpreted as statistical fluctuations in the level density of the compound nucleus. According to these authors, the mean square relative deviation of the total compound cross section from the average value is inversely proportional to the square root of the level density of the intermediate (compound) nucleus. Manero[130] has measured neutron total cross sections for V, In, I, and Bi in the energy range of 3.2–5.2 MeV, with a neutron energy spread of ±30 keV. The results for vanadium and indium are shown in Fig. 45. Now it is known from earlier work,[11] that the level spacing for bismuth (Bi^{209}) and vanadium (V^{51}) at these excitations is considerably smaller than for indium (In^{115}) and iodine (I^{127}). The use of the level density formula given by Ericson[1] for the equidistant spacing model with the values of the parameter a given by Erba *et al.*,[11] gives the respective level densities for compound nuclei for an average neutron energy ϵ_n=4 MeV (Table VII). Thus, according to Calvi *et al.*[129] one should expect large and narrow resonances for vanadium and bismuth, small value of a and smaller but broader resonances of indium and iodine. This indeed seems to be the case (cf. Fig. 45).

Structure in total cross sections for Na, K, and Ca between 4–6-MeV neutron energy has been found also by Stüwer *et al.*[131] Pronounced peaks of 100–150-keV width have been found in each case and their presence attributed to fluctuation in compound nucleus density. Thus although the presence of intermediate resonances in the total cross section seems to be well established,

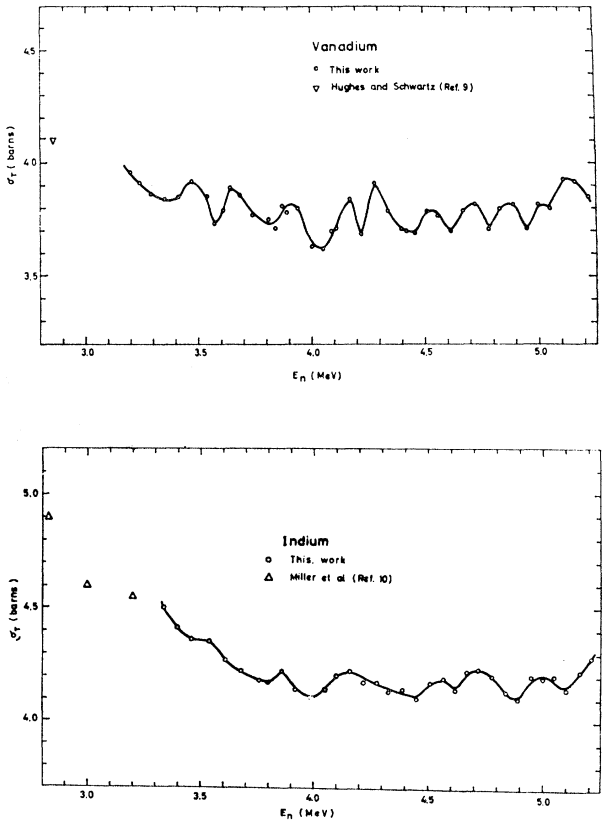

FIG. 45. Fine resolution measurements (ΔE_n=±30 keV) of total cross sections of vanadium and indium plotted vs the incident neutron energy. Each point is the average of at least three determinations of five measurements each. The total statistical error of every point is about 2.5% for vanadium and 2% for indium (Ref. 130).

the problem of finding an adequate interpretation for these resonances is still open to discussion.

D. Isomeric Ratios

Ratios of cross sections leading to two neighboring isomeric states have been used to complement our knowledge about the reaction mechanisms and especially to obtain information about the distribution of spins in the compound nucleus. The so-called spin cutoff factor $2\sigma^2$, present in the spin distribution of level densities,

$$(2J+1)\exp\left[-(J+\tfrac{1}{2})^2/2\sigma^2\right] \qquad (1.49)$$

enters as a crucial parameter in the calculation of isomeric ratios. Thus, if one assumes a compound nucleus mechanism for a specific reaction, the study of experimental isomeric ratios should yield information about this parameter.[132] This method is especially applicable for thermal neutron reactions, where the mechanism is purely a compound nucleus one.[133]

Isomeric ratios of fast neutron induced reactions were measured recently by Meadows *et al.*[134] and Brzosko *et al.*[135] The latter studied the so-called Levkovski effect[115] consisting in the regular decrease of the cross section with the increasing atomic number in (n, p) reactions on different isotopes. They found that a smaller variation in the ratio of Z/A (0.004 for tin and 0.007 for tellurium) than the one reported by Levkovski (0.009) is necessary to reduce the cross section by a factor of two.

Mangal and Gill[136] have measured the isomeric cross section ratios for several $(n, 2n)$ reactions at 14 MeV and compared them to the theory in order to obtain a best fit value of σ in the distribution (1.49). Using the calculations of Huizenga and Vandenbosh[132] and supposing dipole emission only, the value of the parameter σ for several nuclei around $A=100$ was calculated. All the obtained values cluster around 5 (e.g., for Sb^{123} $\sigma=4.5$). A similar analysis was performed by Kolar *et al.* for several neutron induced reactions in order to study the dependence of the isomeric ratios on the respective values of final angular momenta. In the (n, p) and (n, α) reactions studied all the metastates had considerably larger spins than the ground states. However, the measured isomeric ratios were all around unity. Thus the results of Brzosko *et al.*[135] could not be reproduced. Although the statistical model reproduces the experimental results fairly with a cutoff parameter σ corresponding to one-half of the rigid body moment of inertia, these results should be taken with some caution, since they are obtained assuming a very small number of de-excitation gamma rays (in fact $\nu=0$ was used throughout).

TABLE VII. Level densities of V^{51}, In^{115}, I^{127}, and Bi^{209} (see text).

Target nucleus	B_n (MeV)	a (MeV^{-1})	(N) (levels/MeV) for $E_n=4.0$ MeV
V^{51}	7.304	8.8	1.9×10^5
In^{115}	6.610	21.0	4.4×10^{11}
I^{127}	6.760	20.6	3.3×10^{11}
Bi^{209}	4.640	10.8	1.4×10^5

In two recent articles Vonach *et al.*[128] and Bishop *et al.*[139] have used the isomeric ratios in order to distinguish between two models of level densities, the Fermi gas and the superconductor model (see Secs. IA2 and IA3). Although the superconductor model predicts only a slight energy dependence of the nuclear temperature at low excitation energies, in agreement with some, but not all experimental results, the single-particle level densities required to reproduce the absolute values of the experimental nuclear temperatures are considerably smaller than expected. The superconductor model predicts a reduction from the rigid body moment of inertia which is consistent with isomeric ratios for nuclei with an odd number of nucleons.

The two models—a Fermi gas model modified to compensate for pairing interactions (the so-called "shifted" Fermi gas model) and the superconductor model have been used to calculate isomeric ratios for the reactions $Au^{127}(n, 2n)$ $Au^{126g,m}$ and $Cd^{116}(n, 2n)$ $Cd^{115g,m}$ for neutron energies from 12–17.5 MeV. For the first reaction excellent fits for σ_m/σ_g have been obtained with the Fermi gas model with $a=19$ MeV^{-1} ($a=15$ and 30 MeV^{-1} gave no agreement). However, in order to obtain any agreement with the superconductor model, the a value should be set below 15 MeV^{-1}, which is incompatible with other experimental results (Fig. 46). The situation is quite opposite for the reaction $Cd^{116}(n, 2n)$ $Cd^{115g,m}$. A reasonable fit is obtained with the superconductor model with $a=25$ MeV^{-1}, which is reasonable for this model,[140] and the Fermi gas requires $a=30$ MeV^{-1}, which is by far too large [Figs. 47(a) and (b)].

Neither of the models is able to explain satisfactorily all the experimental isomeric ratios. All the cases in which the Fermi gas model is satisfactory are odd–odd residual nuclei, while odd mass nuclei either agree well with the superconductor model or lie in between the two.

II. SCATTERING AND OPTICAL MODEL STUDIES

For the last decade, the elastic neutron scattering has been analyzed in terms of a complex potential.[141] Conversely, information about this potential has been extracted from these data and successfully used to fit neutron inelastic scattering and other nuclear processes. Gradually, the complex potential employed grew in complexity: the square well potential was abandoned in favor of the diffuse edged one[142] and spin orbit interaction has been added to it.[143] In the last few years the energy dependence of the optical model parameters has been, in a sense, circumvented by the use of nonlocal potentials[66] which give a good over-all

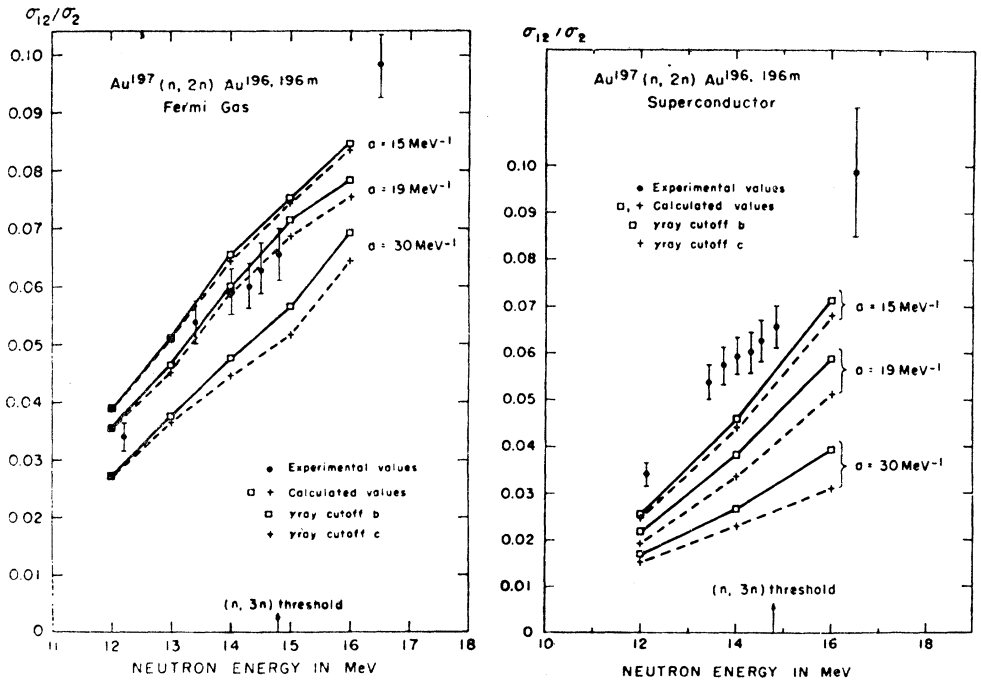

FIG. 46. Comparison of experimental isomeric cross section ratios for the Au^{196} isomers produced by the $Au^{197}(n, 2n)$ reaction with theoretical values calculated with (left) a Fermi gas model for two assumptions about the gamma ray cascade and for several values of the level density parameter a, and (right) a superconductor model for two assumptions about the gamma ray cascade and for two values of the level density parameter a. The effect of the number of gamma rays in a cascade appears to be negligible (Ref. 138).

fit for neutron cross sections over a wide range of energies and elements.

A. Formulation of the Problem

Optical model calculations are nowadays considered as the standard method of analysis of scattering data. They give the expressions necessary to compute the differential elastic cross sections, polarization, and total reaction cross sections. So far the optical model has been applied successfully to particles of spin 0, $\frac{1}{2}$, and 1 incident against 0-spin nuclei. The basic idea of the optical model in its simplest form is to substitute the intricate interaction in the nuclear system by a complex potential well which reproduces the main features of the absorption and the scattering of nuclear particles by atomic nuclei.

The formal statement of the problem[144] starts with the Schrödinger equation

$$[-(\hbar^2/2\mu)\nabla^2+U]\psi=E\psi, \qquad (2.1)$$

where μ and E are the reduced mass and the center of mass energy of incident particle. U is the optical potential that replaces the general particle–nucleus interaction:

$$U=U_{\text{coul}}(r)+U_{NR}(r)+iU_{NI}(r)+\{U_{SR}(r)+iU_{SI}(r)\}\hbar^2(\mathbf{s}\cdot\mathbf{L}). \qquad (2.2)$$

The terms in (2.2) that depend only on the distance r between particle and target are the Coulomb, the central real, the central imaginary, the spin–orbit real, and spin–orbit imaginary potential, respectively, while $\mathbf{s}$ and $\mathbf{L}$ represent, respectively, the spin and orbital angular momentum operators of the incident particle. The expression (2.2) can be amplified to include other terms, notably a tensor term for spin-1 particles,[145] but even the form (2.2) is often too complicated to be used. Equation (2.1) could, in general, be solved only numerically, with the aid of fast computers. Several computer programs, differing in the form factor of the assumed potentials are available.[144] The most commonly used form factors are:

—the Woods–Saxon potential[142] for the real central part

$$U_{NR}(r)=V[1+\exp(r-r_R)/a_R]^{-1}, \qquad (2.2a)$$

—a similar volume

$$U_{NI}(r)=W_V[1+\exp(r-r_I)/a_I]^{-1}, \qquad (2.2b)$$

or the surface potential for the imaginary central part

$$U_{NI}(r)=W_S\exp\{-[(r-r_I)/b]^2\}, \qquad (2.2c)$$

—and a Thomas term for the real and imaginary

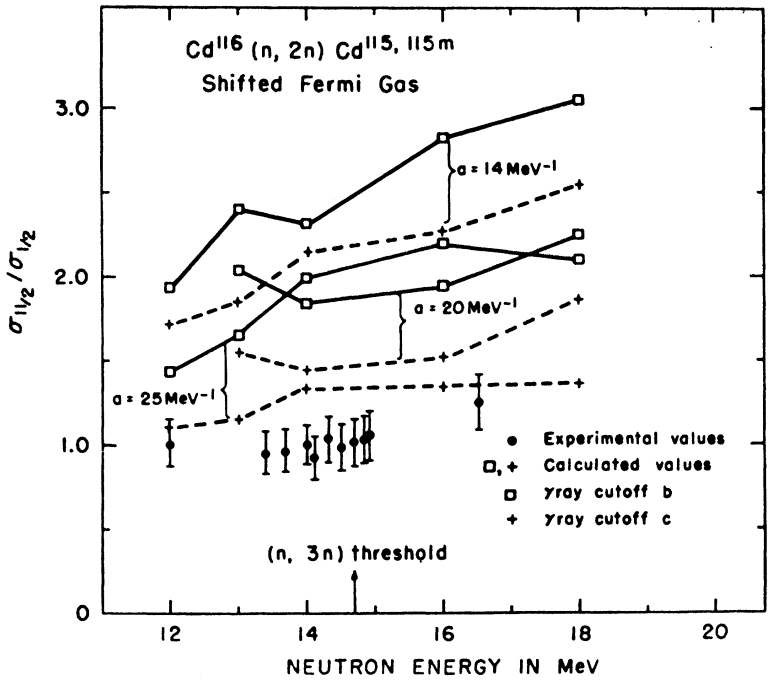

(a)

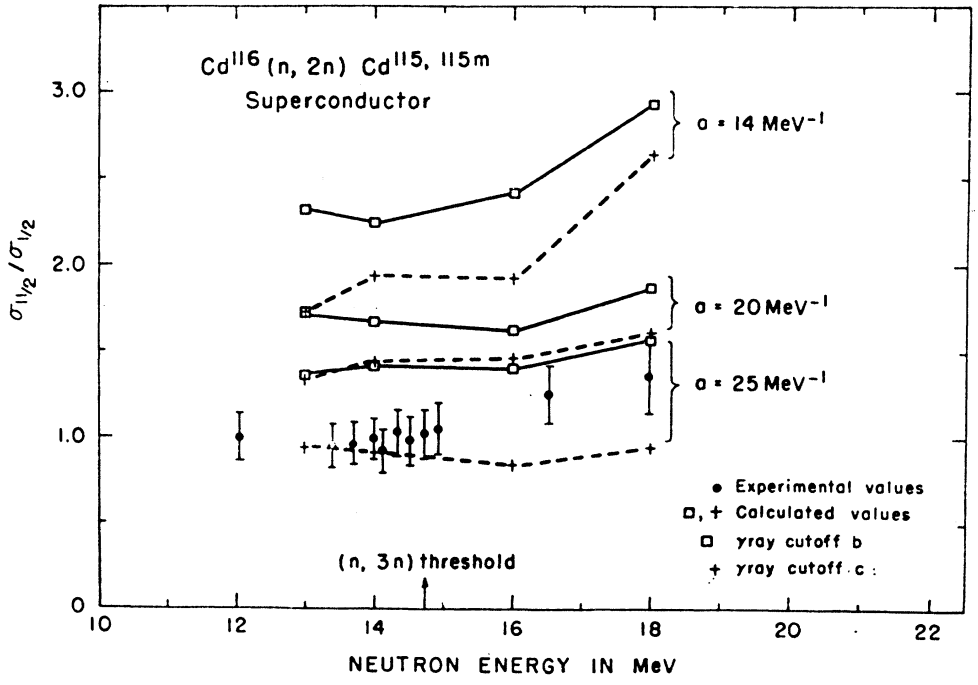

(b)

FIG. 47. (a) Comparison of the experimental isomeric cross section ratios $\sigma_{9/2}/\sigma_{1/2}$ for the Cd^{115} isomers produced by the $Cd^{116}(n, 2n)$ reaction with theoretical values calculated with a shifted Fermi gas model for two assumptions about the gamma ray cascade and for two values of the level density parameter a (Ref. 138). (b) Same as Fig. 47(a), with theoretical values calculated with a superconductor model for two assumptions about the gamma-ray cascade and for two values of the level density parameter a (Ref. 138).

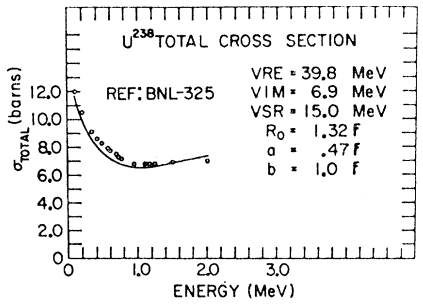

FIG. 48. Experimental and calculated (solid line) total neutron cross sections of U^{238}. The data are from Refs. 148–150. The calculated values are mostly within the 5% errors assigned to the data (Ref. 147).

parts of the spin–orbit potential

$$\left.\begin{matrix} U_{SR} \\ U_{SI} \end{matrix}\right\} = \left.\begin{matrix} V_{SO} \\ W_{SO} \end{matrix}\right\} \frac{2}{\hbar^2 r}\left[\frac{d}{dr}\left(\frac{1}{1+\exp\left[(r-r_{R,I})/a_{R,I}\right]}\right)\right]. \quad (2.2d)$$

Thus the optical potential, in its general form (2.2) allows for at least 11 free parameters, of which 6 can be listed as geometrical (the radii of the Coulomb, real, and imaginary potentials, respectively, and the three shape factors a_R, a_I, and b) and 5 as dynamical (the depths of central and spin–orbit potentials, respectively). Both in practice and in theory some of these parameters are related to each other.

The simple replacing of the nuclear interaction by a complex hole can lead to only the simplest results, i.e., the information that could be obtained from optical model calculations concerns a limited number of physical quantities, such as total cross sections, elastic scattering angular distributions, and polarization. The total cross section is given in terms of the absorption coefficients η_l while the differential cross sections are functions of the scattering amplitude too and differ according to the spins of the incident particles. The explicit formulas for these physical quantities are given in Ref. 144.

B. Comparison with Experimental Data

1. Elastic and Inelastic Scattering

Optical model analysis presently serves both for elastic scattering and total cross sections analysis and for producing input data in inelastic scattering and direct reactions. The inelastic scattering of neutrons has been described by Wolfenstein[14] and by Hauser *et al.*[15] in terms of the compound nucleus theory, while the direct inelastic scattering has been described by Banerjee[146] and others. Elements of the compound nucleus theory of inelastic scattering have been given in Sec. IA3, where the cross section for the transition to a particular state in the residual nucleus is given in terms of initial and final state spins and parities, and the transitions amplitudes are summed over all the accessible states in the compound nucleus. The factors governing the dynamics of the transitions are the particle penetrabilities T_l. The input data in inelastic scattering theories, the particle penetrabilities T_l, are determined from optical model analysis.

A complete set of data would hence comprise elastic and polarization angular distributions and total cross sections, from which optical model parameters can be extracted and used in fitting inelastic scattering data. Such a study has been performed by Auerbach *et al.*[147] who have made an extensive analysis of neutron scattering data between 0.1 and 3 MeV for several heavy elements in the region between Ta^{181} and U^{238}. As this region includes deformed nuclei also, it is not to be expected *a priori* that one will be able to fit the experimental data with a spherical optical potential. Using particle penetrabilities obtained from fitting the elastic scattering and total cross section data by the usual χ^2 method, Auerbach *et al.* have obtained good agreement

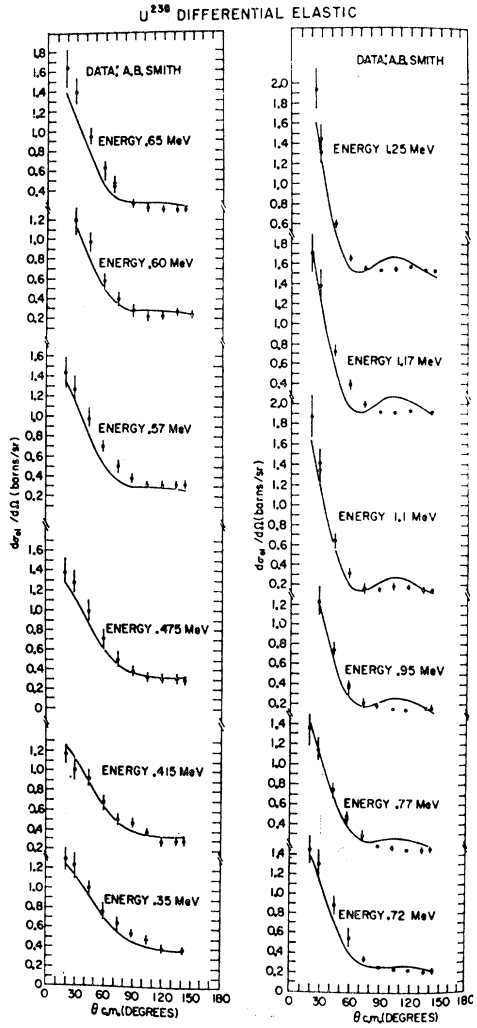

FIG. 49. Experimental and calculated (solid lines) differential elastic cross sections for U for parameters shown in Fig. 48. Calculated values include corrections for compound elastic scattering, using the Hauser–Feshbach theory (Ref. 147).

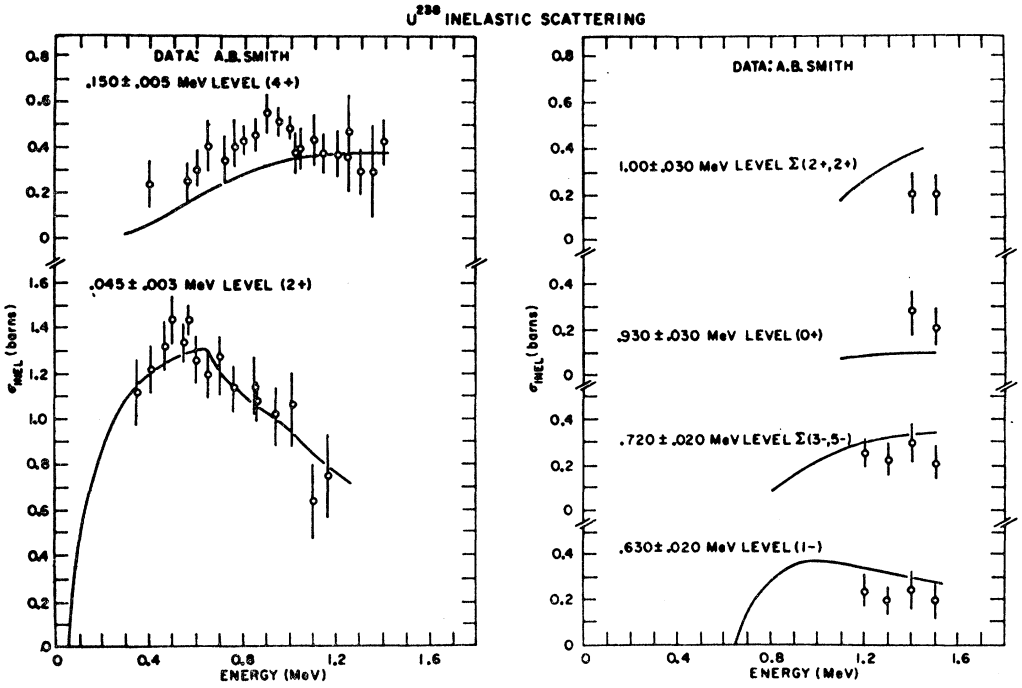

FIG. 50. Calculated values for inelastic scattering of neutrons by U^{238} using the Hauser–Feshbach theory and the optical model parameters determined by fitting the entrance channel data (Ref. 147).

for the inelastic scattering experiments on all the studied nuclei. A typical example of the fits is shown on Figs. 48–50 for the case of U^{238}. Optical model parameters calculated from fitting total cross sections (Fig. 48) and elastic differential cross sections (Fig. 49) were used to determine neutron penetrabilities $T_l(\epsilon)$ to be used as input data in the calculation of inelastic neutron scattering cross sections (Fig. 50).

A detailed inspection of the results of Auerbach *et al.*, shows that the over-all agreement is quite satisfactory. Inclusion of the spin orbit term appears necessary even at such low energies. However, no necessity has been found for the introduction of additional parameters such as different radii of the real and imaginary potential etc. No difference has been observed between spherical and nonspherical nuclei. Thus the optical model does not seem to be sensitive to such details of nuclear structure.[151]

Similar results, but without the additional cross check of total cross section calculations have been obtained by Gilboy *et al.*[152] for elastic and inelastic scattering of neutrons by iron, in the energy range 1–4 MeV. The elastic scattering data have been compared to the predictions of two types of optical potential. The surface absorption potential of Fernbach *et al.*[143] with an absorption depth up to 10 MeV generally yielded a better fit than the non local potential of Perey *et al.*[66] as can be seen from Fig. 51. The latter potential was used in its local energy-dependent approximation. The inelastic scattering angular distributions are all excellently fitted by the Hauser–Feshbach[15] theory using optical model penetrabilities from both the Perey *et al.*[66] and Fernbach *et al.*[143] models (cf. Fig. 52). It appears that the direct interaction contribution to inelastic scattering is negligible. An interesting feature is presented by the excitation function for the 1st excited state in Fe^{56}, which carries the bulk of inelastic scattering at these energies. Penetrabilities calculated from any of the two mentioned potentials did not fit too well this excitation function. Instead, only a strongly energy-dependent ($W_I \propto 1.75\epsilon_0$) imaginary part of the potential yielded acceptable fits.

The available data on absorption, scattering, and polarization by spherical nuclei have been analyzed by Moldauer for neutron energy below 1 MeV. A good fit is obtained with a diffuse surface model, having a sharply peaked absorptive shell at the surface. The comparison has been done through the strength function, Γ_n^0/D, since at very low energy the optical model total cross section approaches

$$\sigma_t = \alpha + \beta/E^{\frac{1}{2}} \tag{2.3}$$

with

$$\alpha = 4\pi R^2 \tag{2.3a}$$

and

$$\beta = 2\pi^2(\epsilon/k^2)(\bar{\Gamma}_n^0/D), \tag{2.3b}$$

where ϵ and k are the incident neutron energy and wave number, respectively, and R the effective radius of interaction. A similar analysis has also been performed by Elwyn *et al.*[154]

Valuable results on elastic and inelastic scattering of fast neutrons have also been obtained by Gilboy *et al.*[155]

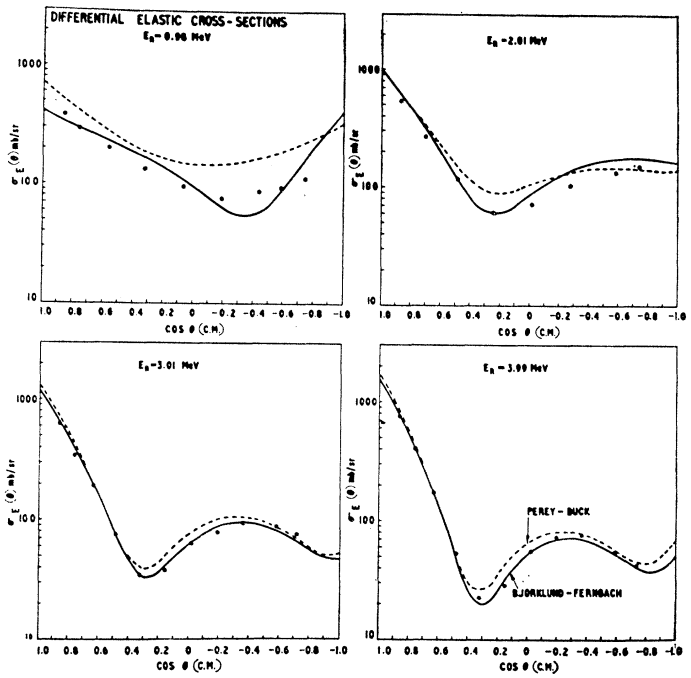

FIG. 51. Differential elastic cross sections for iron at 0.98, 2.01, 3.01, and 3.99 MeV, compared with the theoretical predictions for two types of optical potential: Fernbach *et al.*[143] (solid line) and Perey *et al.*[66] (dashed line). The over-all errors on the measured points are $\leqq 5\%$ (Ref. 152).

in an earlier article ($A=140$–178, $\epsilon_n=1$ MeV) and several other investigators.[156] Total cross sections on Li, U, and Pu isotopes, important in the comparison with neutron cross sections given by the optical model have been measured by MacGregor *et al.*[157]

2. *Polarization and Related Data*

Several references mentioned in the preceding section give also results on polarization of fast neutrons. Scattering of polarized neutrons has been reported by Bucher *et al.*,[158] Kent,[159] Wentzel *et al.*,[160] and Bredin.[161] Optical model analysis has been applied to the scattering of polarized neutrons from the D(d, n) He^3 and T(p, n) He^3 reactions in Refs. 159 and 161, respectively, and satisfactory results have been found in both cases. The angular distribution of elastic polarization of 2-MeV neutrons was found to be strongly element dependent[161] in the region of $A=30$ to 50. Although a surface peaked optical potential yielded excellent fits for all the elements, the sets of optical parameters used differed from element to element. This is hardly unexpected, since it is known that resonances in Al, Si, and Fe do exist. However the same set of parameters gave the best fit for all data (elastic and inelastic scattering and polarization) for each element separately.

Wagner *et al.*[162] have investigated the interaction of polarized and unpolarized 0.35-MeV neutrons with oriented Ho^{165} nuclei in order to search for a possible spin–spin interaction and to study the influence of the deformation of the Ho^{165} nucleus on the interaction. They found that the deformation has some effect on the total cross section of the oriented target. To determine the existence of a possible spin–spin interaction, the total cross section for parallel $\sigma_t^{\uparrow\uparrow}$ and antiparallel $\sigma_t^{\uparrow\downarrow}$ polarizations have been measured. The observed difference

$$\Delta\sigma=\sigma_t^{\uparrow\uparrow}-\sigma_t^{\uparrow\downarrow}$$

has been interpreted as indicating the existence of a spin–spin term to be added to the usual radial+spin–orbit potential.

$$-V_{SS}(\boldsymbol{\sigma}\cdot\mathbf{I})\{1+\exp[(r-r_0A^{\frac{1}{3}})/a]\}^{-1}. \quad (2.4)$$

To account for the observed difference in total cross sections a spin–spin potential depth value V_{SS} of

$$-0.06 \text{ MeV}<V_{SS}<0.13 \text{ MeV}$$

was necessary (Fig. 53). Thus a spin–spin interaction, if present, is practically negligible, since in this case it is less by about two orders of magnitude than the corresponding spin–orbit interaction ($V_{SO}=7.5$ MeV).[163] Other scattering data are discussed in the next chapter.[164,165]

We shall include an interesting application of fast neutron physics to the investigation of the structure of neutrons, which, traditionally is the domain of high-energy physics. This concerns the investigation of the electric polarizability of the neutron by means of small angle elastic scattering, reported by Aleksandrov *et al.*[164] and Walt *et al.*[165] Earlier measurements have shown that the elastic scattering of fast neutrons exhibits an unexpected increase as the angle of scattering is decreased below 15°. Because of its angular dependence this small angle effect could not be attributed either to nuclear or Schwinger scattering effects,[197] the former being a slowly varying function of angle and the latter

being confined to angles below about 2°. It has been suggested by Aleksandrov[164] that the small angle scattering might be produced by the interaction of the nuclear Coulomb field $\mathcal{E}$ with an induced dipole moment $\mathbf{p}=\alpha\mathcal{E}$ of the neutron. This interaction could produce an increase in the forward angle scattering cross section, the magnitude of the increase being dependent on the electric polarizability of the neutron. The analysis of Aleksandrov *et al.*[164] yielded a value of the polarizability $\alpha=8\times10^{-41}$ cm^3 that could account for the observed effects. The data of Walt *et al.*[165] fixed an upper limit for α,

$$\alpha\leq2\times10^{-40}\text{ cm}^3, \tag{2.5}$$

seemingly consistent with Aleksandrov's data and estimates from mesonic effects ($\alpha\doteq2\times10^{-41}$ cm^3). However, a reanalysis of Aleksandrov's data[164] showed that in order to account for the observed effects, a new value of α, equal to 5×10^{-40} cm^3, is required. This value is excluded by the limit (2.5). Thus it appears that the enhanced small angle scattering is not the effect of an induced dipole moment in the neutron.

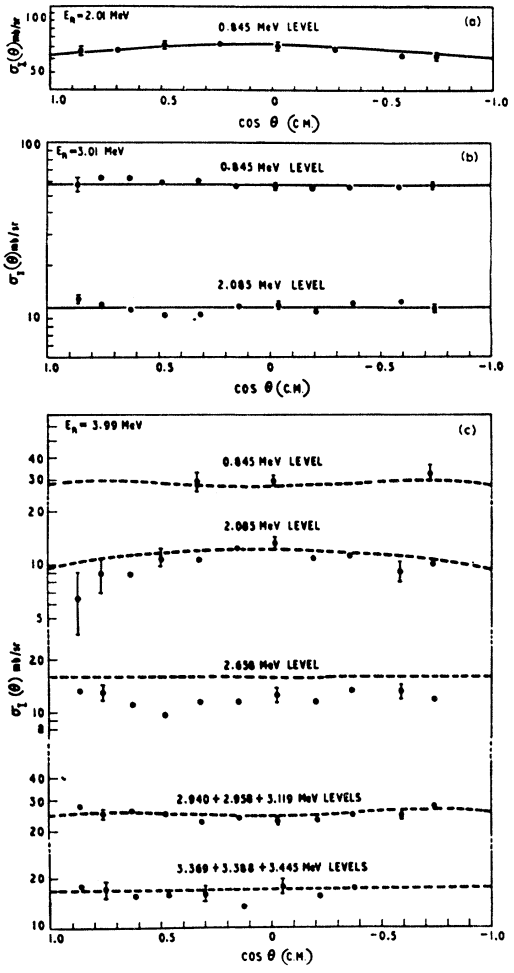

FIG. 52. Differential inelastic scattering cross sections of iron. (a) The 0.845-MeV level at $E_n=2.01$ MeV indicating typical over-all errors. (b) The 0.845- and 2.085-MeV levels at $E_n=3.01$ MeV. (c) Various levels at $E_n=2.99$ MeV. The dashed curves are Hauser–Feshbach[15] predictions (Ref. 152).

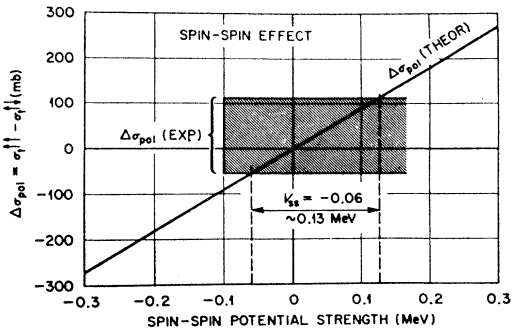

FIG. 53. Cross-section splitting due to a spin–spin interaction, and comparison with experiment (Ref. 162).

3. *Optical Model Data and Conclusions*

As mentioned earlier, the elastic and inelastic scattering and polarization data serve a twofold purpose: first the optical parameters could be extracted and then used as input parameters to fit inelastic scattering and other data. It appears from the preceding discussion that the compound nucleus theory combined with suitable optical model penetrabilities can account for most of the inelastic scattering data. The elastic scattering and polarization data, well fitted by the optical model itself may help to decide between the different forms of optical potentials used, notably the shape of the absorptive part and the depth of the spin–orbit interaction. It seems that consistently better fits are obtained by the use of a surface peaked imaginary potential.[166] No marked difference in favor of nonlocal potentials has been observed so far although an energy dependence of the parameters seems to be necessary.

The existence of shell model effects in the absorptive potential suggested by Lane[167] to account for the very small values of the S-wave strength functions observed in the mass region $A=90$–130 has been substantiated recently by Vonach *et al.*[168] The effect of a closed shell on the imaginary part of the potential can be explained as caused by the reduction of available absorption states near the closed shells. Hence the effects hould be especially large for doubly closed shells. The investigation in Ref. 168 was centered around the doubly closed shell $A=208$. A surface peaked optical potential with $V_{\text{real}}=46$ MeV, $W_{\text{imag}}=14$ MeV and $V_{\text{SO}}=7$ MeV was used. This potential gave good over-all fit to neutron scattering data over a wide range of nuclear masses. Good fit was thus obtained for Au^{197} but the agreement rapidly deteriorated when approaching bismuth (Bi^{209}) through mercury and thalium. However, if one allows W_{imag} to decrease from 14 MeV for Au^{197} to 5 MeV for Bi^{209}, the agreement is again restored.

The presence of spin–orbit interaction is generally considered as necessary in optical model analysis. There

are, however, considerable discrepancies as to its magnitude. In some of the analyses[166] the value of the spin–orbit potential was set equal to zero, but in general a value around 10 MeV is contained that accounts for most of the polarization measurements. Rahman Khan[169] has made an extensive calculation of the polarization of 0.38- and 0.98-MeV neutrons due to elastic scattering over a wide range of nuclei. The calculations generally account for the data and give a spin–orbit interaction strength consistent with the shell model requirements:

$$V_{SO}=7.5 \text{ MeV} \quad \text{for} \quad A<100.$$

$$V_{SO}=15 \text{ MeV} \quad \text{for} \quad A>100.$$

III. NUCLEAR STRUCTURE AND SPECTROSCOPY STUDIES

A. Investigation of Nuclear Levels

The classical method of investigating levels of excited nuclei at neutron binding energies has been the study of the interaction of nuclei with thermal neutrons. A series of interesting measurements has been done in the field of slow neutron capture in several elements[170–173] but we shall not discuss them.

It is well known that fast neutrons as bombarding particles are less suitable for the fine resolution experiments customary in spectroscopic studies. Nevertheless, they have some advantages in comparison to protons and alpha particles. The absence of charge enables the exploration of not too highly excited states and the interpretation of these results, especially for inelastic neutrons scattering is more straightforward than for charged particles. The analysis is performed in terms of either the Hauser–Feshbach[15] or a direct theory of scattering.[20]

Davis *et al.*[174] have investigated the disintegration of C^{12} and O^{16} by fast neutrons in a CO_2 filled ionization chamber. In the energy range below 9 MeV the only reaction leading to charged particles is the (n, α) reaction. While the cross section for the reaction $O^{16}(n, \alpha)$ C^{13} g.s. shows a strong resonant structure (21 resonances were observed in O^{17} in the energy range of $E_n=5.0-8.8$ MeV), no such structure has been observed in the $C^{12}(n, \alpha)$ Be^9 g.s. reaction. No plausible explanation of this phenomenon has been advanced.

The resonances in the lithium isotopes were investigated by studying the polarization and differential cross sections for neutrons scattered from Li^6 and Li^7 by Lane *et al.*[175] The scattering and the polarization of neutrons below 1.5 MeV are defined by the resonance at 0.25 MeV determined by $J^\pi=\frac{5}{2}^-$, corresponding to a Li^7 state at 7.47 MeV. For higher energies the experimental data vary smoothly with the incident energy. Similar data have been obtained for Li^7 and interpreted in terms of the nonlocal optical potential of Perey *et. al.*[66]

Donoghue *et al.*[176] have used the same method to investigate the parity and angular momenta of levels in O^{19} and N^{16} by measuring the elastic scattering of neutrons in a gas filled recoil counter. CO_2 (O^{18} enriched) and N^{15} were used, respectively. About a hundred angular distributions have been measured in the energy range of 0.4–2.7 MeV (Fig. 54). In the analysis, the cross sections were calculated from the phase shifts, using a formula for the elastic scattering of spin-$\frac{1}{2}$ particles on a spin-0 target derived by Bloch.[177] The phase shifts were calculated from Lane and Thomas.[178] The same phase shifts that fitted the distributions fitted the excitation functions too. The parity of states has been established from the asymmetry $(-)$ or symmetry $(+)$ of the angular distributions around $\pi/2$, while the values of the angular momenta J have been obtained in connection with total cross sections. The results are consistent with the shell model predictions of Elliott and Flowers.[179]

A new first excited state of P^{31} at 451 keV has been detected by means of the pick-up reaction on S^{32} by Colli *et al.*[180] From the angular distribution fitted by a $l=0$ curve (Fig. 55), the state is supposed to be a $\frac{1}{2}^+$. Since the level is strongly excited by a pick-up reaction, it should correspond to a hole excitation. This is not in agreement with the spherical shell model, which in this region predicts the angular momentum of the first excited hole state to be a $\frac{5}{2}$ state. A possible explanation might be the supposition of a negative deformation of nuclei with $A\sim30$.

The parities and angular momenta of several states in Fe^{56} have been determined by Donahue *et al.*[181] from the angular distributions of gamma rays from (n, n', γ) reactions using a model proposed by Satchler.[182] In each case good agreement has been obtained with the compound nucleus model.

A new level scheme of Y^{89} has been proposed by Schaffroth *et al.*[182] on the basis of the investigation of gamma ray spectra from the reaction $Y^{89}(n, n'\gamma)$. As the Hauser–Feshbach[15] fit to the excitation functions is very sensitive to the choice of spins, the excitation functions for several states have been measured, thus giving a stronger independent meaning to the ascribed spectral scheme.

A similar investigation was performed by Wagner,[183] who measured the excitation function of inelastic neutron scattering by the 2.3 MeV metastable state in Zr^{90} from threshold to 5 MeV, and found a sharp increase at 2.75 MeV possibly due to the missing 4^- state of the $(p_{1/2}, g_{9/2})$ configuration, equal in energy to the 3^- state observed hitherto at 2.75 MeV.

Precise measurements of total absorption cross sections of neutrons have been performed by Cabe *et al.*[184] in the energy range from 0.4–1.2 MeV and 3.6–5.2 MeV with a resolution of 3 keV for a number of elements.

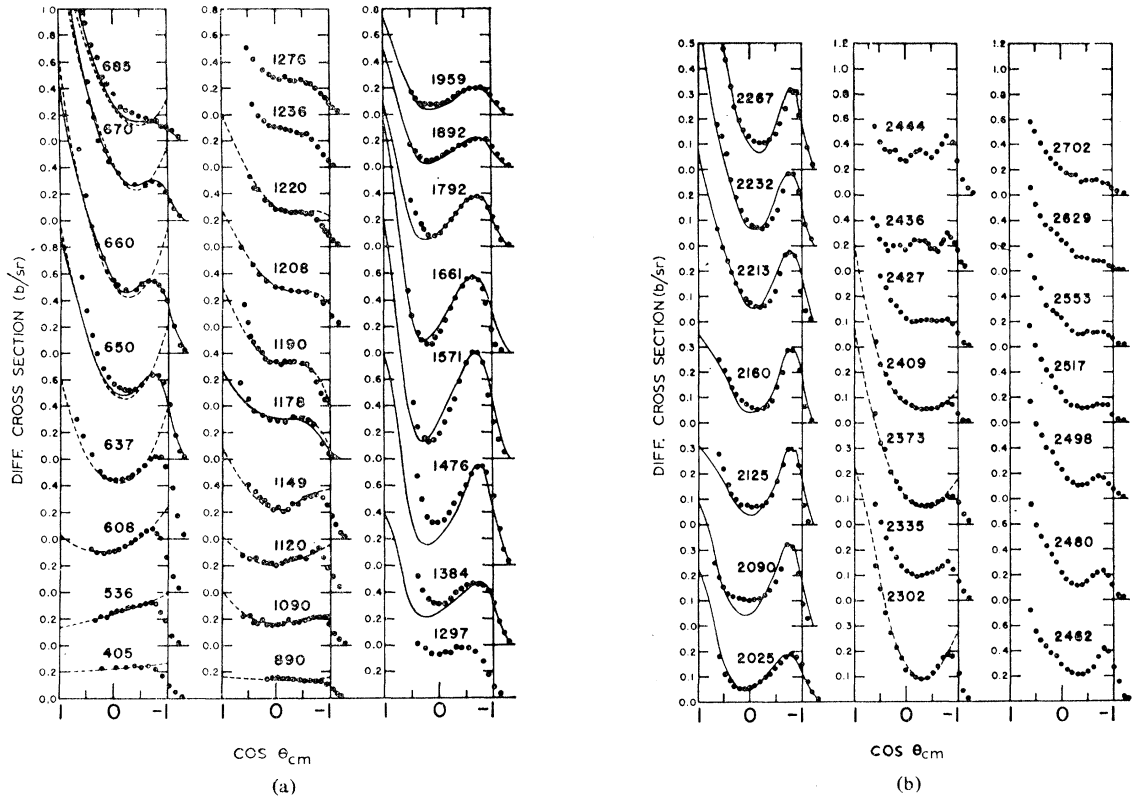

FIG. 54. Representative angular distributions of neutrons elastically scattered from O^{18} for neutron energies (a) below (b) above 2 MeV. The dashed curves represent angular distributions calculated using the phase shifts of Ref. 176. The solid curves represent calculated distributions into which an energy distribution function has been folded (Ref. 176).

A time-of-flight method has been used. These data present a set of valuable data concerning both the total cross sections and the spectroscopic information. A number of new levels, so far unknown, has been found and their angular momenta established using the Breit–Wigner formula. Similar measurements have been presented also by Vaughn *et al.*[185]

B. Nuclear Structure Investigations

Low-energy nuclear reactions have become a tool of increasing importance in the investigation of the nuclear structure. This concerns especially the studies of cluster model configurations and the structure of the nuclear surface.

Bouchez *et al.*[186] have measured the scattering of 14-MeV neutrons from the 7.65-MeV level in C^{12}. The angular distribution exhibits a strong forward maximum and a minimum at $\theta=45°$, suggesting a direct interaction process for $0^+\rightarrow 0^+$ monopole excitation. It is possible to connect this monopole transition to the excitation of an alpha cluster. According to Peele[187] and Wildermuth[188] the angular distribution of inelastically scattered neutrons would in this case take the form

$$\sigma(\theta) \propto j_0^2(kR), \tag{3.1}$$

where j_0 is the zeroth-order spherical Bessel function, k the momentum transfer to the C^{12} nucleus, and R the interaction radius (Fig. 56). The comparison between the experimental curve and the Bessel function is encouraging, although the backward rise should be treated with distorted waves and configuration mixing. The purely backward angular distributions in the reaction O^{16} (n, α) C^{13} (heavy-particle stripping)[29] are a strong additional argument for a four alpha cluster structure of O^{16}.

Some implications about the structure of the nuclear surface can be obtained from the study of (n, α) reactions. Data about nuclear matter at high densities are available from high-energy electron scattering. Far away from the nuclear center the nuclear density decreases. Two alternatives are, however, possible.

(i) as the distance between nucleons increases, the tendency of the nucleons to cluster is not higher than implied by statistics;

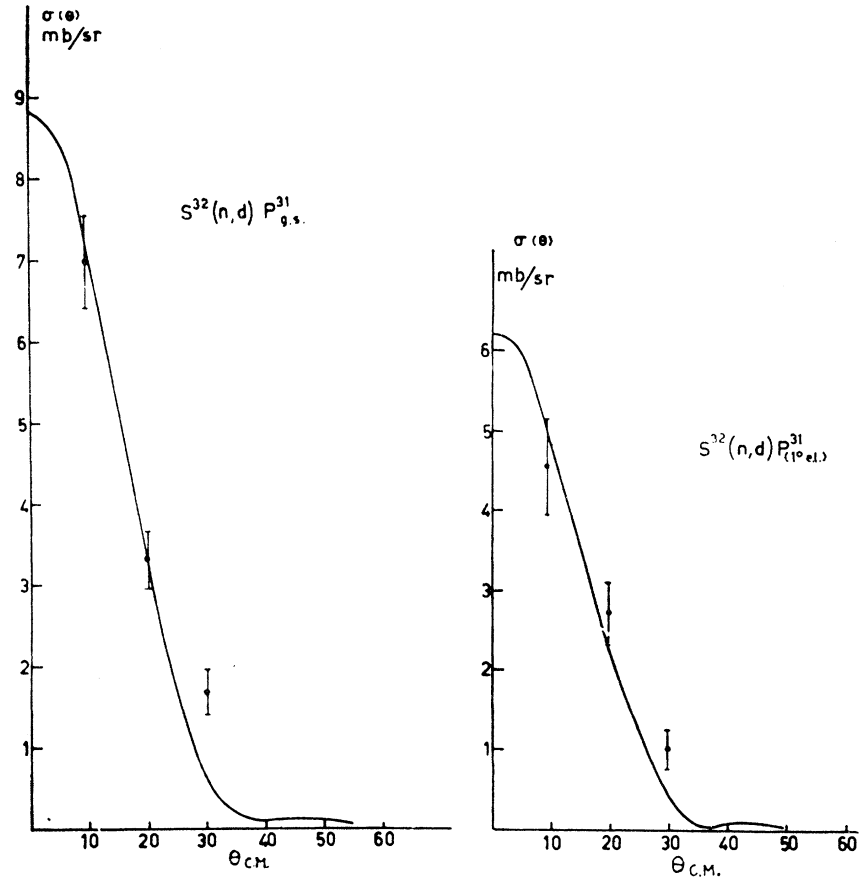

FIG. 55. Angular distribution of deuterons from the reaction $S^{32}(n, d)P^{31}$ ground and first excited states. The full curve has been calculated by the plane wave theory (Ref. 180).

(ii) in spite of the decrease of the over-all density, local densities may attain very high values, i.e., the clustering probability increases.

Hodgson[189] and Wilkinson[190] point out that reactions leading to complex nuclei can be used for the investigation of the texture of the nuclear surface. Using the model proposed by Hodgson, Osakiewicz *et al.*[191] and Kulišić *et al.*[83] have investigated (n, α) reactions on heavy nuclei at 14 MeV in order to calculate the probability of alpha clustering on the nuclear surface. This reaction proceeds through a direct process, (Ref. 60 and others) and, due to the small mean free path of alpha particles in nuclear matter, through a surface interaction. Thus the process might be understood as taking place in a thin layer of the nuclear surface, with the incoming neutron knocking off an alpha particle present on the nuclear surface. Assuming a certain distribution of nuclear matter density on the surface, one can calculate the maximum number N_α of alpha particles that can be built up by the nucleons present on the surface,[192] defined arbitrarily as the region with $\rho<\frac{1}{2}\rho_0$. Then the actual number N of alpha particles present at any time on the surface will be

$$N=pN_\alpha,$$

where p is the fraction of its time that a nucleon on the surface spends incorporated in an α-particle cluster. p is in essence the probability of clustering. Assuming that the (n, α) process proceeds in complete analogy to free neutron–alpha scattering and taking into account

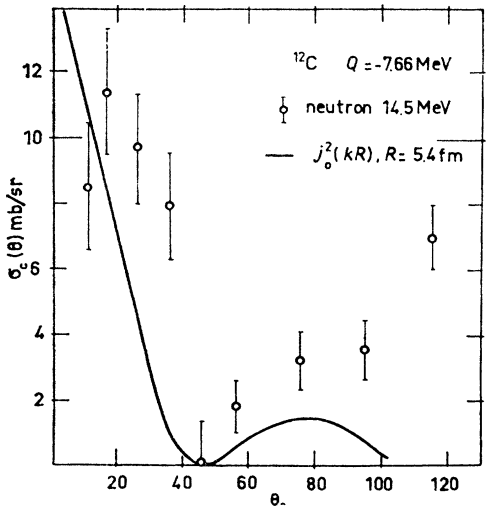

FIG. 56. The experimental angular distribution of 14-MeV neutrons scattered by the 7.65-MeV state in C^{12} and a comparison with a $j_0^2(kR)$ Bessel function (Ref. 186).

that the short mean free path of alphas in nuclear matter prevents its emission *through* the nucleus, the total cross section for the (n, α) reaction can be written as follows (Fig. 57)

$$\sigma(n, \alpha)=\int_V\int_{\theta_1}^{\theta_2}\int_{\phi_1(\theta)}^{\phi_2(\theta)}\gamma p N_\alpha \sigma(\theta)\sin\theta\, d\phi\, d\theta\, dV, \quad (3.2)$$

where γ is the neutron attenuation coefficient in the nucleus, connected with the neutron mean free path λ by[193]

$$\gamma=\exp x/\lambda \quad (3.2a)$$

and $\sigma(\theta)$ the differential cross section for free neutron–alpha scattering. It was estimated that the latter value was 6.4 mb in the energy region where α's were observed.[194] Thus, knowing the experimental (n, α) cross sections at 14 MeV, the quantity p, i.e., the fraction of time a nucleon spends in an alpha-particle configuration can be deduced. The values of p obtained are listed in Table VIII. They are in fair agreement with values obtained by Hodgson[189] and Gauvin[195] for (p, α) reactions.

This way of calculating p can be criticized on the basis of its crudity, and also on other grounds, e.g., the presence of pick-up mechanisms in (n, α) reactions. The first criticism can be mitigated by the fortunate circumstance that the different approximations used in the calculation (3.2) have opposite effects, thus tending to cancel each other.[83] The assumption of a free (n, α) scattering cross section for the collision cross section in nuclear matter and the neglection of the effects of the Pauli principle (prohibiting certain collisions) will certainly decrease the value of p. On the other hand, equating the experimental total (n, α) cross section to the knock-out one certainly minimizes the latter, since some alphas, stemming from other mechanisms of production are counted too; consequently this will tend to increase the value of p (see Fig. 57). Secondary collisions, if present, will have the same effect. As far as the presence of pick-up processes is concerned, several arguments listed by Wilkinson[190] and Lalović *et al.*[84] show that the probability for the formation of a He^3 cluster on the nuclear surface is small compared to that of He.[4]

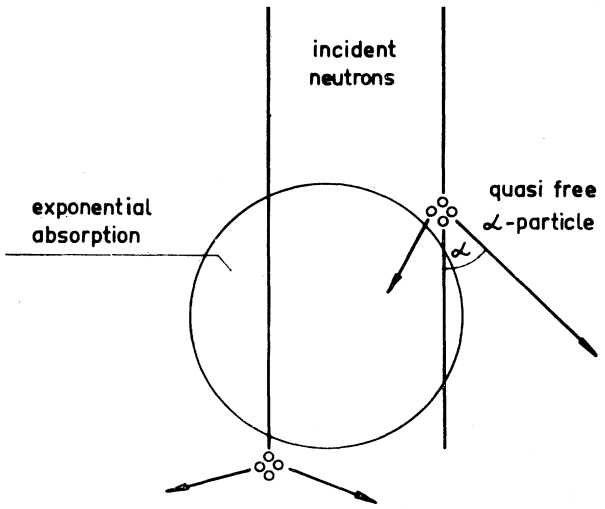

FIG. 57. The process of knocking-out alpha particles from the nuclear surface (Ref. 191).

TABLE VIII. The fraction of its time, p, that a surface nucleon spends incorporated in an alpha cluster.

Reaction	p	Reference
$La^{139}(n, \alpha)$	0.4 0.3	83 191
$Pr^{141}(n, \alpha)$	0.4	83
$Tb^{159}(n, \alpha)$	0.3	83
$Bi^{209}(n, \alpha)$	0.1	83

It has to be nevertheless stressed that the calculations based on Eq. (3.2) yield consistently similar values of p, that are, moreover, in good agreement with values of p obtained by other means.[190]

Structure of alpha and other types discussed in the previous section are obviously of dynamical nature. Following an argument of Serebrennikov[196] one could, along the same lines, calculate the lifetime of an alpha cluster on the nuclear surface. This method is based on the shape of the respective alpha spectra.

In the case of dynamical, decaying alpha structures the static spectrum $N_0(\epsilon)$ of the emitted alpha particles is modified by an exponential factor

$$N(\epsilon)=N_0(\epsilon)\exp(-t_{\text{eff}}/\tau_\alpha), \quad (3.3)$$

where t_{eff} is the effective time the alpha particle spends in traveling to the nuclear surface,

$$t_{\text{eff}}=l/v=\{m_\alpha/2(\epsilon+U)\}^{\frac{1}{2}}l \quad (3.3a)$$

given in terms of the mass m_α, the outgoing energy ϵ and the shell model potential U of the alpha cluster, and its average shortest distance to the nuclear surface, l. The effect of the exponential factor in expression (3.3) will be to cut off the spectrum of alpha particles at much higher energies than predicted by the Coulomb and optical penetrabilities solely. References 83 and 84 in fact report spectra that are sharply cut off at alpha energies around 17 MeV, while the respective penetrabilities at this energy are around 0.5 (Ref. 9). Assuming reasonable values for the parameters in (3.3a) one obtains lifetimes τ_α of the order of 0.5×10^{-22} seconds. Now, 10^{-22} sec is of the order of transit time of 20-MeV nucleons in nuclei. There is a fair chance that a fast nucleon moving in the nucleus will hit at

least one alpha cluster and dissolve it. Our result is not contradictory to this interpretation.

Although the model of Serebrennikov[196] succeeds in explaining the absence of alpha particles around Coulomb barrier energies it fails completely when applied to the higher energy part of the spectrum. In fact, instead of the slow rise determined by the square root of the energy, one has a sharp increase of the number of particles[83] unexplainable in terms of this model.

There is no doubt that calculations of this kind do not include a series of effects and cannot be taken very seriously. However, they still give simple straightforward pictures that yield information in rough accordance with that expected on the basis of more refined and sophisticated models.

REFERENCES

[1] T. Ericson, Advan. Phys. **9,** 425 (1960).
[2] N. Bohr, Nature **137,** 344 (1936).
[3] V. F. Weisskopf, Helv. Phys. Acta **23,** 187 (1950).
[4] H. A. Bethe, Rev. Mod. Phys. **9,** 69 (1937); Phys. Rev. **57,** 1125 (1940).
[5] D. H. Ewing and V. F. Weisskopf, Phys. Rev. **57,** 472, 935 (1940).
[6] J. Blatt and W. F. Weisskopf, *Theoretical Nuclear Physics* (John Wiley & Sons, Inc., New York, 1955).
[7] K. K. Seth, R. M. Vilenzick, and T. A. Griffy, Phys. Letters **11,** 308 (1964).
[8] G. S. Mani, M. A. Melkanoff, and I. Iori, Rapport CEA No. 2379 (1963).
[9] J. Huizenga and G. Igo, ANL Report 6373.
[10] G. S. Mani, M. A. Melkanoff, and I. Iori, Rapport CEA, No. 2380 (1963).
[11] E. Erba, U. Facchini, and E. Saetta Mehichella, Nuovo Cimento **22,** 1237 (1961).
[12] A. G. W. Cameron, Can. J. Phys. **36,** 1040 (1958).
[13] A. Bohr, B. R. Mottelson, and R. Pines, Phys. Rev. **110,** 936 (1958); R. Lang, Nucl. Phys. **42,** 353 (1963).
[14] L. Wolfenstein, Phys. Rev. **82,** 690 (1951).
[15] W. Hauser and H. Feshbach, Phys. Rev. **87,** 366 (1952).
[16] H. Goldstein, in *Fast Neutron Physics,* edited by J. B. Marion and J. L. Fowler (Interscience Publishers, Inc., New York, 1963), Vol. II, p. 1525.
[17] J. M. Blatt and L. C. Biedenharn, Rev. Mod. Phys. **24,** 258 (1952); L. C. Biedenharn and A. Simon, "Revised *Z* Tables of Racah Coefficients," ORNL Report 1501 (1952) and ORNL 1501—Suppl. (1954).
[18] J. Blair, "Inelastic Excitation of Collective Levels," in *Lectures on Nuclear Interactions* (Herceg Novi, Yugoslavia, 1962), Vol. II, p. 1.
[19] N. Austern, "Direct Reaction Theories," in *Fast Neutron Physics,* edited by J. B. Marion and J. Fowler (Interscience Publishers, Inc., New York, 1963), Vol. II, p. 113.
[20] S. T. Butler and A. H. Hittmair, *Nuclear Stripping Reactions* (John Wiley & Sons, Inc., New York, 1957).
[21] N. Glendenning, Ann. Rev. Nucl. Sci. **13,** 191 (1963).
[22] G. E. Brown and H. Muirhead, Phil. Mag. **2,** 473 (1957).
[23] S. T. Butler, Proc. Roy. Soc. (London) **208A,** 559 (1951); Phys. Rev. **106,** 272 (1957).
[24] K. Izumo, Progr. Theoret. Phys. (Kyoto) **26,** 807 (1961).
[25] H. Feshbach, Ann. Phys. (N.Y.) **5,** 357 (1958); **19,** 287 (1962); B. Block and H. Feshbach, Ann. Phys. (N.Y.) **23,** 47 (1963); C. M. Shakin, Ann. Phys. (N.Y.) **22,** 373 (1963); A. Karman, Rodberg, and Young, Phys. Rev. Letters **11,** 422 (1963); R. H. Lemmer and C. M. Shakin, Ann. Phys. (N.Y.) **27,** 13 (1964).
[26] K. J. Le Couteur, Phys. Letters **11,** 53 (1964).
[27] N. Cindro, "Total Cross Section Measurement and Analysis," in *Lectures on Nuclear Interactions* (Herceg Novi, Yugoslavia, 1962), Vol. II, p. 290.
[28] B. Sen, Nucl. Phys. **41,** 435 (1963).
[29] M. L. Chatterjee and B. Sen, Nucl. Phys. **51,** 583 (1964).
[30] R. A. Al Kital and R. A. Peck, Jr., Phys. Rev. **130,** 1500 (1963).
[31] M. L. Chatterjee, Nucl. Phys. **65,** 635 (1963).
[32] D. T. Stewart and P. W. Martin, Nucl. Phys. **60,** 349 (1964).
[33] G. R. Satchler, Phys. Rev. **104,** 104 (1956).
[34] R. Batchelor and J. H. Towle, Nucl. Phys. **47,** 385 (1963).
[35] V. Valković, Nucl. Phys. **54,** 465 (1964); **60,** 581 (1964).
[36] M. R. Zatzik and D. R. Moxon, Phys. Rev. **129,** 1728 (1963).
[37] C. R. Lubitz, "Numerical Table of Butler Born Approximation Stripping Cross Sections" (University of Michigan, 1957).
[38] D. Kovač (private communication).
[39] G. Calvi *et al.*, Nucl. Phys. **39,** 621 (1962); **48,** 408 (1963).
[40] G. Calvi, A. S. Figuera, and R. Potenza, *Proceedings International Conference on Nuclear Physics, Paris* (Dunod & Cie., Paris, 1964).
[41] J. N. Massot, E. El Baz, and J. Lafoucriere, Nucl. Phys. **58,** 273 (1964).
[42] U. Facchini *et al.*, Phys. Letters **1,** 6 (1962).
[43] M. G. Marcazzan, F. Merzari, and F. Tonolini, Phys. Letters **1,** 21 (1962).
[44] M. G. Marcazzan, F. Tonolini, and L. Zetta, Nucl. Phys. **46,** 51 (1963).
[45] G. Anderson Lindström, Z. Naturforsch. **17a,** 238 (1962).
[46] R. Bass, U. Fanger, and F. Saleh, Nucl. Phys. **56,** 569 (1964).
[47] E. A. Davis, Nucl. Phys. **55,** 643 (1964).
[48] W. Patzak and H. Vonach, Nucl. Phys. **39,** 263 (1953).
[49] O. N. Koul, Nucl. Phys. **55,** 127 (1964).
[50] I. Turkiewicz *et al.*, Nucl. Phys. **77,** 276 (1966).
[51] E. Saetta Menichella, F. Tonolini, and L. Tonolini-Severgnini, Nucl. Phys. **51,** 449 (1964); E. Campbell *et al.*, MIT Report No. 73 (1960).
[52] M. Shapiro, Phys. Rev. **90,** 171 (1953).
[53] U. Seebeck and M. Bormann, Nucl. Phys. **68,** 387 (1965).
[54] N. Cindro *et al.*, Proc. 2nd Polish–Yugoslav Symposium on Nuclear Physics, Cracow, 1963.
[55] J. Csikai, J. Baczo, and A. Doroczi, Nucl. Phys. **41,** 141 (1963).
[56] M. Irfan and W. Jack, Proc. Phys. Soc. (London) **47,** 225 (1963).
[57] C. J. D. Jarwis, W. R. Dixon, and R. S. Storey, Nucl. Phys. **44,** 680 (1963).
[58] W. R. Dixon and R. S. Storey, Phys. Letters **5,** 208 (1963).
[59] I. Kumabe *et al.*, Phys. Rev. **106,** 155 (1957).
[60] K. Debertin and E. Rossle (unpublished).
[61] D. B. Thomson, Phys. Rev. **129,** 1649 (1963).
[62] P. Huber *et al.*, Phys. Letters **5,** 202 (1963).
[63] S. G. Buccino *et al.*, Nucl. Phys. **60,** 17 (1964).
[64] K. K. Seth, R. M. Wilenzick, and T. A. Griffy, Phys. Letters **11,** 308 (1964).
[65] R. M. Wilenzick *et al.*, Nucl. Phys. **62,** 511 (1965).
[66] F. G. Perey and B. Buck, Nucl. Phys. **32,** 353 (1962).
[67] T. D. Newton, Can. J. Phys. **34,** 804 (1956).
[68] P. F. A. Klinkenberg, Rev. Mod. Phys. **24,** 63 (1952).
[69] D. W. Lang, Nucl. Phys. **26,** 434 (1961).
[70] P. Kulišić *et al.*, Nucl. Phys. **54,** 17 (1964).
[71] K. J. Le Couteur, Proc. Phys. Soc. (London) **465,** 718 (1952).
[72] N. O. Lassen, Nucl. Phys. **19,** 579 (1960).
[73] V. A. Sidorov *et al.*, Nucl. Phys. **35,** 253 (1963).
[74] R. H. Holbrow and H. H. Barschall, Nucl. Phys. **42,** 264 (1963).
[75] D. Bodansky, Ann. Rev. Nucl. Sci. **12,** 107 (1962).
[76] T. D. Thomas, Nucl. Phys. **53,** 558, 577 (1964).
[77] C. Hurwitz *et al.*, Nucl. Phys. **54,** 65 (1964).
[78] W. R. Dixon, Nucl. Phys. **42,** 27 (1963).
[79] J. C. Robertson, Nucl. Phys. **49,** 306 (1963).
[80] H. S. Hans and R. K. Mohindra, Nucl. Phys. **47,** 473 (1963).
[81] P. Cuzzocrea, S. Notarrigo, and A. Rubbino, Nucl. Phys. **55,** 364 (1964).
[82] D. Veselić *et al.* (private communication).
[83] P. Kulišić *et al.*, Nucl. Phys. **73,** 548 (1965).
[84] B. Lalović *et al.*, *Proceedings of the International Conference on Nuclear Physics, Paris* (Dunod & Cie., Paris, 1964).
[85] U. Facchini *et al.*, Nucl. Phys. **51,** 460 (1964).
[86] E. Rössle (to be published).
[87] W. Maussberg and E. Rössle, Conf. on Solid State Detectors in Nuclear Physics, Liege, September 1963.

[88] R. Batchelor, W. B. Gilboy, and J. H. Towle, Nucl. Phys. **65,** 236 (1965).
[89] A. Adam *et al.*, Nucl. Phys. **49,** 489 (1963).
[90] H. Jeremie, Nucl. Phys. **47,** 225 (1963).
[91] H. Neuert and H. Pollehn, *Tables of Neutron Cross Sections*, EUR 122e, 1963; A. Chatterjee (to be published).
[92] M. Cox, Phys. Rev. **133,** 1337B (1964).
[93] P. Cuzzocrea and G. Pappalardo, Nucl. Phys. **48,** 656 (1963).
[94] R. Potenza, R. Ricamo, and A. Rubbino, Nucl. Phys. **41,** 298 (1963).
[95] J. M. F. Jeronimo *et al.*, Nucl. Phys. **47,** 225 (1963).
[96] Other recent total cross-section measurements: G. C. Bonazzola *et al.*, Nucl. Phys. **51,** 337 (1964). J. Csikai, B. Guyarmati, and I. Hunyadi, Nucl. Phys. **46,** 141 (1963). B. Grimeland and P. Opsahl-Andersen, Nucl. Phys. **51,** 302 (1964). B. Grimeland, E. Kjellsby, and J. Vines, Phys. Rev. **137,** B878 (1963). N. K. Majumdar and A. Chatterjee, Nucl. Phys. **41,** 192 (1963). J. Picard and C. F. Williamson, Nucl. Phys. **63,** 673 (1965). S. R. Salisbury, D. B. Fossan, and F. J. Vaughn, Nucl. Phys. **64,** 343 (1965). H. Spenke, Nucl. Phys. **51,** 329 (1964).
[97] J. Csikai *et al.*, Phys. Letters **4,** 33 (1963).
[98] M. Bormann *et al.*, Z. Physik **174,** 1 (1963).
[99] D. L. Allen, Nucl. Phys. **24,** 274 (1961).
[100] I. L. Preiss and R. W. Fink, Nucl. Phys. **15,** 326 (1960).
[101] G. S. Mani and M. A. Melkanoff, in *Proceedings of the International Conference on Direct Interactions, Padua, 1962* (Interscience Publishers, Inc., New York, 1962).
[102] R. J. Howerton, UCRL Report 5226 (1958).
[103] E. B. Paul and R. L. Cloake, Can. J. Phys. **31,** 267 (1953).
[104] D. L. Allen, Proc. Phys. Soc. (London) **A70,** 195 (1957). L. Allen *et al.*, Phys. Rev. **107,** 1363 (1957).
[105] H. Liskien and A. Paulsen, Nucl. Phys. **63,** 393 (1965).
[106] L. A. Rayburn, Phys. Rev. **130,** 731 (1963).
[107] D. W. Ban, I. C. Browne, and J. S. Gillmore, Phys. Rev. **123,** 859 (1961).
[108] H. Büttner, A. Lindner, and H. Meldner, Nucl. Phys. **63,** 615 (1965).
[109] D. G. Gardner and Yu-Wen Yu, Nucl. Phys. **60,** 49 (1964).
[110] A. Chatterjee, Nucl. Phys. **47,** 511 (1963); **49,** 686 (1963). A. Chatterjee, Phys. Rev. **134,** B374 (1964).
[111] A. Chatterjee, Nucl. Phys. **60,** 273 (1964).
[112] M. Bormann, Nucl. Phys. **65,** 257 (1965).
[113] E. Erba, U. Facchini, and E. Saetta-Menichella, Nuovo Cimento **22,** 1237 (1961).
[114] P. Strohal, N. Cindro, and B. Eman, Nucl. Phys. **30,** 49 (1962).
[115] V. Levkovski, Zh. Eksperim. i Teor. Fiz. **33,** 1520 (1957) [English transl.: Soviet Phys.—JETP **6,** 1154 (1958)].
[116] D. G. Gardner, Nucl. Phys. **29,** 373 (1962). D. G. Gardner and A. Poularikis, Nucl. Phys. **35,** 303 (1962).
[117] N. Rosenzweig, Phys. Rev. **108,** 817 (1957).
[118] A. Rubbino and D. Zubke, Phys. Letters **11,** 333 (1964).
[119] J. E. Brolley, Jr., *et al.*, Phys. Rev. **99,** 330 (1953).
[120] G. S. Mani *et al.*, Nucl. Phys. **19,** 535 (1960).
[121] M. Bormann *et al.*, J. Phys. Radium **22,** 62, 602 (1961).
[122] M. Bormann, Nucl. Phys. **65,** 257 (1965).
[123] E. T. Bramlitt and R. W. Fink, Phys. Rev. **131,** 2649 (1963).
[124] J. Csikai *et al.* (private communication).
[125] K. K. Seth, Phys. Letters **16,** 306 (1965).
[126] J. Csikai (to be published).
[127] R. Cabe *et al.* (to be published).
[128] For the interpretation of total cross-section fluctuations in light elements see: P. Strohal *et al.*, Phys. Letters **10,** 104 (1964); N. Cindro, P. Kulišić, and P. Strohal, Phys. Letters **6,** 205 (1963).
[129] A. J. Elwyn *et al.*, Nucl. Phys. **59,** 113 (1964).
[130] F. Manero, Nucl. Phys. **65,** 419 (1965).
[131] D. Stüwer, H. Gentz, and M. Bormann, Nucl. Phys. **62,** 165 (1965).
[132] J. R. Huizenga and R. Vandenbosch, Phys. Rev. **120,** 1305 (1960).
[133] B. Keisch, Phys. Rev. **129,** 769 (1963).
[134] J. W. Meadows and J. F. Whalen, Phys. Rev. **130,** 2022 (1963).
[135] J. Brzosko, P. Decowski, and Z. Wilhelmi, Nucl. Phys. **45,** 579 (1963).
[136] S. K. Mangal and P. S. Gill, Nucl. Phys. **49,** 510 (1963).
[137] Z. Kolar, P. Strohal, and N. Cindro, J. Inorg. Nucl. Chem. **27,** 2471 (1965).
[138] H. K. Vonach, R. Vandenbosch, and J. R. Huizenga, Nucl. Phys. **60,** 70 (1964).
[139] C. T. Bishop, H. K. Vonach, and J. R. Huizenga, Nucl. Phys. **60,** 241 (1964).
[140] The superconductor model gives, in general, larger values for the level density parameter a than the Fermi gas model.
[141] H. Feshbach, C. E. Porter, and V. F. Weisskopf, Phys. Rev. **97,** 448 (1954).
[142] R. W. Woods and D. S. Saxon, Phys. Rev. **95,** 577(L) (1954).
[143] S. Fernbach, W. Heckrotte, and J. V. Lepore, Phys. Rev. **97,** 1059 (1955); F. Björklund and S. Fernbach, Phys. Rev. **109,** 1295 (1958).
[144] M. A. Melkanoff, J. Roynal, and T. Sawada, in *Methods of Computational Physics*, edited by B. Alder, S. Fernbach, and M. Rotenberg (Academic Press Inc., New York, to be published) Vol. V.
[145] J. Raynal, Phys. Letters **3,** 331 (1963); **7,** 281 (1963).
[146] M. K. Banerjee, "Theory of Stripping and Pickup Reactions," in *Nuclear Spectroscopy*, edited by F. Ajzenberg-Selove (Academic Press Inc., New York, 1960).
[147] E. H. Auerbach and S. O. Moore, Phys. Rev. **135,** B895 (1964).
[148] D. J. Hughes and R. B. Schwartz, *Neutron Cross Sections* (U.S. Government Printing Office, Washington, D.C., 1958), 2nd ed.
[149] H. H. Barshall *et al.*, Los Alamos Report, LA-1060, 1950 (unpublished).
[150] R. L. Henkel *et al.*, Phys. Rev. **94,** 141 (1954).
[151] It is true that the analysis of Auerbach *et al.*[147] does not require, but also does not prejudice the use of additional parameters.
[152] W. B. Gilboy and J. H. Towle, Nucl. Phys. **64,** 130 (1965).
[153] P. A. Moldauer, Nucl. Phys. **47,** 65 (1963).
[154] A. J. Elwin *et al.*, Phys. Rev. **133,** B80 (1964).
[155] W. Gilboy and J. H. Towle, Nucl. Phys. **42,** 86 (1963).
[156] D. Winterhalter, Nucl. Phys. **43,** 339 (1963). D. Reitmann, C. A. Engelbrecht, and A. B. Smith, Nucl. Phys. **48,** 593 (1963). A. H. Armstrong *et al.*, Nucl. Phys. **52,** 505 (1964). D. J. Hooton, Phys. Rev. **138,** B48 (1965).
[157] M. H. Mac Gregor, R. Booth, and W. B. Ball, Phys. Rev. **130,** 1471 (1963).
[158] W. P. Bucher and D. W. Kent, Phys. Rev. **134,** B361 (1963).
[159] D. W. Kent, Phys. Rev. **137,** B401 (1965).
[160] B. E. Wentzel and M. F. Steuer, Phys. Rev. **137,** B80 (1965).
[161] D. J. Bredin, Phys. Rev. **135,** B412 (1964).
[162] R. Wagner *et al.*, Phys. Letters **10,** 316 (1964).
[163] See also Sec. III.
[164] Y. A. Aleksandrov and I. I. Bondarenko, Zh. Eksperim. i Teor. Fiz. **31,** 726 (1956) [English transl.: Soviet Phys.—JETP **4,** 612 (1957)].
[165] M. Walt and D. B. Fossan, Phys. Rev. **137,** B629 (1965).
[166] W. J. MacDonald and J. M. Robson, Nucl. Phys. **59,** 321 (1964). P. W. Martin, D. T. Stewart, and J. Martin, Nucl. Phys. **61,** 524 (1965). M. Conjeaud, B. Fernandez, S. Harar, J. Picard, and G. Souchere, Nucl. Phys. **62,** 225 (1965).
[167] A. M. Lane, Phys. Rev. Letters **2,** 424 (1954).
[168] W. G. Vonach, A. B. Smith, and P. A. Moldauer, Phys. Letters **11,** 331 (1964).
[169] M. Z. Rahman Khan, Nucl. Phys. **59,** 580 (1964).
[170] S. S. Glickstein and R. G. Winter, Phys. Rev. **129,** 1281 (1963).
[171] J. A. Moore, H. Palewsky, and R. E. Clursen, Phys. Rev. **132,** 801 (1963).
[172] R. E. Seegel, R. K. Smither, and R. T. Carpenter, Phys. Rev. **133,** B583 (1964).
[173] L. V. Groshev *et al.*, Nucl. Phys. **58,** 465 (1964).
[174] E. A. Davis *et al.*, Nucl. Phys. **48,** 196 (1963).
[175] R. O. Lane, A. J. Elwyn, and A. Langsdorf, Phys. Rev. **136,** B1710 (1964).
[176] T. R. Donoghue, A. F. Behoff, and S. E. Darden, Nucl. Phys. **54,** 33, 49 (1964).
[177] F. Bloch, Phys. Rev. **58,** 824 (1940).
[178] A. M. Lane and R. G. Thomas, Rev. Mod. Phys. **30,** 257 (1958).

[179] J. P. Elliott and B. H. Flowers, Proc. Phys. Soc. (London) **242A,** 57 (1957).
[180] L. Colli, P. Forti, and E. Gadioli, Nucl. Phys. **54,** 253 (1964).
[181] D. J. Donahue and R. D. Roberts, Nucl. Phys. **50,** 641 (1964).
[182] G. R. Satchler, Phys. Rev. **104,** 1198 (1956); **411,** 1747 (1958). S. M. Shaffroth, P. N. Trehan, and D. M. Van Patter, Phys. Rev. **129,** 704 (1963).
[183] R. T. Wagner, E. R. Shrunk, and R. B. Day, Phys. Rev. **130,** 1926 (1963).
[184] J. Cabe, M. Laurat, and P. Yvon (to be published).
[185] F. J. Vaughn *et al.*, Nucl. Phys. **64,** 336 (1965).
[186] R. Bouchez, J. Duclos, and P. Perrin, Nucl. Phys. **43,** 628 (1963).
[187] R. W. Peele, Phys. Rev. **105,** 1311 (1957).
[188] K. W. Wildermuth (private communication quoted in Ref. 187).
[189] P. E. Hodgson, Nucl. Phys. **8,** 1 (1958).
[190] D. H. Wilkinson, Proceedings of the International Rutherford Jubellee Conference, Manchester, 1960.
[191] W. Osakiewicz *et al.*, Institute of Nuclear Research, Warsaw, Report No. 505/5, March 1964.
[192] A useful expression for the distribution of density of nuclear matter is the one given by Hahn *et al.* [Phys. Rev. **101,** 1131 (1956)]:

$$\rho(r)=\begin{cases}\rho_0 & 0<r<c-z_3\\ \rho_0(c+z_3-r) & c-z_3<r<c+z_3\\ 0 & r>c+z_3,\end{cases}$$

with

$\rho_0=0.18$ nucl/F^3
$c=5.54$ (for La^{138})
$z_3=1.5$ F.

[193] The mean free path of neutrons in nuclear matter is given by

$$\lambda=\hbar/W[(\epsilon_0+V)/2m]^{\frac{1}{2}},$$

where V and W are the real and imaginary part of the optical potential and ϵ_0 and m are the neutron energy and mass, respectively.
[194] M. Arnold *et al.*, Nucl. Phys. **19,** 500 (1960).
[195] H. Gauvin, M. Lefort, and X. Tanago, Nucl. Phys. **39,** 447 (1962).
[196] J. I. Serebrennikov, Zh. Eksperim. i Teor. Fiz. **35,** 789 (1958) [English transl.: Soviet Phys.—JETP **8,** 547 (1959)].
[197] The so-called Schwinger scattering results from the interaction of the neutron magnetic moment with the Coulomb field of the nucleus.